THE MANAGEMENT OF TRACK-BRIDGE INTERACTION USING MONITORING BASED CALIBRATION

DYLAN JACOBS

A dissertation proposal submitted in partial fulfilment of the requirements for the degree of

MASTER OF ENGINEERING (TRANSPORTATION ENGINEERING)

In the

FACULTY OF ENGINEERING, THE BUILT ENVIRONMENT AND INFORMATION TECHNOLOGY

UNIVERSITY OF PRETORIA

DECEMBER 2021

DISSERTATION SUMMARY

THE MANAGEMENT OF TRACK-BRIDGE INTERACTION USING MONITORING BASED CALIBRATION

DYLAN JACOBS

Supervisor: Professor P.J. Gräbe

Department: Civil Engineering

University: University of Pretoria

Degree: Master of Engineering (Transportation Engineering)

Continuous welded rail (CWR) has become an attractive solution in modern railway track to improve safety and rider comfort as well as decrease maintenance. CWR on railway bridges also has several advantages, however, additional rail stress can be expected and it is, therefore, important that the track-bridge interaction phenomenon is understood. Considerable longitudinal rail forces and displacements may develop in CWR track on long-span bridges. Any movement of the bridge deck induces a movement of the CWR track and additional rail stress. To reduce longitudinal stress in the rail, the length of the bridge can be reduced to a maximum expansion length that does not result in excessive bridge deck displacements, by altering the static arrangement of the bridge to relocate the "thermal fixed point". An alternative method to reduce longitudinal rail forces and displacements on long-span bridges is to install a rail expansion joint (REJ). However, this is not an attractive solution as these devices cause local disturbance of the vertical track stiffness and track geometry which requires intensive maintenance.

The study first evaluates bridge temperature as an input parameter to the evaluation of the track-bridge interaction phenomenon. The results of the study confirm that the concept of an effective bridge temperature, supported by literature published by Emerson et al. (1976), is an effective means of defining the uniform bridge deck temperature and calculated effective bridge temperature results correlated well with bridge displacement measurements. Thereafter the study evaluates site data obtained to understand the mechanisms contributing to additional compressive stresses in the rail due to track-bridge interaction. This

was compared to permissible levels of rail compressive stress which were taken from established codes of practice. The need for a rail expansion joint on the Majuba Rail Bridge was confirmed by numerical modelling and high compressive rail stresses resulting in lateral buckling can be expected in the absence of an REJ. The vast difference in recommended values in various literature, ranging from 30 m to 200 m, supports the need for further evaluation of track-bridge interaction due to total bridge expansion length. The numerical analysis also confirmed that alternatives to an REJ, such as ballasted track or Zero Longitudinal Restraints (ZLR's) were ineffective on a bridge expansion length of 314 m. Finally, results from the numerical model demonstrate that additional compressive rail stress can be reduced to permissible values, as per UIC Code 774-3R (2001), by reducing the total bridge expansion length, by altering the static arrangement of the bridge, from 314 m to 120 m which compares well with results published by Esveld et al. (1995), Rhodes & Baxter (2016) and McManus et al. (2017).

The site investigation was undertaken on the newly constructed 68 km Majuba Rail Corridor to measure various parameters that influence track-bridge interaction. The structure is a continuous concrete bridge girder spanning 314 m over the Vaal River approximately 37 km south of Ermelo. Analysis of the bridge displacement, rail displacement and rail creep data indicate that although the rail is fastened directly to the bridge deck by means of elastic fastenings, a relative displacement of up to 6.5 mm, occurred between the bridge deck and rail. This is understood to be as a result of rail creep and "breathing length" associated with thermal loading. Approximately 78% of the displacement at the REJ is due to the high fixity Slab Track rail being pulled by the bridge and the remaining 22% is due to the ballasted rail track on the embankment "breathing" towards the discontinuity at the REJ. Rail creep for the high fixity switch blade accounted for less than 2% of the total rail creep. Rail creep is, therefore, primarily a function of "breathing length" from the ballasted track on the embankment for this bridge and REJ configuration. Midas Civil 2021 was used for numerical modelling. Displacement and axial stress results from a calibrated model compared well with the site data and published stress profile diagrams.

DECLARATION

I, the undersigned hereby declare that:

- I understand what plagiarism is and I am aware of the University's policy in this regard;

- The work contained in this dissertation proposal is my own original work;

- I did not refer to work of current or previous students, lecture notes, handbooks, or any other study material without proper referencing;

- Where other people's work has been used this has been properly acknowledged and referenced;

- I have not allowed anyone to copy any part of my dissertation proposal;

- I have not previously in its entirety or in part submitted this dissertation or its proposal at any university for a degree.

Signature of student: *Dylan Jacobs*

Name of student: Dylan Jacobs

Student number: 29023239

Date: 15/02/2022

ACKNOWLEDGEMENTS

TABLE OF CONTENTS

LIST OF ABBREVIATIONS

BEJ	Bridge Expansion Joint
CAD	Computer-aided Design
CWR	Continuous Welded Rail
HDPE	High-density Polyethylene
LHS	Left Hand Side
LVDT	Linear Variable Differential Transformer
MSL	Mean Sea Level
PTFE	Polytetrafluoroethylene
PRASA	Passenger Rail Authority of South Africa's
REJ	Rail Expansion Joint
RHS	Right Hand Side
RLR	Reduced Longitudinal Restraint
RSR	Rail Safety Regulator
SAR	South African Railways
SFT	Stress Free Temperature
SBR	Styrene Butadiene Rubber
TMT	Tubular Modular Track
UIC	Union Internationale des Chemins de fer (International Union of Railways)

WILMA   Wayside Intelligent Longstress Management

ZLR   Zero Longitudinal Restraint

LIST OF TABLES

LIST OF FIGURES

1 INTRODUCTION

Continuous welded rail (CWR) is the most common track configuration and is an attractive solution due to its ability to overcome the disadvantages associated with jointed track. Although CWR resolves several disadvantages of jointed track, CWR must be managed in such a way that the potential failure that accompanies it does not compromise the safety of the track (Gräbe et al., 2007). On railway bridges with CWR installation, additional rail stress is generated as the movement of the bridge superstructure imposes deformation on the track fastening system. The track-bridge interaction phenomenon is discussed in various design codes with recommendations of trackform structures and span lengths to reduce the effect of additional rail stress induced by bridge movement.

This chapter discusses the background of the track-bridge interaction phenomenon, defines the objectives of this study and discusses the scope limitations and methodology associated with the objectives of this study.

1.1 BACKGROUND

Due to temperature variations, considerable longitudinal rail forces and displacements may develop in continuous welded rail (CWR) on long-span bridges (Esveld et al., 1995). Any movement of the bridge deck induces a movement of the CWR track and additional rail stresses (Mirković et al., 2017). For rail bridges, the track structure and bridge are interlinked, regardless of whether the track is on ballast or Slab Track. This interaction affects the behaviour of the bridge and track structure and can be defined as the track-bridge interaction phenomenon (Kumar & Upadhyay, 2012).

To reduce longitudinal stresses in the rail, the length of the bridge can be reduced to a maximum expansion length that does not result in excessive bridge deck displacements by altering the static arrangement of the bridge to relocate the "thermal fixed point". However, if this maximum expansion length cannot be achieved, due to topography or other constraints, it is necessary to reduce additional rail stress using various alternative methods.

According to UIC Code 774-3R (2001), for a single bridge deck carrying CWR, without alternative methods to reduce additional rail stress (such as a rail expansion device), it is generally accepted that the maximum expansion length will be:

- 60 m for steel structures carrying ballasted track;

- 90 m for steel / concrete structures with concrete slab carrying ballasted track.

It should be noted that UIC Code 774-3R (2001) recommends a specific evaluation for unballasted track systems. Network Rail in the UK limits the bridge expansion length to 30 m (Rhodes & Baxter, 2016) while the South African Railways (SAR), now known as Transnet, limits the use of ballasted CWR track to a maximum expansion length of 200 m. It can be seen that there is a large variation in recommended bridge expansion lengths, which requires further investigation.

According to UIC Code 774-3R (2001), if the expansion length of a concrete bridge is 90 m or shorter, the additional axial stress of the rail is understood to be within acceptable stress limits. For longer bridge expansions, alternative methods are available to reduce the additional rail axial stress, such as rail expansion joints (REJ's) or Zero Longitudinal Restraints (ZLR's). REJ's have been successfully implemented on long-span continuous bridges but there is limited evidence to support the use of ZLR's on continuous spans longer than ~120 m (Esveld et al., 1995; Rhodes & Baxter, 2016; McManus et al., 2017).

Rails can be attached to a bridge structure in many ways. One of the most common mechanisms is the use of direct fix fastenings with spring clips. Alternatively, rigid rail clips have been used in the vicinity of substructure units with fixed bearings (Transportation Research Board, 2000). Reduced longitudinal restraint (RLR) or zero longitudinal restraint (ZLR) fastenings can be applied across sections of the bridge to somewhat decrease the additional stress of the rail across the entire section of the bridge (Lee et al., 2017).

In many cases, an REJ is provided on a bridge to provide stress relief when CWR experiences high compressive forces. There are various suppliers of REJ's in the industry and they can be used in a wide variety of applications including passenger rail and heavy haul operations. Due to the inherent irregular geometry issues associated in the vicinity of an REJ, a need to eliminate REJ's within a rail network has been identified. In both passenger and heavy haul operations, it has been found that REJ's are not an attractive solution as these devices cause local disturbance of the vertical track stiffness and track geometry which requires intensive maintenance (Kumar & Upadhyay, 2012). In further investigating the possibility of eliminating an REJ, it is imperative that the factors constituting the need for such a device are fully understood. The factors to be considered are as follows:

- Longitudinal displacement of the rail along the length of the concrete bridge;

- Relative displacement of the rail and the concrete bridge;

- Compressive longitudinal forces generated in the rail due to varying expansion rates.

To fully understand the effect of various fastening systems on additional rail stress, it is important that the track-bridge interaction is understood. Due to the varying expansion coefficients of concrete and steel, differential expansion between the concrete bridge and steel track can be expected which will cause additional longitudinal stress in the rail.

To determine the expected additional rail stress, it is vital to understand how the bridge may displace due to temperature. Bridges expand and contract due to change in temperature. This movement is accommodated by the use of bearings and expansion joints or by deformation of the piers and abutments with integral construction (Roeder, 2002). Research has shown that bridge expansion and contraction depend upon change in average bridge temperatures rather than air temperature. The actual calculation of the effective bridge temperature is complex, but two simplified methods exist, namely, the Emerson Method (1976) and Kuppa Method (1991).

1.2   OBJECTIVES OF THE STUDY

UIC Code 774-3R (2001) recommends a specific evaluation for unballasted track systems on bridges as opposed to recommending maximum bridge expansion lengths for ballasted tracks. The Transport Research Board (2000) discusses alternative methods to reduce additional longitudinal rail stress on bridges, including various fastening systems.

The objective of this study was, therefore, to develop a calibrated numerical model of an unballasted track system on a long-span bridge. The numerical model was calibrated using temperature and displacement (bridge and rail) data obtained from continuous monitoring on an incrementally launched Slab Track bridge, with a bridge expansion length of 314 m. The numerical model was then used to evaluate the effect of various alternative methods (REJ's, ZLR's, expansion length) on the additional rail stress due to thermal loading of the track and bridge structure.

The objectives achieved through the scope of this study can be further defined as follows:

- Evaluate the accuracy of the proposed method by Emerson et al. (1976) used to determine an effective bridge temperature;

- Evaluate the factors that contribute to the track-bridge interaction phenomenon, due to thermal loading, such as bridge displacement, rail displacement and rail creep. Use displacement, creep and temperature results to calibrate a numerical model for ballastless trackform on long-span bridges;

- Confirm the need for a rail expansion joint (REJ) on the 314 m Slab Track bridge;

- Evaluate alternative methods to manage track-bridge interaction, such as adopting ballasted track or installing zero longitudinal restraints on long-span bridges;

- Determine the maximum allowable bridge expansion length that results in permissible additional compressive rail stress and compare the results with recommendations by Network Rail, UIC Code 774-3R, De Wet (1989), Meyer & Mistry (2014) and Esveld et al. (1995).

1.3 SCOPE OF THE STUDY

The focus on this study was the evaluation of additional compressive rail stress, subject to varying fastening strengths and bridge expansion length, due to thermal loading. It should be noted for the purpose of this study that the "length of the bridge" or "bridge expansion length" is the distance from the "thermal fixed point" to the free end of a bridge deck between expansion joints. The additional compressive rail stress was quantified due to thermal loading of the bridge and rail only and the effect of the bridge substructures (stiffness of piers, bearing supports etc.) was not considered. Instead, longitudinal bridge displacement data served as input into the numerical model to calculate the resultant rail movement and stress. This enabled the ability to evaluate the effect of varying fastening strengths on longitudinal rail stress, due to thermal loading only and confirm the need for a rail expansion joint on the bridge.

It is understood that the track-bridge interaction phenomenon is influenced by various factors including temperature, vehicle braking/acceleration and vertical bending effects. According to Lee et al. (2015), the effect related to temperature load accounts for 50~70% of the total additional axial force whereas 20~40% is related to traction/braking and 5~10% is related to vertical load. Given that thermal loading accounts for most of the additional compressive rail stress, the study evaluated additional compressive rail stress due to thermal loading only with the effect of traction/braking and vertical loading recommended as a further study to this dissertation. In addition, the field investigations were undertaken shortly after the construction of the rail bridge before any traffic

was permitted. This provided the opportunity to evaluate the effect of thermal loading only without disturbance from other external forces.

It is understood that there are various finite element modelling techniques available that may influence the outcome of the track-bridge interaction study. The various modelling techniques and the associated benefits of the models are documented in several research papers. However, as this study was focussed on evaluating the additional compressive rail stress, emphasis was not placed on the alternative finite element model methods available. Instead, the finite element recommendation proposed in UIC Code 774-3R (2001) was used which models the bridge and rail as beam elements and the fastening system as bi-linear spring elements. Midas Civil Track-Structure Interaction (TSI) Wizard was used for this purpose and evidence was provided that the TSI Wizard provides similar outputs recommended by the UIC Code 774-3R (2001) test case.

This study primarily focused on and was limited to calculation of additional compressive stresses in the rail due to track-bridge interaction. This was compared to permissible levels of rail compressive stress which were taken from established codes of practice. Noting that the confirmation of bridge expansion length was not the primary focus of this study, it was limited to the comparison of lateral buckling permissible levels of rail stress with the assumption that lateral buckling is the critical failure mode associated with the 314 m Majuba Rail Bridge. Due to the season in which the site investigation was undertaken, site data associated with rail breaks due to contraction of rails was not obtained and, therefore, rail break failure modes were not investigated. Further recommendations are provided in Chapter 6 to assess rail break failure modes.

Support reactions in the bridge structure are a key consequence to consider in the track-bridge interaction phenomenon. It is believed that methods proposed in this dissertation to reduce the additional rail stress may have negative consequences on the bridge structure support reactions. The impact on the structure support reactions is recommended as a further study to this dissertation.

The location for this study is a 314 m incrementally launched concrete box girder bridge. The bridge was constructed over the Vaal River in 2016 as part of the 68 km heavy haul corridor to the Majuba Power Station. The bridge expands in one direction and expansion is facilitated by pot bearings with low frictional resistance. To accommodate the expansion of the rail, an REJ was installed on the southern end of the bridge and allows for a maximum expansion of 300 mm.

1.4   METHODOLOGY

The methodology is broadly divided into four main sections:

- A literature review was undertaken to identify and review relevant information related to this field of study. The literature review includes a brief discussion of the various track components, including track fastening systems and Slab Track and their association with the bridge track structure. This was followed by a discussion on bridge temperature and expansion and the methods available to determine an effective bridge temperature from field measurements. The chapter then concludes with a detailed discussion on track-bridge interaction and the factors influencing this phenomenon.

- A site investigation was undertaken to obtain various site data results to serve as input to calibrate a finite element model. The site investigation was undertaken over a total period of three weeks during different seasons of the year. Site data included the following continuously monitored parameters; total bridge displacement, total rail displacement, rail temperature, bridge temperature (throughout the cross-section), air temperature and precipitation. In addition, ad-hoc displacement and strain measurements were taken at key locations to determine rail slip at intermediate locations on the bridge.

- Data analysis was then undertaken on the measured site data to evaluate trends associated with track-bridge interaction and was used to define key input data to serve as calibration for the numerical model.

- Once the finite element model was developed, an analysis was undertaken to confirm the need for an REJ on the 314 m Slab Track bridge. The effect of the fastening system, including ZLR's and high fixity, were then evaluated by altering the bi-linear spring element properties to determine a resultant additional compressive rail stress. This analysis provided the ability to evaluate the effect of fastening strength on additional longitudinal rail stress as a result of thermal loading of long-span bridges. Finally, the finite element model was then used to challenge the maximum bridge expansion lengths recommended in the literature including Network Rail, UIC Code 774-3R, De Wet (1989), Meyer & Mistry (2014) and Esveld et al. (1995).

- Conclusions and recommendations for future research in the field of track-bridge interaction were then made.

1.5   ORGANISATION OF THE DISSERTATION

The dissertation consists of the following chapters:

- Chapter 1 provides an introduction and background to the dissertation, outlining the objectives, scope, methodology and organisation of the research project.

- Chapter 2 serves as a review of applicable literature related to the expansion of concrete bridges due to temperature, management of continuous welded rail, track components on rail bridges and track-bridge interaction phenomenon.

- Chapter 3 discusses the various parameters measured to evaluate track-bridge interaction. A detailed description of the equipment and experimental setup is provided. The results from the site investigation are then presented.

- Chapter 4 describes the analysis of the field investigation data, evaluates trends related to track-bridge interaction and summarises key inputs to serve as calibration parameters for the finite element model.

- Chapter 5 describes the development and calibration of the finite element model and discusses the results related to additional compressive rail stress due to the REJ and various fastening systems.

- Chapter 6 contains the conclusions of the dissertation objectives and provides recommendations for further research in the field.

- Chapter 7 provides a list of references used in this dissertation.

2 LITERATURE REVIEW

This chapter provides a detailed review of literature applicable to this study. Firstly, an introduction to track components, applicable to railway bridges, is provided with specific focus on Slab Track structures and the fastening system at the rail-sleeper interface. The focus of the literature review then shifts to literature related to railway bridges, initially discussing the expansion of concrete bridges and then discussing methods available to determine an effective bridge temperature from field measurements. Track loading, specifically related to thermal stresses, is then discussed in further detail. Thereafter, emphasis is placed on the track-bridge interaction phenomenon with specific focus on the behaviour of the rails through the fastening system and the bridge expansion length influencing the track-bridge interaction phenomenon.

2.1 TRACK COMPONENTS AND TERMINOLOGY

According to Selig and Waters (1994), the purpose of a railway track structure is to provide safe and economical transportation. To achieve this function, each track component must be able to perform satisfactorily in response to train loads and imposed environmental loads, such as temperature changes.

Railway track structures can be broadly defined by two main categories, namely, ballasted and unballasted (slab) track. According to Selig and Waters (1994), the track structure can be subdivided into superstructure and substructure. The classic railway track, namely ballasted track, consists of a framework composed of rails and sleepers which is supported on ballast and formation. The ballast bed rests on a subballast layer which forms the transition layer into the formation (Esveld, 2001). Since the inception of railways, the principle of the ballasted track structure has not changed substantially. Figure 2.1 illustrates a longitudinal view of the track structure components associated with ballasted track.

According to Esveld (2001), due to certain disadvantages associated with ballasted track, an alternative track structure, namely Slab Track, is evolving into a very competitive alternative. The disadvantages associated with ballasted track, in comparison to Slab Track, are:

- Tendency of track to "float" in both longitudinal and lateral direction over time;

- Limited non-compensated lateral acceleration in curves caused by limited lateral resistance provided by ballast;

- Pulverisation of the ballast grains in the ballast bed resulting in particles damaging rails and wheels;

- Reduced permeability to contamination, the wear of the ballast and intrusion of fine particles from the subgrade;

- A relatively heavy and high track structure requiring stronger construction for bridges and viaducts.
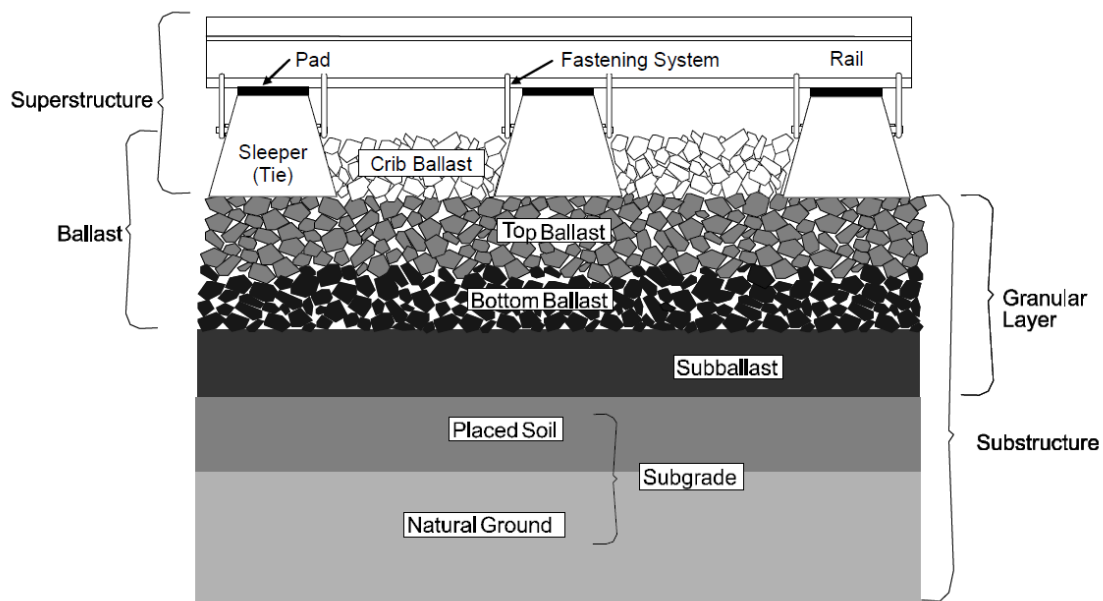
Figure 2.1: Longitudinal view of ballasted track structure (Selig & Waters, 1994)

The major advantages of Slab Track are low maintenance, high availability, low structure height and low weight (Esveld, 2001).

Based on the disadvantages associated with ballasted track, the use of Slab Track on bridges may have several advantages including the reduction in the tendency of the track to "float" in the longitudinal direction and the low weight of the track structure, reducing dead load on bridges and viaducts. However, the continuation of Slab Track on bridges could pose problems as the bridge acts as a discontinuity due to temperature changes causing longitudinal movements of the bridge structure (Esveld, 2001). This issue, known as the track-bridge interaction phenomenon, is the focus of this dissertation. The study focusses on bridges with Slab Track and, therefore, the literature review of track components excludes track components related to ballasted track.

2.1.1 Rails

Rails are the longitudinal steel members that guide the train wheel evenly and continuously. The rail must have sufficient stiffness to serve as a beam, transferring concentrated wheel loads to the supporting sleepers without excessive deflection in the rail (Selig & Waters, 1994).

The rail can be seen as the most important component of the track structure and has the following important functions (Esveld, 2001):

- It accommodates the wheel loads and distributes these loads over the sleepers and supports;

- It guides the wheel in a lateral direction with any horizontal transverse forces on the rail head being transferred to and distributed over the sleepers and supports;

- It provides a smooth-running surface and distributes accelerating and braking forces by means of adhesion;

- It acts as an electrical conductor;

- It conducts signal currents.

Rail profiles which are used extensively worldwide include the 54 E1 (UIC 54) and 60 E1 (UIC 60), where the numbers refer to the rounded weight in kg/m. The greater the mass and moment of inertia, the greater the resistance to heavier traffic loading.

Over the past 200 years, increasingly heavier rail has been required to handle the increased weight of locomotives and rolling stock associated with traffic volume increases (AREMA, 2003). Economic development in South Africa resulted in increased rail traffic over the years with heavier train loads and more powerful locomotives. With increased traffic load and frequency, rails of a greater mass were required. The UIC60 (60E1) was first introduced to the South African network in 1976 on the Iron ore line and later to the Coal line (Louw, 2009).

2.1.2 Rail Fastener

The term "fastening system" is considered to include all components that form the structural connection between the rail and sleeper. There are several methods available to fasten the rail to a conventional sleeper or Slab Track system. According to AREMA (2003), rail fastenings are aimed primarily at reducing movement between the rail and sleeper, both vertically and laterally. Originally, a spike was used to provide lateral support to the rail, however, with the need to

continuously improve rail systems and specifically rail fastenings, an elastic fastener was developed that provided longitudinal restraint as well.

The purpose of the fastening system is to retain the rail against the sleeper to prevent lateral, longitudinal, and vertical displacement of the rail when loaded. The forces inducing these displacements may be due to wheel loads and temperature changes in the rail (Selig & Waters, 1994). The longitudinal resistance of the fastening system should be much greater than the longitudinal resistance between the sleeper and ballast (Tzanakakis, 2013).

According to Esveld (2001), the general functions and requirements of rail fastenings are:

- To absorb rail forces elastically and transfer them to the sleeper;

- To damp vibrations and impacts caused by traffic as much as possible;

- To retain the track gauge and rail inclination within certain tolerances;

- To provide electrical insulation between the rails and sleepers.

The fastening system can be broadly divided into two main categories, namely, direct and indirect fastening systems. For a direct fastening system, the rail and baseplate are fixed to the sleeper using the same fastener whereas the indirect fastening system connects the rail to an intermediate component, such as a baseplate, which is then fixed to the sleeper.

According to Esveld (2001), with the introduction of CWR, the need for elastic fastening systems becomes essential due to its ability to provide longitudinal resistance in addition to vertical and lateral restraint. Elastic fastening systems can reduce rail creep making them effective in the use of long CWR sections. A variety of elastic fastening systems are available in the market which include the Pandrol Fastening System, the Pandrol Fastclip and the Vossloh Fastening System. Figure 2.2 illustrates the conventional Pandrol and Vossloh elastic fastening systems respectively.

Figure 2.2: Pandrol elastic fastening (a) and Vossloh elastic fastening (b)

An effective elastic rail fastening entails that the spring displacement is large, resulting in considerable clamping force. The clamping force of an elastic fastener varies for different products but is generally between 10 and 15 kN. According to Esveld (2003), the low stiffness and great spring displacement associated with elastic fastenings make the clamping force on the track less susceptible to:

- Elastic movements during wheel passage;

- Dimensional changes and inherent inaccuracies in the clip holder;

- Possible slight loosening of the fastenings; and

- Wear.

With a conventional direct fix elastic fastening system, the fastener provides isolation of the wheel/rail impact forces, electrical isolation, vertical elasticity for noise and vibration attenuation and longitudinal/lateral resistance to temperature and train forces. Although high clamping force and longitudinal resistance, associated with elastic fastenings, is the desired outcome in most applications, there may be instances where it is an attractive solution to increase or decrease the level of longitudinal resistance. An example of where a low level of longitudinal resistance is a desired outcome is on railway bridges where the bridge deck expansion causes additional stress in the rail, resulting in track-bridge interaction.

Low-restraint, moderate-restraint and high-restraint fastening systems are available where in some instances, zero longitudinal restraint may also be required.

Zero longitudinal restraint (ZLR) clips are a specialised fastening system with a sliding facility that purposely does not restrain the rail in a longitudinal direction. The ZLR consists of a special steel baseplate which is fastened to the sleeper by means of a Pandrol clip. In the absence of lateral loads, there is a small opening between the rail foot and the toe insulator. However, when the rail is subject to lateral loads, the toe insulator is engaged and resists overturning of the rail. The baseplate of the rail is made of a low friction material, such as Teflon, providing an almost zero frictional force in the absence of train vertical loads (Esveld et al., 1995).

One of the objectives of this dissertation, as described in Section 1.2, is to evaluate the effect of applying varied fastening strengths on long-span unballasted track bridges. The application of using a range of high-restraint, low-restraint and zero-restraint fastening systems is, therefore, an important aspect of this study and is further reviewed and discussed in Section 2.5.

Although the rail fastener is a key component responsible for providing longitudinal restraint to the rail, the ability of the rail to move through the fastening system is also a function of the rail pad material properties. The rail pad is, therefore, further investigated and discussed in Section 2.1.3.

2.1.3 Rail Pad

The main function of a rail pad is to transfer train vertical loads to the sleeper while also dampening high frequency force components (Esveld, 2001). The rail pad plays an important role in track dynamics and influences the overall track stiffness. In a loaded condition, a soft rail pad permits a larger deflection of the rail and the axle load from the train is distributed over more sleepers. In addition, soft rail pads isolate high frequency vibrations to the sleepers and further down to the ballast (Tzanakakis, 2013).

The rail pad is placed between the rail and sleeper to fulfil the following functions:

- Reduce vibration and impact transmission from rail to sleeper by providing resilience and impact attenuation;

- Provide adequate resistance to longitudinal and rotational movement of the rail;

- Minimise rail foot corrosion and concrete sleeper erosion;

- Provide increased longitudinal restraint, in addition to the rail fastener, to minimise longitudinal creep as a result of thermal expansion;

- Provide electrical resistance between the rail and sleeper;

- Provide a conforming layer between the rail and sleeper to avoid high contact area pressures.

Rhodes et al. (1989) discuss the significance of different properties of the rail pad, particularly resilience and durability. A brief history of the development of rail pads in heavy haul application is discussed. When concrete sleepers were first introduced on heavy haul lines, rubber pads, made of Styrene Butadiene Rubber (SBR) or Neoprene, were used. It became evident that these rubber pads were not durable, even under light traffic loads and had to be replaced long before the rail needed to be replaced. The use of rubber rail pads is still restricted on Transnet's rail network with a specific exclusion quoted in the Transnet Freight Rail Specification for Rail Fastening Systems (Meyer et al., 2013).

In the 1970's, an alternative pad with higher durability was introduced and manufactured from plastic materials such as high-density polyethylene (HDPE) which had a much longer service life than rubber pads. One of the issues associated with HDPE pads is their tendency to be brittle in cold temperatures. This was, however, overcome by adding a polyvinyl acetate to form a co-polymer (EVA). Although HDPE largely overcame the durability and service life issues associated with rubber pads, after several years in service, it became evident that HDPE pads could result in cracking of concrete sleepers. The issues associated with HDPE pads can be largely mitigated by introducing resilient rail pads, such as the Hytrel Pad.
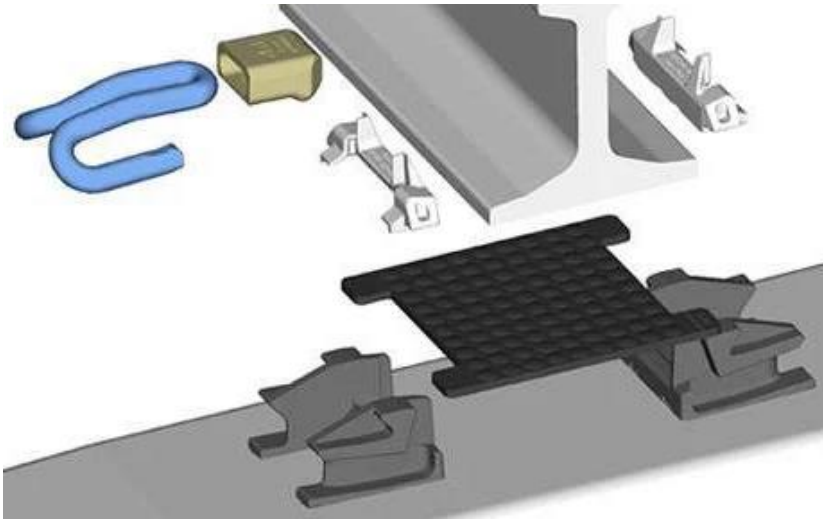
Figure 2.3: Pandrol Hytrel rail pad

The Pandrol Hytrel resilient rail pad is a two-part component moulded primarily from a thermoplastic elastomer. The material of the pad allows the pad to provide additional resilience in comparison to a rubber pad, however, with an increased service life.

A case study from the late 1980's related to improved track elasticity by providing more resilient pads, such as the Hytrel pad described above, is presented by Maree (1993) and Rhodes et al., (2005). The case study discusses track problems that occurred on the heavy haul Coal export line in South Africa after the axle loading had been increased to 26 ton/axle, resulting in skewed sleepers and crushed/powdered ballast. Pandrol was approached to analyse the impact of the existing rail pads, namely 12 mm thick High-density Polyethylene (HDPE). Studies showed that a permanent displacement of 1 mm occurred after 16 seconds under traction forces from four electric locomotives. The rail operator, Transnet Freight Rail (previously known as Spoornet), thus recognised the need for rail pads that would assist in reducing vibration, stabilise load distribution and reduce wear. Pandrol and Transnet Freight Rail tested a range of resilient rail pads that would accommodate larger forces and displacement and be more likely to recover elastically. The Hytrel thermoplastic elastomer provided the required resilience resulting in a maximum relative longitudinal displacement between the rail and sleeper of 0.2 mm (Dupont, 2021).

By proposing more resilient rail pads, the impacts of high vertical loads and large traction forces from electric locomotives could be mitigated. The main conclusions from the investigation were as follows:

- More resilient rail pads give better creep resistance with new Hytrel pads providing 23% better creep resistance than new HDPE pads;

- Hytrel rail pads prevent vibrations from rolling stock to the ballast and no powdering/crushing of ballast had been observed where Hytrel pads were installed.

Rhodes et al. (1989) recognised that as well as considering resilience, it is important to consider the durability of the rail pad which can be achieved by using material with high abrasion resistance associated with high hardness and stiffness. Unfortunately, these properties conflict with the requirement for a rail pad to provide resilience. It is understood that a non-resilient pad, such as HDPE, may result in a longer rail pad life in comparison to a resilient pad, such as a Hytrel pad. However, a Hytrel pad may extend the life of other track components such as sleepers. The selection of rail pads is, therefore, a complex decision dependent on many factors such as traffic loading, environment and track geometry (steep gradients and sharp curves). It is worth noting that the Transnet Freight Rail Specification for Rail Fastening Systems (Meyer et al., 2013) makes provision for resilient and non-resilient rail pads.

Although the use of resilient rail pads may not always be justified on conventional ballasted track, ballastless track structures, such as Tubular Modular Track or Slab Track, lack the resilience usually provided by the ballast bed. In these instances, resilient rail pads play an important role in dampening dynamic forces which cause accelerated deterioration of structural components such as fasteners and Slab Track modules. In a study conducted by Gräbe & Lubout (2012), a studded Hytrel pad is recommended for the Tubular Modular Track structure.

With the increased need for higher axle loads and increased train frequency in heavy haul operations, components such as the rail pad have evolved. Rhodes & Cox (2013) presented a paper related to the design of rail fastenings for extreme longitudinal forces for various climate conditions. Sleeper displacement, resulting in skewed sleepers, occurs as a result of slip between the rail and the sleeper and the sleeper and the ballast due to train acceleration and braking. To mitigate this effect, it is necessary that the ballast and formation have uniform properties and are compacted well. Further improvement can, however, be made using a rail pad that allows the largest elastic longitudinal displacement before slip occurs.

2.2 SLAB TRACK

With major rail projects now being assessed over the full life cycle of the asset, as opposed to capital expenditure only, Slab Track is a competitive alternative to ballasted track due to the reduced maintenance effort and increased availability. According to Lichtberger (2011), Slab Track systems are efficient in terms of construction, durability, strength and economy.

According to Esveld (2001), Slab Track provides far higher lateral and longitudinal stability resulting in improved track geometry with smaller deviations and a slower rate of deterioration. Slab track does, however, have several disadvantages in comparison to ballasted track including:

- Higher construction costs;

- Higher airborne noise reflection;

- Major alterations to track geometry requiring a substantial amount of work, as opposed to the tamping of ballasted track;

- Relatively small adaptability to large displacements on embankments;

- Much more time and effort to repair track in the event of a derailment;

- Ballasted to Slab Track transition required.

Slab track also requires a well-prepared foundation and homogenous sublayers resulting in minimal settlement when loaded. The extensive measures and capital expenditure required to meet the minimum settlement criteria have prevented the widespread use of Slab Track (Esveld, 2001).

The use of Slab Track is generally limited to high-speed rail, light rail and civil structures such as bridges or tunnels. A variety of Slab Track systems are available and can be broadly defined as systems with discrete rail supports or continuous rail supports. The discrete rail supports can be further subdivided into systems with sleepers/blocks and systems without sleepers. Table 2.1 summarises the Slab Track systems available with an example for each system.

Table 2.1: An overview of Slab Track systems and construction methods (Esveld, 2001)

Discrete Rail Supports				Continuous Rail Supports	
With Sleepers		Without Sleepers		Embedded Rail	Clamped and Supported
Concrete Embedded	On Top of Asphalt	Prefabricated	Monolithic in-situ		
Rheda Züblin Sonneville LVT	ATD (asphalt track bed)	Shinkansen Bögl	Paved-in track on civil structure	Paved-in track Light rail Road crossing Deck track	CoconTrack ERL (continuously supported grooved rail system) Vanguard KES (Continuous elastic support system)

In general, there are two ways of designing Slab Track. The first method involves Slab Track and subgrade with high stiffness, such as bridges or tunnels, where no differential displacement is expected. This Slab Track system has no bending resistance with reinforcement placed in the neutral axis to control crack width. The second method involves constructing slabs with top and bottom reinforcement with bending resistance which is more attractive on soil subgrades with some settlement.

2.2.1 Typical Slab Track Systems in South Africa

The use of Slab Track in South Africa is generally limited to tunnels constructed after the 1960's and long-span bridges. The main reason for the limited use of Slab Track systems in South Africa is the high cost of construction, which is typically two to three times more than the cost of ballasted track (Anon., 2018). In a South African context, although Slab Track offers lower maintenance with increased traffic density and the cost has been justified on the basis of life cycle cost by some rail authorities, the high construction cost still remains a deterrent.

Increased use of Slab Track on the Passenger Rail Authority of South Africa's (PRASA) network can be attributed to the need to maintain horizontal and vertical geometry through passenger platforms following the introduction of more stringent tolerances imposed by the Railway Safety Regulator (RSR). As these strict maintenance tolerances are not imposed on freight lines, Slab Track is still mostly limited to tunnels, where maintenance access is limited and on long-span

bridges where rail expansion joints are installed to manage large bridge temperature expansion movements.

Due to the simplified construction process, flat slabs have been widely used in the past and early South African Slab Track systems also used this method. To attach the rail to the Slab Track and provide rail inclination, cast iron rail chairs were typically used. A major disadvantage associated with the flat Slab Track system and cast-iron rail chairs is the complexity of fixing the fastening system within a desired tolerance. This generally requires skilled labour to set up jigs and apply epoxy plinths beneath the chairs. The largest cost associated with this Slab Track system is, therefore, due to the complexity associated with the rail chair (Anon., 2018).

As the high cost of Slab Track can be attributed to the costly installation of the rail chair, eliminating the need for this component results in a more economical Slab Track system. The resulting design in response to the costly rail chair is the development of the PY Track Slab system which aims to meet all the technical and functional requirements of traditional Slab Track, however, at a reduced cost. The PY Track Slab system has been in use since the early 1970's when heavy haul lines were constructed in South Africa.

The "PY" is derived from the PY sleeper, a common sleeper used in heavy haul applications in South Africa which uses a Pandrol fastening system. The PY Track Slab has the same cross-section and dimensions as the PY sleeper, however, is extruded into longitudinal panels. Using the same profile and fastening system as a PY sleeper ensures an economical and compliant Slab Track design which suits current market stock items and rail maintenance procedures (Anon., 2018).

Figure 2.4: PY Track Slab construction (Photograph: Transnet Capital Projects)

In the PY Tack Slab construction method, fastenings are directly cast into the slab using a method to suspend and hold rail fastenings in position to a 1 mm tolerance at 5 m intervals. This construction method is achieved by using robust steel fabricated jigs. By using jigs to achieve the desired construction tolerance of Slab Track, costly, skilled labour can be minimised, contributing to the economic viability of the PY Track Slab system.

Slab track in South Africa was used on various corridors in the 1970's and 1980's and included various tunnels on the Coal line, Natal line and the Hex River Tunnel. However, after a long break in track construction, various track components used for these Slab Track systems were discontinued. In recent years, BridgePort and RCE re-developed the system to accommodate current Pandrol fastening systems with improved construction tolerances. Slab Track and more specifically, the PY Track Slab system has been applied to track between passenger stations on the PRASA network, in tunnels, runways for heavy-duty gantry cranes and on railway viaducts. These projects are generally small-scale, intermittent and geographically distributed which dictate a Slab Track system that has low site establishment cost, is simple to construct and scalable to accommodate various project sizes (Wagner & Gräbe, 2018).

Recent projects in South Africa that have implemented the PY Track Slab system include the reconstruction of the Metrorail route between Pretoria and Walker Street Station as well as the 314 m incrementally launched bridge over the Vaal River as part of the Majuba Rail Project (Wagner & Gräbe, 2018). This dissertation focuses on the track-bridge interaction on the Vaal River Bridge and the PY Track Slab is, therefore, relevant to this study.

2.3   THERMAL EXPANSION OF CONCRETE BRIDGES

Bridges are exposed to daily, seasonal and yearly temperature variations throughout the expected design life. Temperature variations in a structure are a function of solar radiation, ambient air temperature, humidity and wind speed. Furthermore, temperature variations are affected by orientation of the structure, material of the structure, deck surface finishing layer, structure dimensions and cross-section geometry (Krkoška & Moravčik, 2015).

It is understood that the two main parameters influencing bridge temperature and resultant displacement is ambient air temperature and solar radiation (Ni et al., 2007). The angle between the direction of the sun and a specific surface is a key parameter in determining the magnitude of solar radiation on a given surface. If a surface is directly perpendicular to the sun, it receives a maximum amount of solar radiation. If the surface is angled to the sun, the solar radiation is reduced by the cosine angle between the direction of the sun and the perpendicular line the sun would take for maximum receipt of solar radiation (Dickinson, 2003).
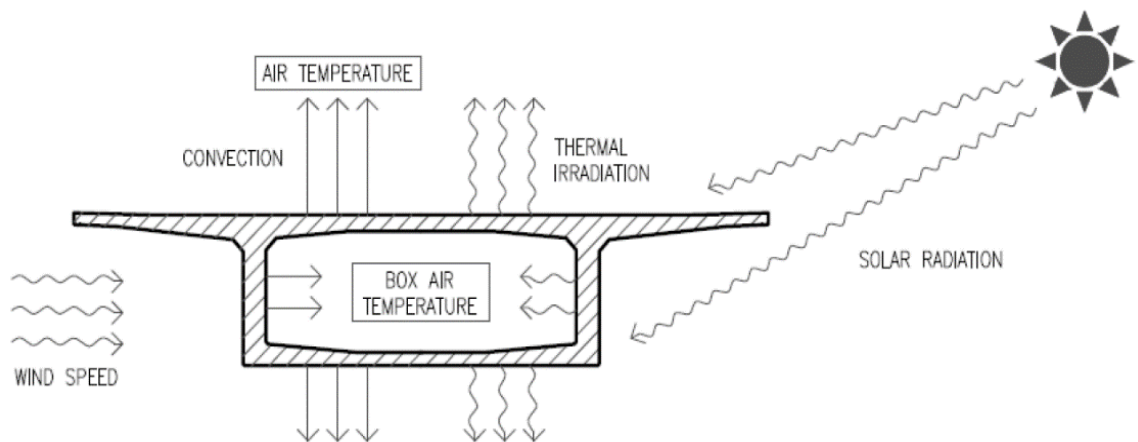
Figure 2.5: Environmental effects on bridge temperature (Krkoška & Moravčik, 2015)

A uniform temperature change causes significant expansion or contraction movements in a bridge structure. Restricting the temperature variation movements in a bridge deck can cause large internal forces that may result in damage of critical members in the structure. These forces may lead to severe damage if movements are not properly accommodated through joints and bearings (Roeder, 2002). Bearings, expansion joints or deformation of the piers accommodate the thermal expansion in a bridge.

Thermal expansion in a structure is computed by the following equation:

$$\Delta L = \alpha\, L\, \Delta T \hspace{6cm} \text{(Eq. 2-1)}$$

Where:

L = Original bridge length (m)

ΔL = Change in bridge length (m)

α = Expansion coefficient of concrete $\left(\frac{1}{\circ C}\right)$

ΔT = Change in temperature for a prescribed period (°C)

The thermal expansion is an important parameter when designing bridge expansion joints and bearings. Understanding direction and magnitude of the design movement with reasonable accuracy is important as restrained movements result in large forces in the bridge structure.

Underestimating the design movement results in damage to a structure. Conversely, overestimating the design movement results in increased capital cost during construction and increased maintenance cost during the lifecycle of the structure. The risk and cost associated with thermal movement supports the need for accurate understanding and determination of the parameters affecting thermal movement.

The key input parameter to determine thermal expansion is bridge temperature. Bridge temperature determination is, therefore, discussed in further detail in Section 2.3.1.

2.3.1 Bridge Temperature

The temperature distribution within an individual structural element can be categorised into the following four fundamental components:

- A uniform temperature component (a)

- A linearly varying temperature difference component about the z-z axis (b)

- A linearly varying temperature difference component about the z-z axis (c)

- A non-linear temperature difference component which results in a system of self-equilibrated stresses which produce no net load effect on the element (d)
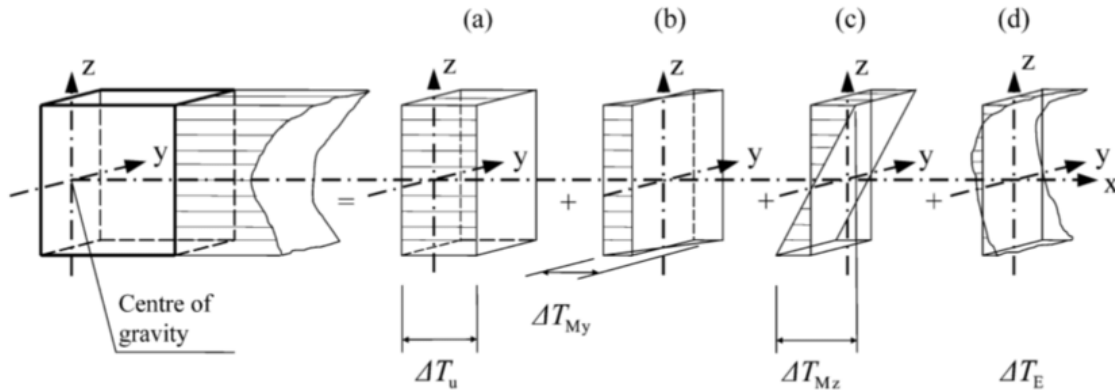
Figure 2.6: Diagrammatic representation of temperature profile components (STN EN 1991-1-5)

Generally, it is assumed that the uniform temperature component results in longitudinal movement of an unrestrained bridge. Longitudinal movement in a bridge is limited by the following effects:

- Longitudinal restraints (elastomeric bearings);

- Friction at roller or sliding bearings;

- Non-linear geometric effects;

- Track-bridge interaction.

The longitudinal bridge movement associated with uniform bridge temperature can be determined by linear elastic methods for statically determinate structures.

The effective temperature of a bridge is defined as the temperature which governs the longitudinal movement and can be derived from the sum of the products of areas (A_N) between isotherms and their mean temperatures (ΔT_N), divided by the total area of the cross-section of the bridge deck. In practice, it is difficult to locate isotherms but an approximation can be made by dividing the cross-section into temperature isotherms where the mean temperature per area can be determined by experimental measurement (Emerson, 1976).

$$\Delta T_e = \left(\frac{A_1 \Delta T_1 + A_2 \Delta T_2}{A_1 + A_2} \right)$$
(Eq. 2-2)

Where ΔT_e represents the change in effective temperature for a bridge structure. The equation for determining effective bridge temperature is derived by considering two adjacent bridge sections of unit length and the derivation is provided in Appendix A for further information.

2.4 TRACK LOADING

Significant longitudinal forces are imposed on the track due to thermal loads. A change in temperature of the rail causes expansion or contraction of the steel rails. Any restraint to this change in length induces thermal stresses in the longitudinal direction of the rail. Under compression force, in the absence of sufficient resistance, buckling of the rail can occur in both the horizontal and vertical plane (University of Pretoria, 2010).

2.4.1 Continuous Welded Rail

Long welded rails, also known as continuous welded rails (CWR), first appeared in South Africa in 1938. Continuous welded rails are now used on all major freight and passenger rail networks in South Africa.

CWR is used on most modern railways worldwide and is a key component of a modern railway system, allowing trains to travel at higher speeds with increased axle loading. Without the presence of joints along the rail, CWR results in decreased deterioration of vertical geometry, plastic deformation of the rail head, dangerous rail cracks as well as damage to sleepers and fastenings, resulting in an increased service life of all track components.

CWR has several advantages over previous conventional non-welded rail systems. CWR has been preferred over its predecessor, fish-plated joints and other conventional non-welded rail systems due to the problems associated with high-speed and heavy axle loads of modern freight trains (Szelazek, 1992). Fish-plated joints limit trains from achieving the desired operating speeds and, therefore, reduces the efficiency of the system (Sung et al., 2005). CWR reduces track maintenance as well as increases the service life of track components (Lim et al., 2003). According to Strauss et al. (2018), only CWR offers suitable serviceability with respect to today's increasing train speeds, as the deformation of joints often affects geometry of jointed track which increases maintenance.

There are, however, several disadvantages to the use of CWR. According to Gräbe et al. (2007), CWR must be managed in such a way that the potential failure that accompanies it does not compromise the safety of the track. Statistics from the Coal export line in South Africa revealed that 50-60% of train delays are stress related.

The stability of CWR can be affected by high resultant temperature forces. With an increase in temperature, high compressive forces are induced in the rail which may cause the track to buckle

in the lateral direction. Stability of lateral forces in the rail is provided by the resistance of the sleepers within the ballast and the mass of the rail itself (Lombard, 1978).

Figure 2.7: Rail kick out due to compressive forces

UIC Code 774-3R (2001) reviews the basic principles governing CWR in conventional track. According to UIC Code 774-3R (2001), the rail is fixed to the sleepers with fasteners with a predefined clamping force. The fastening system is designed to transmit the longitudinal movement in the rail to the sleepers which is in turn resisted by the ballast bed.
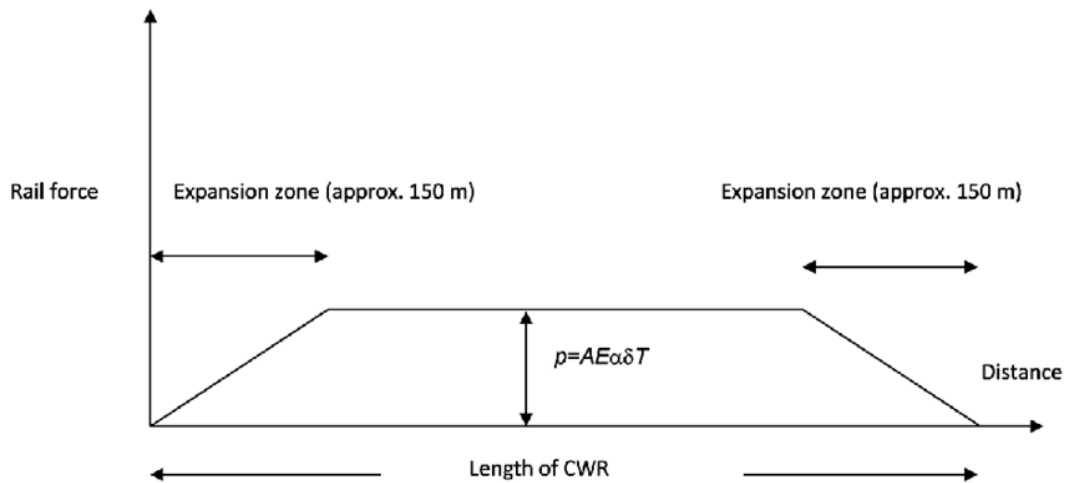
Figure 2.8: Force diagram for CWR under temperature variations (UIC Code 774-3R)

As the free movement of the rail is restrained by the ballast bed, longitudinal rail forces develop in the rail. UIC Code 774-3R (2001) defines the zone in which expansion and contraction are prevented as the "central zone". The "breather zone" is defined at each end of the CWR and is

approximately 150 m long. "Breather zones" are experienced in locations where there is a gap in the rail. A typical example of where the CWR experiences a gap in the rail is at an REJ. The force (P) induced in a rail, in the central zone of CWR, when a change in temperature has occurred may be derived from the analogy of a beam fixed at both ends undergoing a temperature increase.

$$P = \alpha \, \Delta T \; E \; A \qquad\qquad\qquad (Eq. \ 2\text{-}3)$$

Where:

ε_T = Strain due to temperature change

ε_P = Strain due to induced force

L = Length of rail (m)

α = Expansion coefficient of steel $(^1/_{^\circ C})$

ΔT = Change in temperature (°C)

E = Elastic Modulusof rail steel (GPa)

A = Cross sectional area of rail (m^2)

P = Force induced in the rail (N)

σ_P = Stress induced in rail caused by induced force (MPa)

Wheree temperature change (ΔT) is the difference between the current rail temperature (T_R) and the stress free temperature.

$$\Delta T = Rail \ temperature - SFT \qquad\qquad\qquad (Eq. \ 2\text{-}4)$$

From Equation 2-3, parameters such as Elastic Modulus, cross-sectional area and the expansion coefficient of a rail is generally well defined. The rail temperature can also be determined through temperature measurement probes or correlation to air temperature. The stress free temperature, however, is a complex parameter to determine and is a key input required to calculate the thermal loading in a track structure.

Another critical failure mode to be considered in the design and maintenance of CWR is rail breaks associated with rail deterioration and high tensile forces when the rail temperature decreases below the SFT. Rail deterioration is increased by operational conditions such as train speed, axle load, rail material type, wheel material type, rail size, rail profile, track construction, bogie characteristic, curvature, weather and environment (Chattopadhyay et al., 2006). Rail longitudinal compressive and tensile stresses are mainly concentrated in the head and foot of the rail whereas shear forces

are mainly concentrated in the web of the rail (Cope, 1993). Contributions to rail break failure modes generally consists of:

- Worn rail by wheel contact;

- Abrasive contact of sleeper on rail foot;

- Corrosion that leads to loss of rail section;

- Surface cracks that lead to reduced fatigue resistance.

A rail break occurs as the last phase of rail crack development processes. As the rail crack increases in length and depth, stress concentration increases in the rail and a break occurs due to additional external forces such as temperature loading (high tensile forces), rolling stock acceleration/braking and track-bridge interaction. Not all rail breaks impose a derailment risk but rail breaks are a major contributor to rail and wheel degradation. Rail breaks and associated derailments are key considerations for rail operators as they may result in loss of revenue, property and environmental damage or loss of life. Analysis of these risks with associated cost estimations are important in planning effective maintenance strategies (Reddy, 2004).

2.4.2 Rail Creep

Rail fastenings, and in particular resilient rail fastenings, serve a critical function to restrain the rail longitudinally to control rail creep. The amount of rail creep is a function of tensile and compressive forces generated from temperature variations, rolling stock acceleration and braking as well as track-bridge interaction. The amount of longitudinal rail restraint and associated rail creep varies from one application to the other. Rail creep can be defined as the movement of the rail through the rail fastener and this can occur in an "elastic" or "plastic" zone as discussed in Section 2.5.3. The "uncontrolled" rail creep through the rail fastener is more generally known as the "plastic zone", where the rail has moved past the "elastic zone" associated with the properties of the elastic fastening and rail pad.

According to Rhodes & Coats (2008), there are four main reasons to control rail creep:

- To constrain CWR when it is subjected to temperature loading;

- To prevent movement of the rail when it is loaded longitudinally by rolling stock acceleration/braking;

- To prevent excessive longitudinal forces on turnouts and insulated rail joints;

- To limit longitudinal forces transferred between the track and other structures such as bridge decks.

When rail slips in an uncontrolled manner, large displacements of the rail can accumulate to a localised point which will result in high compressive forces generated in the rail and ultimately track buckling. Conversely, at the ends of bridges and in transitions from one trackform to another it may be necessary to allow the rail to slip through the fastening in a controlled way by means of ZLR's as discussed in Section 2.1.2.

2.5 TRACK-BRIDGE INTERACTION

As the need for improved efficiency, increased speeds and higher axle loads grow, modern track solutions need to provide a system that results in improved safety and reduced maintenance. As discussed in Section 2.4.1, CWR has become an attractive solution in modern railway track to improve safety and rider comfort as well as decrease maintenance. CWR on railway bridges also has several advantages, however, additional rail stress can be expected and it is, therefore, important that the track-bridge interaction phenomenon is understood.

Due to temperature variations, considerable longitudinal rail forces and displacements may develop in CWR track on long-span bridges (Esveld et al., 1995). On ballasted bridges, this can result in excessive relative displacement between ballast and sleepers impacting the stability of the track. Any movement of the bridge deck induces a movement of the CWR track and additional rail stress (Mirković et al., 2017).

For rail bridges, the track structure and bridge are interlinked, regardless of whether the track is on ballasted or Slab Track. This interaction affects the behaviour of the bridge and track structure and can be defined as the track-bridge interaction phenomenon (Kumar & Upadhyay, 2012).

Longitudinal and vertical displacement of the bridge occurs due to various external forces which causes additional axial stress in the rail. In these instances, the bridge and track cause member force and displacement that structurally influence each other (Lee et al., 2017).

When CWR is fixed to sleepers with the aid of elastic fasteners and rests on a bridge deck with or without a ballast cushion, interaction between the track and the bridge deck takes place as the two are not free to move independently (Kumar & Upadhyay, 2012). This results in additional longitudinal forces in the rail. According to Kumar & Upadhyay (2012), additional rail forces can be expected on bridge structures due to the following reasons:

- Thermal expansion of the bridge deck;

- Longitudinal braking and acceleration;

- End rotations of the deck due to vertical traffic loads;

- Bridge deck deformation/bending.

To reduce longitudinal stress in the rail, the length of the bridge can be reduced to a maximum expansion length that does not result in excessive bridge deck displacements by altering the static arrangement of the bridge to relocate the "thermal fixed point". However, if this maximum expansion length cannot be achieved, due to topography or other constraints, it is necessary to reduce additional rail stress using various alternative methods.

In order to reduce longitudinal rail forces and displacements on long-span, it is common practice to install a rail expansion joints (REJ). However, this is not an attractive solution as these devices cause local disturbance of the vertical track stiffness and track geometry which would require intensive maintenance (Esveld et al., 1995).

According to Mirković et al. (2017), REJ's should be omitted due to their:

- High price of production and installation;

- High maintenance costs;

- Adverse influence on the driving and passenger comfort.

2.5.1 Track-bridge Interaction Code (UIC 774-3R)

According to UIC Code 774-3R (2001), the use of an expandable deck, capable of moving relative to CWR track, introduces a discontinuity into the characteristics of the track bed. This discontinuity is responsible for relative movement between the track bed and the track as the deck expands and contracts. This relative movement causes forces to be applied to the rails and the structure, as well as changes in the additional stresses due to forces induced by traffic loads. The parameters influencing the track-bridge interaction can be subdivided into "bridge parameters" and "track parameters" and can be summarised as follows:

Table 2.2: Parameters affecting the track-bridge interaction phenomenon

Bridge Parameters	Track Parameters
Bridge expansion length Bridge span length Bridge support stiffness Bending stiffness of the deck Height of the deck	Track resistance Cross-sectional area of the rail

The relationship between the force applied to the track and the track resistance is a function of the track structure adopted, the standard of maintenance, defects present and the magnitude and frequency of the vertical load applied.

The relationship between the force applied to the bridge and the bridge resistance is a function of static arrangement of the bridge, behaviour of bearings, behaviour of supports, total support stiffness and bending behaviour of the deck. According UIC Code 774-3R (2001), the load cases to be considered for track-bridge interaction are as follows:

- Expansion of the deck only or expansion of the deck and rail with an REJ;

- Horizontal braking and acceleration;

- Deck rotation due to bending caused by vertical loading;

- Deformation of the concrete structure due to creep and shrinkage;

- Longitudinal displacement of supports due to thermal gradient;

- Deformation of the structure due to vertical temperature gradient.

UIC Code 774-3R (2001) defines the consequences for the track and bridge, due to the load cases listed, as:

- Combining load case effects;

- Permissible additional stresses in CWR on the bridge **(objective of this study)**;

- Absolute and relative displacement of the bridge and track;

- End rotations of the track;

- Support reactions;

- Need for rail expansion joint (REJ) **(objective of this study)**.

As discussed in Section 1.3, one of the focus areas of this dissertation was to evaluate additional compressive rail stress due to thermal loading only as this accounts for 50~70% of the total additional axial force in the rail (Lee et al., 2015).

When considering load cases due to temperature only, the change in temperature of the uniform component and the difference in temperature between the deck and rails (with expansion joints) must be considered. According to UIC Code 774-3R (2001), the bridge deck temperature does not vary from its neutral temperature by more than 35 ºC whereas the rail temperature does not vary by more than 50 ºC. In the case of CWR without an expansion joint, the rail does not displace and, therefore, is assumed to have no interaction effect on the deck. For UIC 60 on concrete sleepers with well consolidated ballasted track (ballast depth greater than 300 mm) and a minimum curve radius of 1500 m, additional permissible rail stresses due to track-bridge interaction can be considered. According to UIC Code 774-3R (2001), the additional permissible compressive rail stress is 72 MPa and the additional permissible tensile rail stress is 92 MPa.

It is understood that the additional permissible rail stress in UIC Code 774-3R is derived from buckling analysis of ballasted track. Additional permissible rail stress of 112 MPa for Slab Track is documented in BS PD CEN/TR 17231 (2017).

An additional objective of this study was to confirm the need for an REJ. According to UIC Code 774-3R (2001), it is preferable to avoid REJ's, but an REJ should always be installed at the free end of the deck if the additional rail stress exceeds the permissible values. Considering the possibility of having the fixed support of a bridge in the middle of the deck allows the length of CWR, without an expansion joint, to double. According to UIC Code 774-3R (2001), for ballasted track on concrete bridges of 90 m, no expansion joint is required (180 m if fixed bearing of deck is in the middle of the bridge). In contrast to the recommended value by UIC Code 774-3R (2001), Network Rail in the UK limits the bridge expansion length to 30 m (Rhodes & Baxter, 2016).

To investigate the consequences of (1) additional permissible compressive rail stress and (2) the need for a rail expansion joint, a further understanding of the parameters affecting the track-bridge interaction phenomenon (Table 2.2) is required. As described in Table 2.2, these parameters can broadly be defined as "bridge parameters" and "track parameters".

Of the parameters listed in Table 2.2, the main ones investigated in this dissertation are the "bridge expansion length" and the "track resistance". With the exception of the bending stiffness of the deck, the remaining parameters that are considered in this dissertation are as follows:

- **Bridge span length:** know parameter from plan layout construction drawings;

- **Bridge support stiffness:** know parameter (pot bearings) from construction drawings;

- **Height of the deck:** known parameter from cross-section construction drawings;

- **Cross-sectional area of rail:** know parameter from track construction drawings.

2.5.2 Bridge Parameters – Expansion Length

The bridge "expansion length", that influences the rail stress due to thermal expansion, is the distance from the "thermal fixed point" to the free end of a bridge deck (Rhodes & Baxter, 2016). Various static bridge arrangements are considered in UIC Code 774-3R (2001) and include simply-supported, continuous with fixed support at one end, continuous with intermediate fixed support and a series of simply supported spans. All these arrangements are considered with or without an REJ. The static bridge arrangement most applicable to the Majuba Rail Bridge and this dissertation is the "continuous deck with REJ and fixed support at one end".
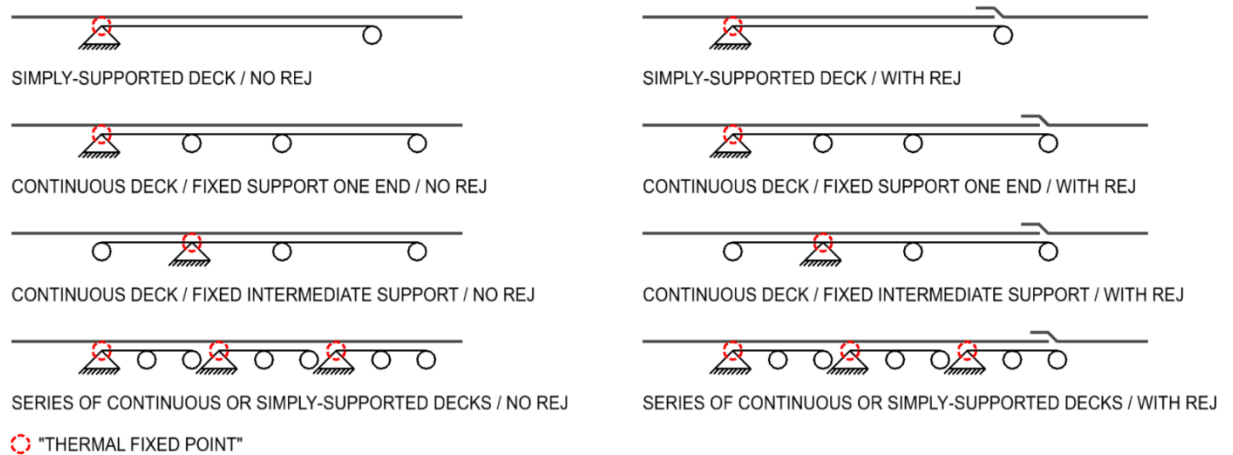
Figure 2.9: Common static arrangements for rail bridges (UIC Code 774-3R, 2001)

Although UIC Code 774-3R (2001) recommends concrete bridges with ballasted track do not exceed an expansion length of 90 m, significant examples of longer span bridges without REJ's do exist. One of the most notable examples of a long-span ballasted bridge without an REJ is the Olifants River Bridge on the iron ore export line in South Africa. The bridge deck is 1035 m long with twenty 45 m spans. After incremental launching, the central span was detached to form two expansion joints with 495 m continuous decks either side the 45 m simply supported deck.

Although REJ's were specified by the bridge designer, these were never installed. The 495 m continuous sections are, therefore, the longest known sections supporting CWR in the world (De Wet, 1989). On September 24th, 1982, a derailment occurred on the Olifants River Bridge due to a compression kick-out associated with track-bridge interaction forces and the absence of an REJ. Although an REJ was considered shortly after the derailment, a monitor/alarm system was recommended instead due to the large movement and unique REJ required and a weak point being created in the track. In addition, winged sleepers were installed for additional lateral stability (Maree, 1987). An additional measure on the Olifants River Bridge was the successful installation of zero longitudinal restraints (ZLR) (Esveld et al., 1995).

According to De Wet (1989), the South African Railways (SAR) deemed the restrictive operating conditions and level of risk associated with operation of the Olifants River Bridge as unacceptable. The SAR, therefore, limited the use of ballasted CWR track to a maximum expansion length of 200 m where winged sleepers and ballast kerbs are recommended for expansion lengths greater than 100 m. For bridge expansion lengths greater than 200m, the SAR recommended concrete Slab Track with an REJ. At the free expansion end, the REJ is placed at a CWR breathing length from the ballasted track off the bridge to ensure local disturbance of the ballast does not occur. As described in Section 2.4.1, the CWR expansion length can be as long as 150m. To ensure the REJ is not placed too far from the bridge expansion joint, SAR recommended that the breathing distance of the REJ could be significantly reduced by using closely spaced rail clips over the length of the REJ concrete slab. This also reduces the expansion joint capacity of the REJ, enabling the use of standard REJ's on bridge expansion lengths of up to 400 m (De Wet, 1989). It is evident that the Slab Track structure, recommended by SAR in the 1980's, for bridge expansion lengths greater than 200 m, is a similar design as the track structure that has been adopted on the newly constructed Majuba Rail Bridge, designed by H. De Wet at Protekon. Figure 2.10 illustrates the REJ on the Majuba Rail Bridge which has the same configuration as Figure 7 from De Wet (1989).

Figure 2.10: Rail Expansion Joint (Photograph: Transnet Capital Projects)

Prior to the installation of the REJ on the Majuba Rail Bridge, Transnet Freight Rail released a "User Requirement Specification for Rail Expansion Joints (BBG2478)" (Meyer & Mistry, 2014). This specification states that REJ's are required on ballasted and Slab Track bridges for long-span bridges with a deck length of 500 m. It is worth noting that the 500 m length is significantly longer than the maximum ballast deck expansion length of 200 m previously recommended by the SAR. There is no evidence of site investigations or numerical modelling undertaken to support the 500 m length stated in specification BBG2478.

A recent example of a ballasted bridge with an expansion length in excess of 200 m is the 1.125 km long-span bridge on the Seaford Rail Expansion Project south of Adelaide, Australia. The bridge consists of 22 spans with the longest expansion length being 7 no. 52.3 m spans (~366 m long). After consideration of the lessons learnt from the Olifants River Bridge track-bridge interaction problems, a series of REJ's were installed on the bridge to manage rail stress. In addition, the project considered ZLR's, however, the option was abandoned due to the lack of documented performance of extensive ZLR clip usage in similar applications (Turner et al., 2011).

Although there are no defined standards or recommendations for track-bridge interaction on Slab Track, there are several examples of long-span Slab Track bridges that traditionally use REJ's to manage excessive rail stress, such as the Majuba Rail Project (South Africa) and the Seaford Rail Expansion Project (Australia), discussed above.

An alternative track-bridge interaction mitigation measure, using ZLR's, has successfully been implemented on several long-span ballasted bridges, for example, the Olifants River Bridge (South

2-28

Africa) and a bridge on a high-speed line between Brussels – Lille on the junction for London/Paris (Esveld et al., 1995). The use of ZLR on Slab Track, however, has been limited in new railway projects due to lack of confidence in the design procedure and the non-availability of a dedicated design standard for Slab Track (Rhodes & Baxter, 2016).

Nevertheless, as high-speed rail on long-span bridges becomes more popular, the need to eliminate REJ's is exacerbated. A recent example of this occurred on the Bangkok MRTA Green Line where the design consultant worked with Pandrol to analyse additional rail stresses on continuous structures to justify the use of CWR with ZLR at peak stress locations as opposed to installing an REJ. Another example of an alternative to REJ's on long-span Slab Track bridges was the use of low longitudinal resistance fastening systems either side of pier locations on the Caulfield to Dandenong Level Crossing Removal Project in Melbourne, Australia (McManus et al., 2017).

There are many other examples of Slab Track used on long-span bridges used internationally such as the Beijing-Tianjin intercity railway line in China, the Cologne-Rhine/Main 300 km/hour high-speed line in Germany, Shinkansen lines in Japan and the Taichung and Yunlin Elevated Railway in Taiwan. This provides additional evidence of the need to manage track-bridge interaction on long-span bridges but are not discussed further in this literature review to maintain brevity.

Figure 2.11: Example of ZLR's installed on rail bridge

From the discussion above, it is clear that the bridge expansion length is a key parameter in understanding the track-bridge interaction. Various track structure examples were discussed and interact closely with bridge expansion for both ballasted and Slab Track, with or without REJ's. The parameter that connects the bridge expansion length to the associated track structure is known as the track longitudinal resistance which is discussed in further detail in Section 2.5.3.

2.5.3 Track Parameters – Longitudinal Resistance

Longitudinal resistance of the track is provided by clips, pads, sleeper and ballast. In a ballasted track system, the sleeper (with fastening system) and ballast contributes 30 - 40% whereas the crib ballast contributes 60 - 70% and 5% is provided by the shoulder ballast (Bartlett et al., 1961). The sleeper resistance varies between 4 - 14 kN/sleeper for newly constructed to well consolidated track with an average of ~9 kN/sleeper (which results in approximately 12 kN/m for 700 mm sleeper spacing).

According to UIC Code 774-3R (2001), the resistance of the track per unit length (k) to longitudinal displacement (u) is an important parameter and is a function of the following factors:

- Trackform (ballasted or Slab Track);

- Loaded/unloaded track (vertical);

- Frozen ballast;

- Maintenance condition;

- Defects in the track.

Track resistance (k) to longitudinal displacement (u) is a function of the rail displacement relative to its supporting structure. At low displacement, the resistance increases rapidly, however, once a certain displacement (u) is reached, the rail slips and longitudinal resistance (k) remains virtually constant (UIC Code 774-3R, 2001). It is generally accepted that this non-linear relationship between longitudinal track resistance (k) and displacement (u) is simplified to a bi-linear function as represented in Figure 2.12. According to UIC Code 774-3R (2001), this bi-linear function allows the longitudinal track resistance to be represented to a level of precision sufficient for calculation purposes.

From Figure 2.12 it can be seen that the displacement between the elastic and plastic zone, where rail slip occurs, has various conditions depending on track structure, environmental factors and loading conditions. For ballasted track, there are two sets of bi-linear conditions, namely, (1) resistance of sleeper in the ballast and (2) resistance of rail in the sleeper. These conditions are then repeated for loaded and unloaded for vehicle loading. For Slab Track, only the resistance of the rail in the sleeper is considered which, therefore, contributes to the increased longitudinal track resistance. In the case of frozen ballast, this is assumed to perform similar to Slab Track with no displacement between the sleeper and ballast.
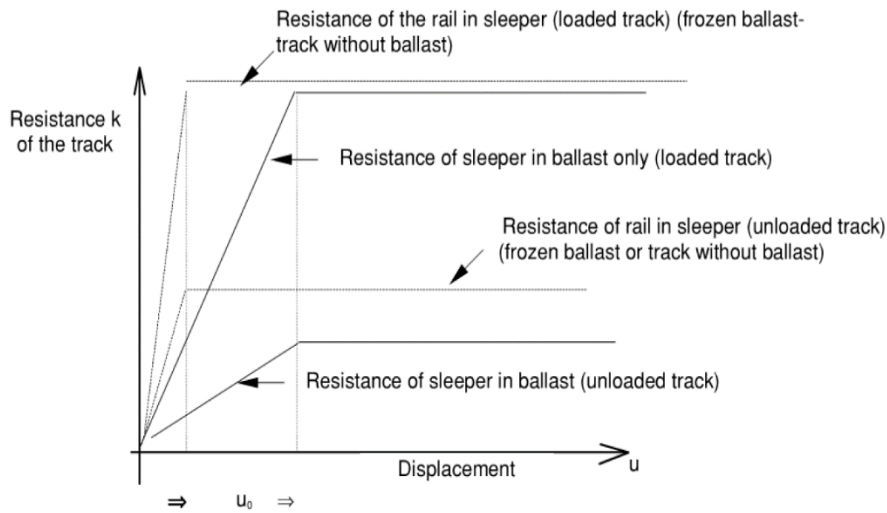
Figure 2.12: Longitudinal resistance (k) per unit length as a function of displacement (u)

Table 2.3 provides a summary of the various longitudinal track resistance parameters (k) at the displacement between the elastic and plastic zone (u) as documented in UIC Code 774-3R (2001).

Table 2.3: Longitudinal track resistance parameter (k) at the plastic zone

Track Structure / Condition	Track Resistance (k)
Resistance of sleeper in ballast, moderate maintenance (unloaded)	12 kN/m
Resistance of sleeper in ballast, good maintenance (unloaded)	20 kN/m
Resistance of loaded track or track with frozen ballast	60 kN/m
Slab track (unloaded)	40 kN/m
Slab track (loaded)	60 kN/m
Embedded rail (unloaded)	13 kN/mm
Embedded rail (loaded)	19 kN/mm

It can be seen from Table 2.3 that the longitudinal track resistance of ballasted track is significantly less than slab track and is mainly due to the ability of the sleeper to displace in the ballast as opposed to a slab track system fixed to the supporting foundation. The lower track resistance in ballasted track may result in less longitudinal stress generated in the rail, however, the resistance of slab to lateral buckling as a result of longitudinal stress in the rail is significantly more than ballasted track.

In addition, the use of ballasted track on bridges results in additional dead load transferred to the deck and substructure as well as increased maintenance.

As discussed in Section 2.4.1, an important aspect of CWR is the "breathing length". A breathing length occurs at the end of a sufficiently long CWR track where a discontinuity is introduced, such as an REJ or fish-plated joint. As the longitudinal track resistance decreases towards the joint, longitudinal rail displacement increases and the compressive force in the rail decreases.

The "breathing length" can, however, be decreased if the joint (REJ or fish-plated joint) provides additional longitudinal resistance to end of track movement. As described in Section 2.5.2, the REJ on the Majuba Rail Bridge uses closely spaced clips on a flat concrete slab to limit the REJ "breathing length" and minimise local disturbance of the ballast. The "breathing length" can be calculated by dividing the CWR axial force by the longitudinal resistance of the track structure (k) and the resistance of the REJ (K).

2.6   RAIL STRESS PROFILE ON A BRIDGE

The rail stress profile of a rail directly fastened to a bridge deck varies depending on the presence of an REJ. Figure 2.13 illustrates the additional stress in CWR track generated due to variation in temperature of the bridge deck.
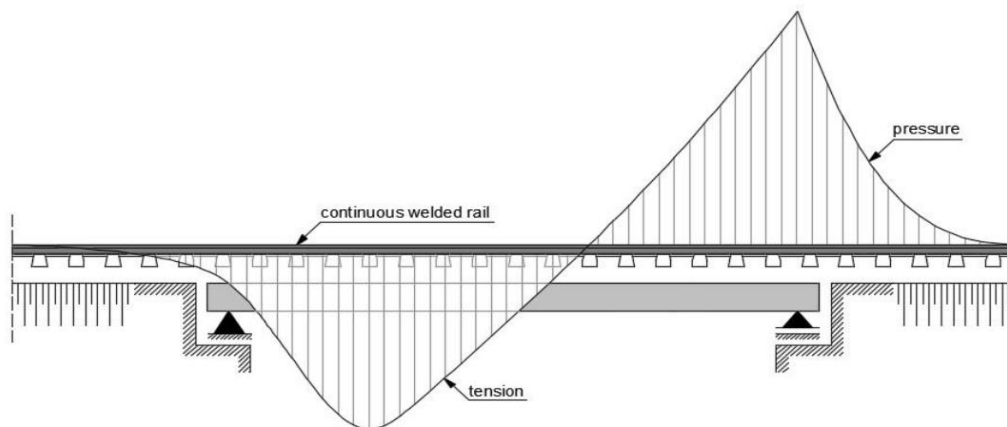
Figure 2.13: Additional rail stress due to temperature variations in bridge deck (Mirković et al., 2017)

However, when an REJ is installed at one end of the bridge deck, the additional rail stress is generally linear across the length of the bridge and decreases to zero at the end of the REJ, as illustrated in Figure 2.14.
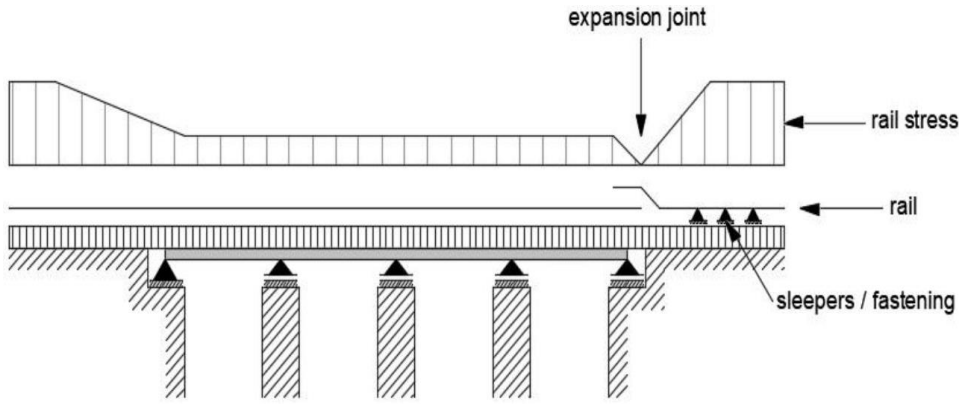
Figure 2.14: Strain in the rail at the movable end of the bridge with REJ (Mirković et al., 2017)

2.7 SUMMARY

Section 2.1 discusses various track components and more particularly, the influence of these components on longitudinal track resistance, which is a key parameter in determining the track-bridge interaction effect. Various types of rail fasteners are introduced including direct fastenings, elastic fastenings and low/zero longitudinal restraint fastenings. The functions of these fastenings and their application are then further discussed where it is concluded that direct fastenings, in contrast to elastic fastenings, are ineffective in providing longitudinal track restraints whereas elastic fastenings significantly reduce longitudinal creep. Low/zero longitudinal restraints are then introduced in the literature and their specific application on a railway bridge is discussed with reference to a study undertaken by Esveld et al. (1995). Thereafter, the rail pad is introduced including HDPE, Hytrel and rubber pads. The role of the different rail pad material properties in providing longitudinal resistance is then investigated. A study from the late 1980's, undertaken by Maree (1993), provides insight into the advantages of using Hytrel pads under heavy axle and large traction forces to minimise skewed sleepers and reduce crushed ballast.

Following the literature study of track components, Slab Track systems are further investigated in Section 2.2 including discrete/continuous rail supports with/without sleepers. At first, common Slab Track systems used internationally are discussed before the focus is shifted to the PY Track Slab system, developed and used in South Africa. As this Slab Track system is implemented on the Majuba Rail Bridge, it is a key structural component for the analysis undertaken in this dissertation. One of the main advantages of this Slab Track system is the use of a typical South African trackform

cross-section imitating the PY sleeper. This allows the use of track components readily available in the market making it a competitive solution in comparison to ballasted track when considering the full life-cycle cost. Once a literature review of the track superstructure components was complete, the thermal expansion of concrete bridges was then introduced before a detailed discussion was provided on the determination of an effective bridge temperature from the bridge cross-section (Emerson, 1976). The site investigation undertaken as part of this dissertation included continuous temperature monitoring through the bridge cross-section. An objective of this study is, therefore, to determine an effective bridge temperature, using the Emerson Method (1976), from the site data to correlate it to the bridge expansion.

The literature study concludes with a review of longitudinal track loading with particular focus on the parameters influencing longitudinal track loading and resistance related to the track-bridge interaction phenomenon. A key objective of this study is to confirm the need for an REJ on the Majuba Rail Bridge. The most important parameter that determines the need for an REJ is the bridge expansion length. A literature review of recommended maximum expansion lengths for CWR, without REJ's, was undertaken. The research shows a large variation in recommended parameters from 30 m for Network Rail, 90 m for UIC Code 774-3R (2001) and a maximum of 200 m recommended by SAR in the 1980's. An interesting expansion length of 500 m has been published in the Transnet specification for splice joints (BBG2478), however, there is no site investigations or numerical modelling data to support this parameter. An extensive review of literature related to the Olifants River Bridge derailment in 1982 revealed that the Olifants River Bridge still operates with 495 m of CWR and monitors the exceedance of rail stresses, which occurs 3 times a year according to De Wet (1989). Although the restrictive operations and risk profile associated with the Olifants River Bridge expansion length may be deemed unacceptable in modern railways, the vast difference between this expansion length (495 m) and the examples quoted by Network Rail (30 m) and UIC Code 774-3R (90 m) is questionable and, therefore, an investigation of the bridge expansion length remains an objective of this study.

Several examples of long-span bridges (ballasted and Slab Track) without REJ's are given in the literature review including Esveld et al. (1995), Turner et al. (2011), Rhodes and Baxter (2016) and McManus et al. (2017). The elimination of REJ's from long-span bridges is achieved through the introduction of low/zero longitudinal restraints at key locations of the bridge, such as bridge piers. However, the expansion length upper limit on long-span bridges with ZLR's has not been quantified in literature.

3 EXPERIMENTAL SETUP & SITE INVESTIGATION

A site investigation was undertaken to measure various parameters that influence the track-bridge interaction. The site data includes rail displacement, rail slip, rail temperature, change in rail strain, bridge displacement, bridge temperature and weather station data such as air temperature and precipitation. This data was used to study the relationship between key parameters and determine their effect on the track-bridge interaction phenomenon. This chapter describes the experimental setup and methodology followed to measure the track and bridge parameters.

The site investigation took place on the newly constructed Majuba Rail Corridor. The signature structure on the Majuba Rail Corridor is a 314 m long incrementally launched rail bridge.
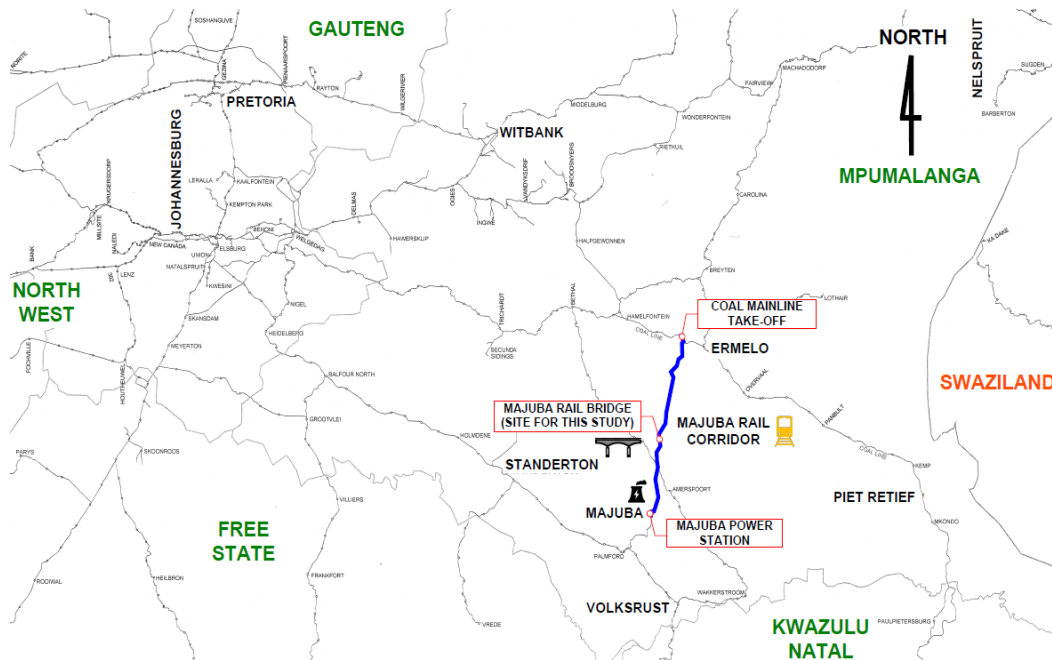
Figure 3.1: Majuba Rail Corridor Locality Plan

The structure is a continuous concrete bridge girder spanning the Vaal River approximately 37 km south of Ermelo. The centre of the structure is at km 35.57 with the 0 km chainage being at the mainline take-off. The 314 m long continuous concrete deck is fixed to the northern abutment, with moment transfer between the deck and the abutment but no movement allowed, and expands freely on pot bearings towards the south. The track structure on the bridge is PY Track Slab (refer Section 2.2.1) with ballasted track either side of the northern and southern abutments. A rail expansion joint

(REJ) is installed a breathing length from the ballasted track at the southern abutment to manage additional rail stress induced by the track-bridge interaction phenomenon.

3.1   PURPOSE OF THE INVESTIGATION

The purpose of the site investigation can be summarised as follows:

1. Measure the temperature of the concrete bridge girder at various locations through the cross-section. Use this data to validate the effective bridge temperature equation by Emerson (1976).

2. Measure displacement at the bridge expansion joint (BEJ) and correlate the displacement with the calculated effective bridge temperature to confirm the bridge expansion length.

3. Compare the total bridge expansion and total rail expansion, at the BEJ and REJ respectively, to determine total rail creep/slip on the structure.

4. Measure the differential displacement between the bridge deck (Slab Track) and rails, at several locations along the length of the bridge to determine the rail creep/slip profile. Use this data to analyse the rail breathing length and verify the longitudinal track resistance bi-linear relationship.

5. Measure the change in rail strain, at several locations along the length of the bridge, to determine the rail stress profile between the fixed northern abutment and the REJ.

6. Analyse the site investigation results and develop parameters to be used in the calibration of a numerical model.

3.2   METHODOLOGY

The following methodology was followed to obtain parameters, such as expansion length and track longitudinal resistance, for further analysis of the track-bridge interaction phenomenon and calibration of a numerical model.

Firstly, a suitable site was identified to undertake the site investigation. The Majuba Rail Bridge on the Majuba Rail Corridor was selected as a suitable site for the investigation as it has a significant continuous span with an expansion joint in the bridge and rail to measure displacement with ease. The Majuba Rail Bridge is on tangent track for the length of the span which removes the effect of lateral forces associated with curves, facilitating an investigation of longitudinal displacement effects only. In addition, at the time of the site investigation, the Majuba Rail Bridge was newly

constructed which provided the opportunity to investigate the performance of new components (clamping force, pad friction etc).

Once a site was selected, various site investigations were planned to undertake the necessary data collection. Three separate site investigations were initiated with the first investigation taking place in March 2018, approaching winter in Ermelo. The second site investigation was undertaken in September 2018, approaching summer in Ermelo with a third site investigation undertaken in March 2019 for additional testing and repeatability.

3.3 SITE DESCRIPTION

The Majuba Rail Corridor is a component of the Eskom Road-Rail initiative with the construction of a railway line that links the Majuba Power Station to the main coal railway hub in Ermelo, Mpumalanga. The 68 km corridor is the first large greenfield freight-rail infrastructure project to be carried out in South Africa since 1986 and will be operated by Transnet Freight Rail (TFR).

The 68 km Majuba Rail Corridor takes off from the Broodsnyersplaas mainline approximately 10 km east of the Ermelo TFR Depot. The centre of the 314 m Majuba Rail Bridge is located at approximately km 35.57 with the 0 km chainage being at the TFR Broodsnyersplaas mainline take-off. The bridge is orientated in a north-south direction with the low chainage end on the north and the high chainage end on the south. The bridge is located on tangent track with an 800 m radius curve approximately 1.5 km north of the bridge and an 800 m radius curve approximately 0.5 km south of the bridge. Figure 3.2 provides an aerial view of the Majuba Rail Bridge site layout.
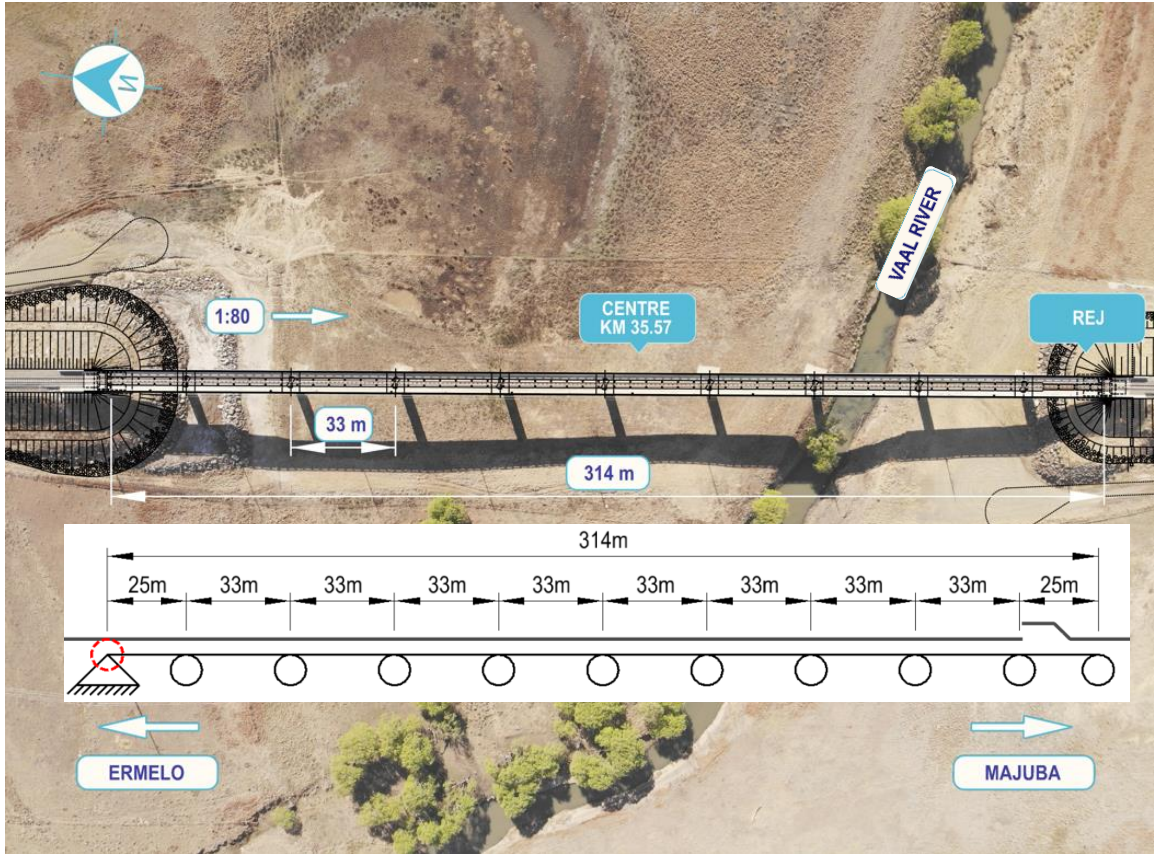
Figure 3.2: Majuba Rail Bridge Site Layout

The vertical gradient of the bridge is 1:80 (1.25%) sloping towards the southern abutment with the bridge soffit varying between an elevation of 1585 m ~ 1590 m above MSL. A further description of the various bridge and track components is provided below.
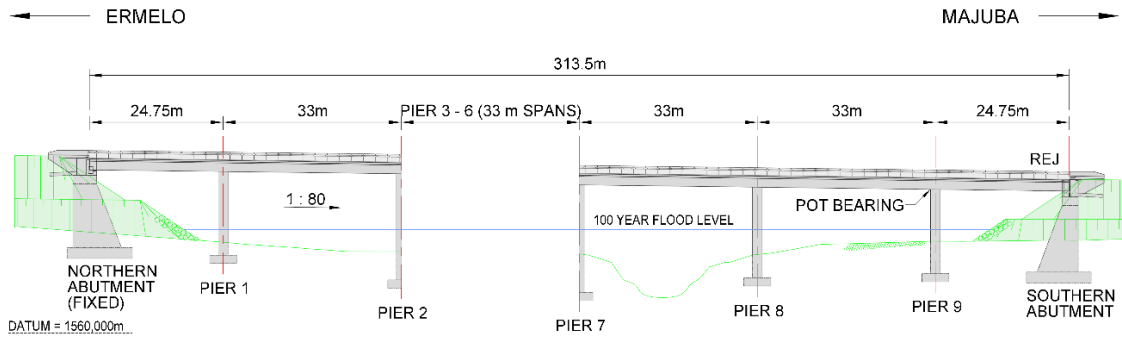
Figure 3.3: Majuba Rail Bridge Longitudinal Section

3.3.1 Bridge Deck

The Majuba Rail Bridge deck is a reinforced concrete box girder 314 m long with ten continuous pre-stressed concrete spans, designed to be constructed by the incremental launch method (launched from the southern abutment in a northerly direction). The concrete strength is 50 MPa with 19 mm stone and approximately 486 tons of reinforcement. The total depth of the box girder is 2.5 m with a total deck width of 6.4 m to facilitate a single track.
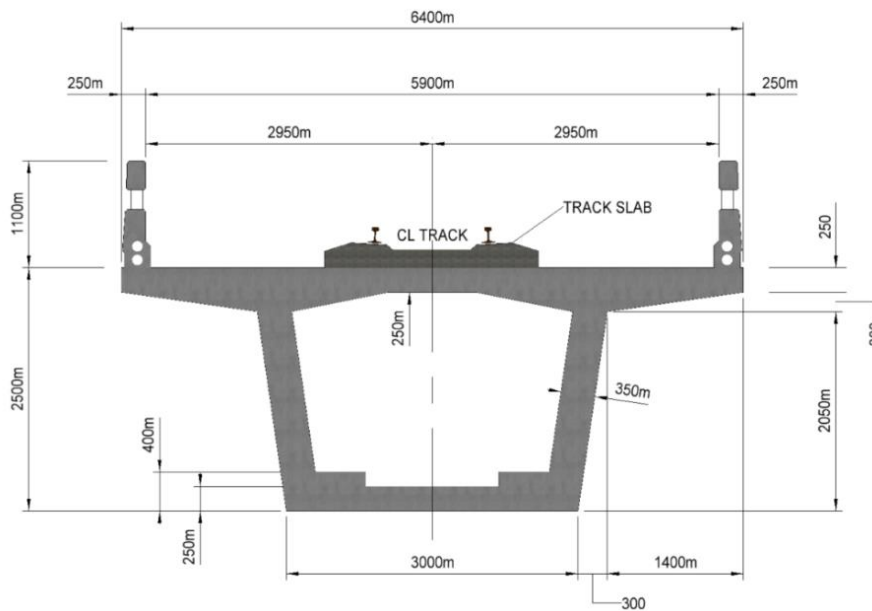
Figure 3.4: Majuba Rail Bridge Cross Section

3.3.2 Bridge Bearings

The continuous bridge deck has a bridge expansion joint at the southern abutment. The bridge deck expansion occurs on pot type mechanical bearings with horizontal movement taken up by metal bearings sliding on Teflon. The maximum coefficient of friction between the sliding surfaces of the bearing is 0.05 for permanent vertical load and 0.03 for maximum vertical load. The direction of preset is away from the fixed point at the northern abutment and parallel to the bridge centre line. The bridge deck is anchored to the northern abutment expanding towards the southern abutment, facilitated by bearings on the 9 bridge piers.

Figure 3.5: Majuba Rail Bridge Pot Bearings from Northern Abutment

3.3.3 Substructure

The substructure comprises box abutments and prismatic piers founded on spread footings. The average height of the piers is approximately 18 m with the highest being Pier 7 at 19.59 m high. The pad footings are 6.5 m x 5.5 m in plan with a depth of 1.5 m. The typical geology, at Pier 7 for example, includes transported silty sand, sandy clay and sand for approximately the first 6 m and is typically sandstone below this level. The water table is approximately 3 m below surface. An example of a bore hole log taken in the vicinity of Pier 7 is given in Figure 3.6.
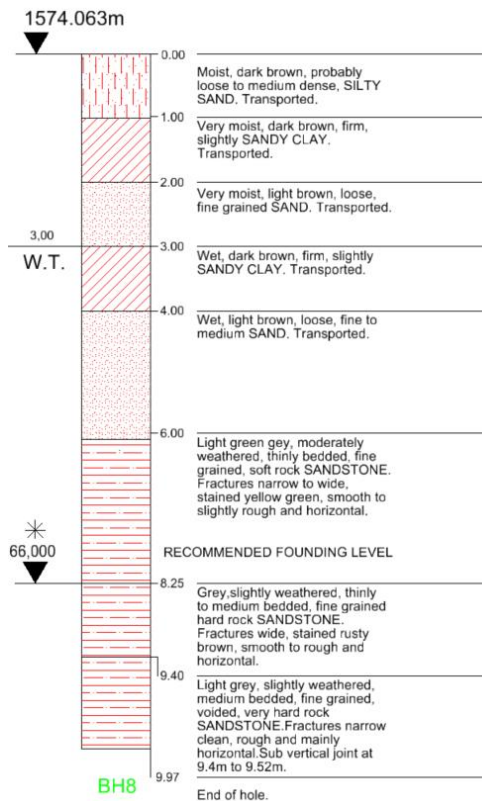
Figure 3.6: Typical Bore Hole Log at Majuba Rail Bridge

3.3.4 PY Track Slab

The PY Track Slab system was designed and developed by Henry de Wet who is currently the Chief Design Engineer for Bridges and Ports at RCE Consultants in South Africa (Wagner & Gräbe, 2018). Features of the PY Track Slab can be summarised as follows:

- The slab is manually constructed using jigs to achieve a profiled top surface with 1:20 canted rail seats. The concrete grade is 50 MPa with 19 mm stone;

- The continuity of the slab is divided into 5 m long segments with notches in the side extending approximately one half of the sleeper. This notch assists with rail welding procedures;

- The rail is supported by discrete rubber pads at 720 mm spacing which can be decreased to 360 mm spacing in the event of heavy loading;

- The rail fastenings are not drilled and epoxied, instead, the rail fastening shoulder is cast directly into the concrete during in-situ slab construction.

The PY Track Slab is subdivided into three sections, namely, Stage 1, 2 and 3. Table 3.1 provides a summary of the Majuba Rail Bridge Track Slab stage dimensions, position and structure.

Table 3.1: Majuba Rail Bridge Track Slab Details

Stage	Track Slab Structure	Length (m)	Position
1	Fixed PY Track Slab	288.10	From northern abutment
2	Sliding PY Track Slab	13.63	From southern abutment
3	Fixed Flat Track Slab	14.03	In between Stage 1 and 2

The Stage 1 PY Track Slab and Stage 3 Flat Slab are fixed to the concrete deck by means of Y12-E42 shear connectors and are, therefore, not expected to expand at different rates. The Stage 2 PY Track Slab is fixed to the southern abutment by means of a male-female structural connection with the male connection cast into the southern abutment and the female connection cast into the Stage 2 PY Track Slab. With the southern end of the Stage 2 PY Track Slab fixed to the southern

abutment, the remaining section is suspended on 64 no. (32 either side of track CL) pads, composed of PTFE (Teflon) bonded to rubber, with a total thickness of 24 mm. This section of Slab Track serves as an anchor for the southern half of the REJ where the Slab Track and rail are not subject to bridge expansion interaction as this section moves independently of the bridge over the Teflon support pads.

FEMALE CONNECTION   MALE CONNECTION
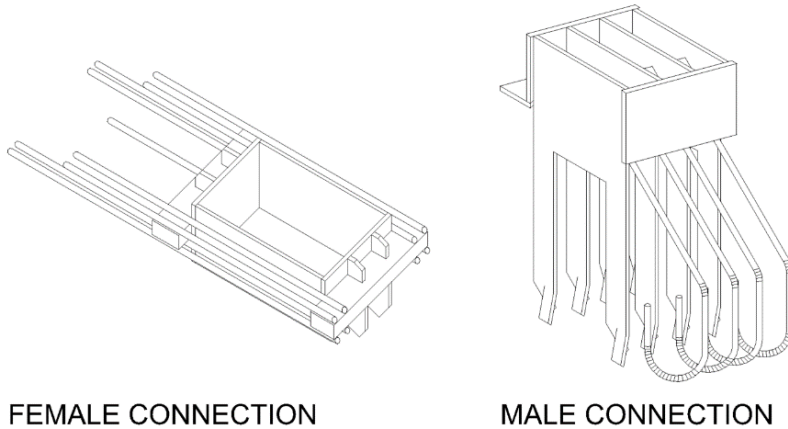
Figure 3.7: Typical sketch of Stage 3 male-female connection

Figure 3.8: Construction of Stage 3 PY Track Slab

3.3.5 Rail Expansion Joint

The Rail Expansion Joint, designed by VAE SA (Pty) Ltd., comprises a switch blade (gauge side) and stock rail (field side). The switch blade, located north of the rail expansion reference point, is anchored to the Stage 3 Flat Slab Track and is, therefore, anchored to the bridge. The stock rail, located south of the rail expansion reference point, is anchored to the Stage 2 PY Track Slab by means of resilient fasteners but is not anchored to the Stage 3 Flat Track Slab and instead is free to expand on the bridge by means of low restraint fasteners. The switch blade, which does not facilitate sliding, is anchored by means of various high toe load fasteners which include a combination of K-clip KP60-306/307 fastening clips and switch blade rail support buttresses which facilitate fastening to the base plate and the switch blade web resulting in high fixity fasteners. These components are fastened with a combination of Nordlock Washer and Nylock Nuts.

The stock rail, which does facilitate sliding, is guided on the Stage 3 Flat Track Slab by a combination of low restraint fasteners which include a combination of K-clip KP60-309 fastening clips and stock rail support buttresses that are only fastened to the baseplate and are not fastened to the stock rail. The K-clip KP60-309 fastening clips are similar to ZLR's and have a 0.8 mm gap between the toe of the rail and the underside of the clip which provides lateral support for overturning of the rail but allows free longitudinal expansion. As the stock rail buttress support is not fastened to the stock rail, it also provides lateral support only while allowing free longitudinal expansion with only minor steel to steel friction. The REJ has a total of 25 fastener positions which include 5 fixed fastening pairs on the switch blade and 6 sliding fastening pairs on the stock rail with the remaining fasteners being a combination of fixed K-clips and fixed buttress supports on the switch blade as well as sliding K-clips and sliding buttress supports on the stock rail.

All the fasteners within the REJ section, for both the switch blade and stock rail, are steel to steel connections only without any resilient pads. The switch blade and stock rail fastenings are then fastened to steel baseplates. A resilient pad is placed underneath the steel baseplate to provide elasticity to the track structure. The steel baseplates are then levelled with an epoxy and connected to the Stage 3 Flat Track Slab by means of drilled M24 grade 8.8 bolts with a Nylock nut and flat washer. As the switch blade is fixed to the bridge Slab Track by means of multiple high restraint fasteners, displacement of the switch blade is expected to be similar to the displacement of the bridge with the exception of minor creep through the fasteners. The stock rail, however, is expected to displace significantly more than the switch blade as it is fixed to the sliding Stage 2 PY Track Slab and is only connected by means of low restraint fasteners on the Stage 3 Flat Track Slab.
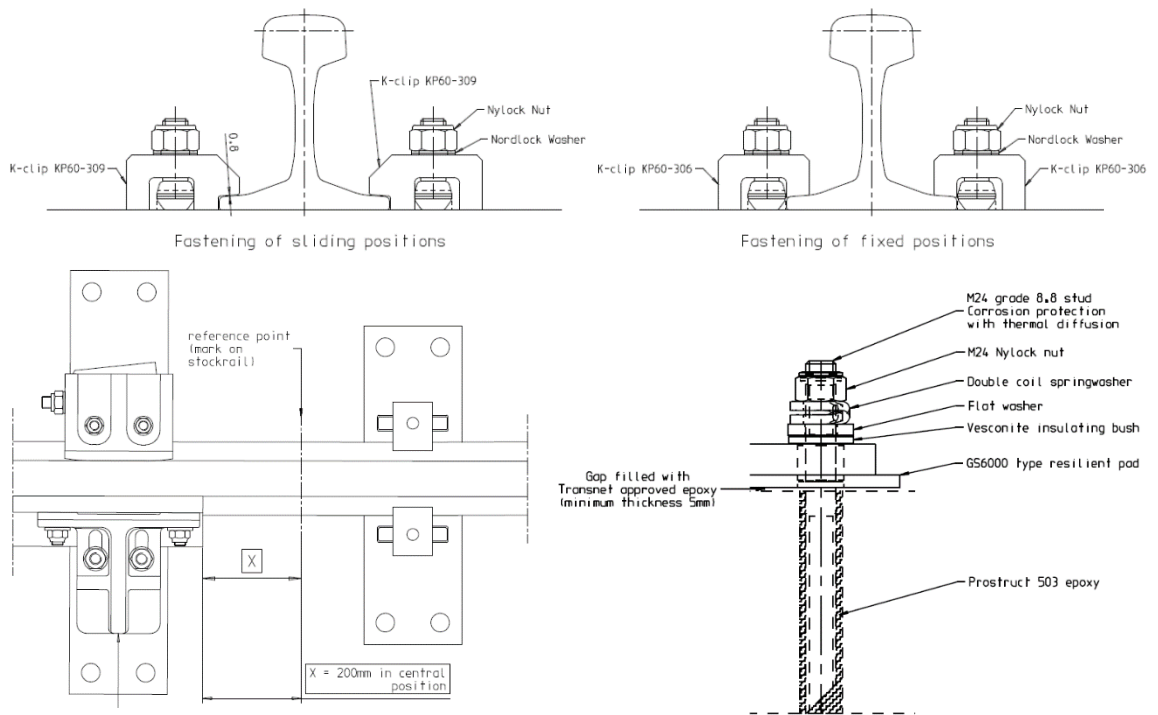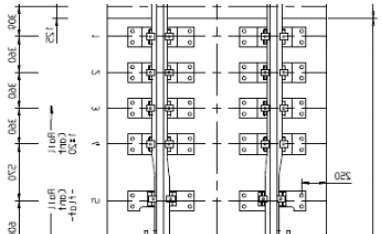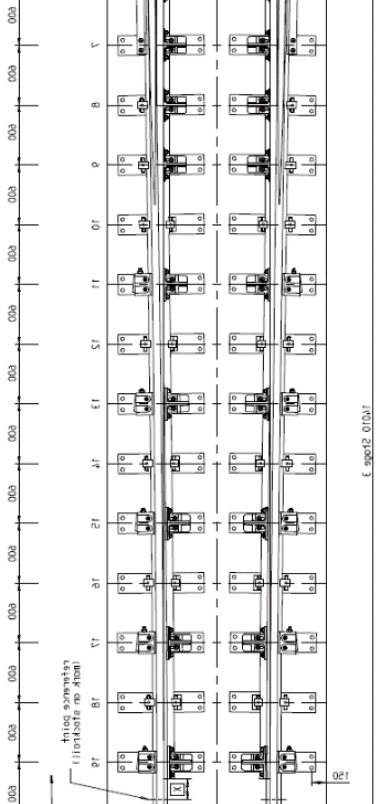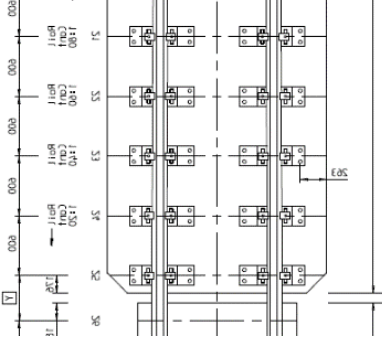
Figure 3.9: Stock rail fasteners (top left) and switch blade fasteners (top right)

Figure 3.10: Rail Expansion Joint on Stage 3 Flat Track Slab

Table 3.2: Majuba Rail Bridge Track Slab Fastening Details

Position	Fastening Type	Spacing
1 - 5	Fixed Fastening K-clip KP60-306 inside and outside	
6 – 9	Fixed buttress rail support inside Sliding K-clip KP60-309 outside	
10, 12, 14, 16, 18	Fixed Fastening K-clip KP60-306 inside Sliding K-clip KP60-309 outside	
11, 13, 15, 17, 19	Fixed buttress rail support inside Sliding buttress rail support inside	
20 - 25	Sliding K-clip KP60-309 inside and outside	

3.3.6 Slab Track Rail Fasteners

The Majuba Rail Bridge Stage 1 PY Track Slab is approximately 288.1 m long and comprises 56 no. 5 m long slabs with 6 mm deep recesses (150 mm x 250 mm) spaced at 360 mm intervals. Every second recess has Pandrol shoulders cast into the Slab Track which results in a fastening spacing of 720 mm.

A 60E1 rail profile is used with Pandrol e-clips and T23 Gauge Plate Insulators (internal) and T17 Gauge Plate Insulators (external) resulting in a gauge of 1072 mm.
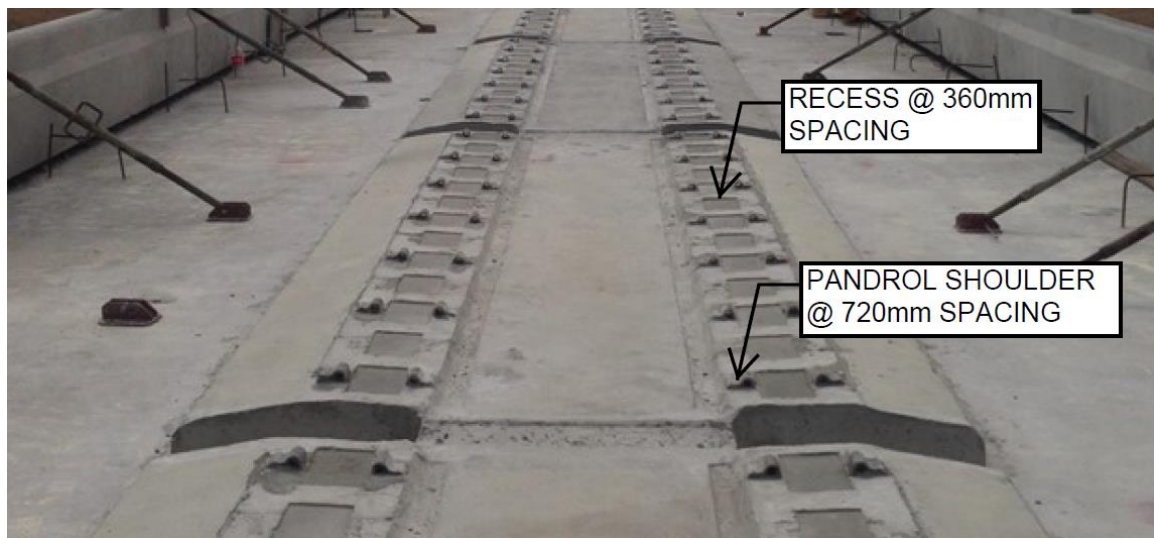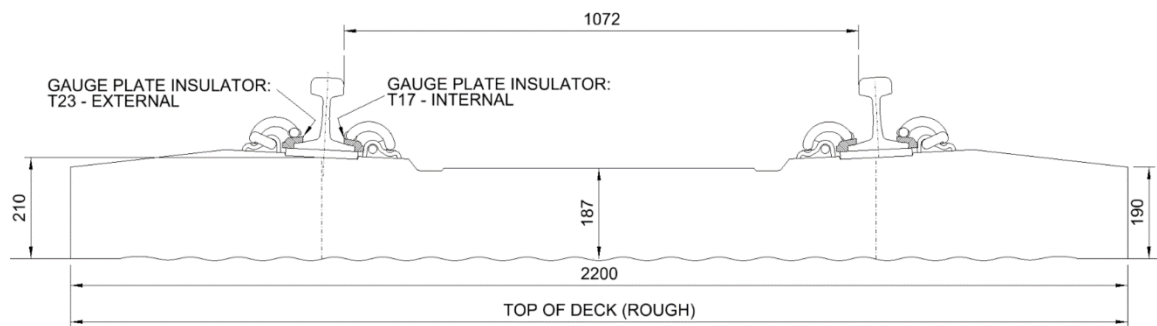
Figure 3.11: Recess and Pandrol shoulder for rail pads / fasteners

The original PY Track Slab design specified a 150 mm x 250 mm grooved rubber pad (16 mm thick). However, as rubber pads are not approved for use on Transnet lines, in accordance with Section 6.3 of BBF9273, an alternative pad was recommended by Transnet Track Technology. The rail pad proposed for the Majuba Rail Bridge is a Sylodyn ® rail pad by Getzner. It is understood

that this rail pad provides improved elasticity with proven durability which results in less wear on superstructure components. A case study was undertaken by Getzner to evaluate the effect of improved elasticity on superstructure components whilst confirming the durability of the rail pad. The case study involved installing Sylodyn ® rail pads on a 100 m heavy haul section of track in Brazil over a period of 6 years. This section of track had a high rate of rail and fastening fractures due to high traffic loading with reduced elasticity. The results of the study were satisfactory with no rail fractures over the 6 year test period and no signs of wear to the rail pad following visual and laboratory inspections (Getzner, 2019).

In addition to the improved elasticity and durability, it is understood that the Sylodyn ® rail pad provides increased longitudinal restraint in comparison to rubber pads. To confirm the improved longitudinal restraint, a creep test was undertaken by Transnet Track Technology. The creep test involved applying a longitudinal force to a short section of rail, which was fastened to a track slab section with cast-in shoulders and Pandrol e-clips. The same rail fastening assembly was used for both pads to eliminate variability. The results of the creep test are presented in Table 3.3.

Table 3.3: Creep test results on rail pads

Pad Type	Creep Force (kN)		
	Test 1	Test 2	Test 3
Rubber rail pad	13.7	12.7	11.1
Sylodyn ® rail pad	18.9	18.4	18.1

The results of the creep test indicate a significant improvement in longitudinal restraint for the Sylodyn ® rail pad in comparison to the rubber pad.

The creep force results obtained for both pad types are satisfactory in accordance with BS EN 13146-1 (2012) which requires a minimum longitudinal rail restraint of 7 kN on conventional railway lines and a minimum of 9 kN on high-speed lines as defined in BS EN 13481-5 (2012) Section 5.2. BS EN 13146-1 (2012) specifies a laboratory test procedure for determining the maximum axial force required to cause plastic displacement ("rail slip/creep"). The rail is secured to a sleeper or Slab Track element with a full fastening assembly which consists of:

- Fastening assembly including rail;

- Short length of rail (approximately 0.5 m);

- Slab Track, sleeper or half sleeper;

- Load-displacement measuring instrumentation;

- Rigid support and restraint to prevent rotation.

Figure 3.12: Example of longitudinal restraint test arrangement

An additional test is recommended in BS EN 13146-4 (2012) to determine the longitudinal restraint of a fastening system following repeated cyclic loading. This test provides an indication of the performance and durability of the fastening system following repeated loads in service.

From the longitudinal restraint (rail creep force) laboratory test results provided by Transnet Track Technology and the recommended values in BS EN 13481-5 (2012) Section 5.2, it can be seen that a wide range of longitudinal restraint values exist and are a function of the type of rail pad and clip used. In addition, technical specifications indicate a minimum of 9 kN longitudinal restraint is provided by the Pandrol elastic fastening systems.

3.3.7 Conventional Track Structure

The ballasted track structure, either side of the northern and southern abutments, comprises the following components:

- 900 mm deep track formation (SSB-layer, SB-layer, A-layer, B-layer in accordance with Transnet S410 Specification for Railway Earthworks);

- 300 mm deep ballast bed (below sleeper level);

- PY concrete sleeper (2200 mm long);

- Pandrol e-clip fasteners;

- HDPE rail pads;

- 60E1 rail profile.
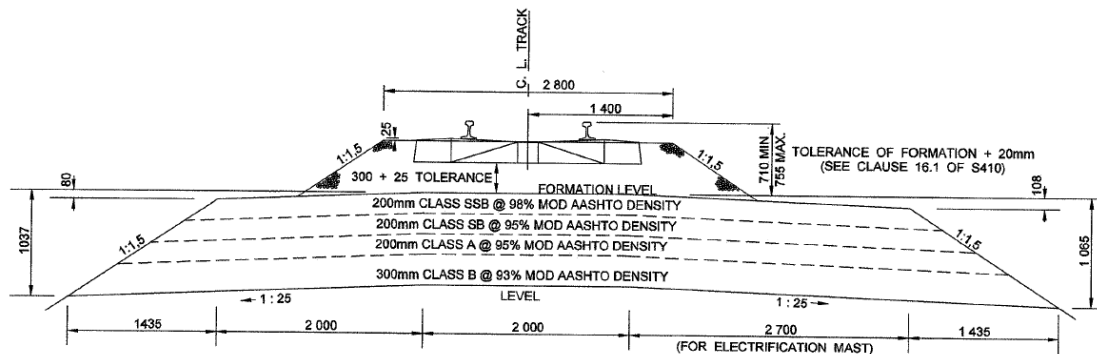
Figure 3.13: Typical conventional track structure on Majuba Rail Corridor

The track structure comprises CWR which is made up of 240 m rail lengths that were mobile flash butt welded into 480 m long rail panels. The 480 m long panels were destressed in the "A-range" particular to this geographical location in accordance with Annexure 16 of the Transnet Manual for Track Maintenance (BBB0481). As the "tensor method" was used to destress the rails, a stress free temperature (SFT) of 30 °C, in the midpoint of the "A-range", was generally achieved.

3.4 INSTRUMENTATION

The following parameters were measured during the site investigations in March 2018, September 2018 and March 2019:

- Bridge Temperature and Displacement;

- Rail Temperature and Displacement;

- Rail Stress;

- Ambient Air Temperature;

- Precipitation;

- Rail Slip/Creep.

These parameters were measured with various equipment and data loggers including temperature probes (thermistors), Linear Variable Differential Transformers (LVDT's), strain gauges, a weather station and three different data loggers. This section describes the instrumentation used during the site investigations.

3.4.1 Thermistors

Temperature was measured using 5 kΩ thermistors which consist of a micro NTC ceramic chip soldered between two solid silver plated nickel leads. The thermistors were soldered to data cables and covered in heat shrink material to improve durability and prevent water ingress.

Figure 3.14: 5 kΩ Thermistor with Heat Shrink Application

Thermistors measure the resistance of a wire of a specified metal by passing a current through it and then convert the reading to temperature using a calibration equation. The Steinhart-Hart Equation was used as the calibration equation for the conversion of Ohms to Celsius:

$$1/_T = A + B * \ln\left(R/_{R_{25}}\right) + C * \ln^2\left(R/_{R_{25}}\right) + D * \ln^3\left(R/_{R_{25}}\right) \qquad \text{(Eq. 3-1)}$$

Where:

T = Temperature (°C)
$A = 3.354 * 10^{-3}$
$B = 0.257 * 10^{-3}$
$C = 2.606 * 10^{-3}$
$D = 0.063 * 10^{-3}$
$R = 5000 \, \Omega$
R_{25} = Resistance at 25 °C

Once the thermistors had been soldered and heat shrink was applied, the calibration equation used was validated by placing the thermistors in a bowl of water with a known temperature measured by a thermocouple. Submerging the thermistors in water also confirmed that the heat shrink would be effective in preventing water ingress on site.

3.4.2 Linear Variable Differential Transformer (LVDT's)

Bridge displacement, rail displacement and rail creep were measured using Linear Variable Differential Transformers (LVDT's). The LVDT's used for this site investigation were DCC Series 4-20 mA 2-wire Output Displacement Transformers supplied by RDP Group. The LVDT's are stainless steel with high accuracy, cycle life and resolution. This series of LVDT's are available as either guided, captive or spring return version. A spring return version of the LVDT's was used for this site investigation which is appropriate where it is not possible to connect the transformer armature to the moving component being measured.

Figure 3.15: LVDT measuring bridge displacement on Majuba Rail Bridge

Two different types of spring return DCC Series 4-20 mA 2-wire LVDT's were used, namely, DCC100A and DCC150A. The main difference between the DCC100A and DCC150A type is the range of measurement which is 100 mm and 150 mm respectively. Table 3.4 provides an overview of the specification for each LVDT type.

Table 3.4: DCC Series 4-20 mA 2-wire Output LVDT Specifications

Description	DCC100A Type	DCC150A Type
Range (mm)	100	150
Linearity Error (%F.S)	±0.5 / ±0.25 / ±0.1	±0.5 / ±0.25 / ±0.1
Length (mm)	324	436
Centre of Range (X) (mm)	75	114
Total Weight (g)	398	511
Spring Force at X (N)	1.8	6.0
Spring Rate (N/cm)	0.2	0.4
Inwards Over Travel (mm)	8	15
Outwards Over Travel (mm)	14	15

3.4.3 Strain Gauges

Four strain gauges were used to measure longitudinal axial strain for both the left and right rail. The strain gauges were supplied by TLC Engineering Solutions, South Africa.

Figure 3.16: Encapsulated strain gauge supplied by TLC Engineering Solutions

The strain gauges used were 350 Ω encapsulated longitudinal strain sensors with a Half-bridge Type I Wheatstone Circuit. The strain gauges comprise a quarter-bridge active element and a quarter-bridge temperature compensation element.
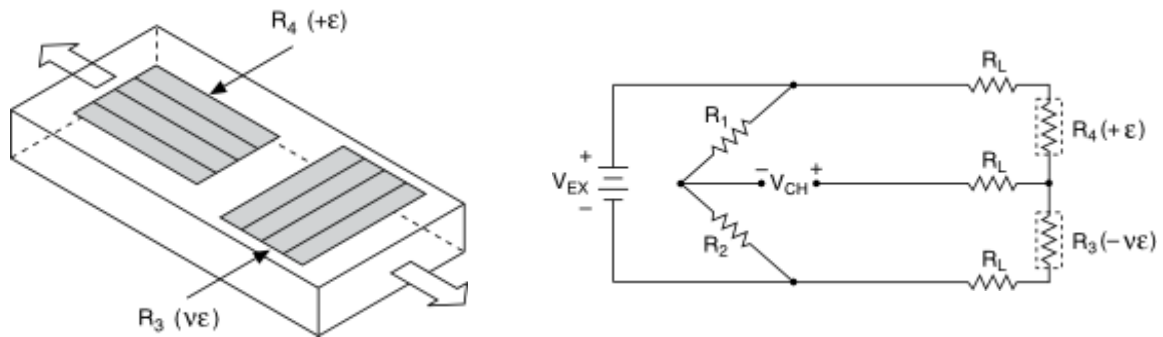
Figure 3.17: Half-bridge Type 1 axial configuration with temperature compensation

3.4.4 Weather Station

The ATMOS 41 all-in-one weather station, from METER Group, was used for this site investigation. Literature presented on the ATMOS 41 weather station was obtained from METER Group (2018).

Figure 3.18: ATMOS 41 all-in-one weather station

This weather station is designed for continuous monitoring of various environmental variables which include:

- Solar radiation;

- Precipitation;

- Air temperature;

- Vapor pressure;

- Relative humidity;

- Wind speed;

- Wind direction.

Key parameters for this study include precipitation, air temperature and solar radiation. Precipitation is measured by means of a 93.1 mm rain gauge. During a rain event, a flared hole forms the rain into drops that then pass through a drip counter. A spring is attached to the flared hole which prevents large particles from entering the drip counter while still allowing enough flow.

Air temperature is measured by means of a small stainless steel needle which contains a tiny thermistor. An advantage of the ATMOS 41 temperature sensor is increased accuracy in calculating temperature as solar radiation and wind speed are measured too, which are two main parameters that determine the error between measured and actual air temperature.
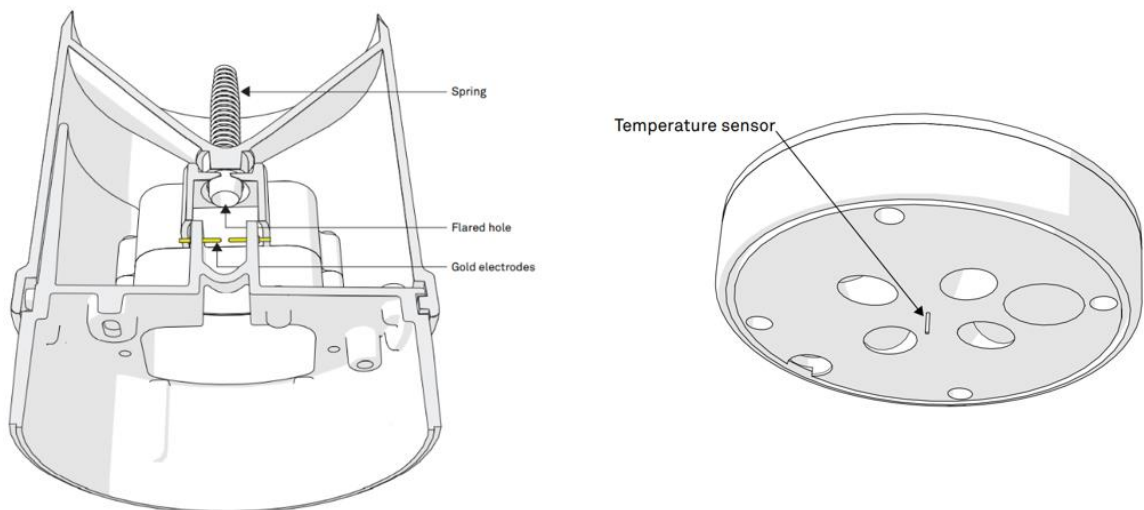
Figure 3.19: ATMOS 41 rain gauge (left) and temperature sensor (right)

Specifications for precipitation, air temperature and solar radiation are presented in Table 3.5 and include the range, resolution and accuracy for each parameter.

Table 3.5: ATMOS 41 Measurement Specification

Description	Range	Resolution	Accuracy
Precipitation	0 – 400 mm/h	0.017 mm	±5% of measurement from 0 to 50 mm/h
Air Temperature	-50 to 60 °C	0.1 °C	±0.6 °C
Solar Radiation	0 – 1750 W/m2	1 W/m2	±5% of measurement typical

3.4.5 Data Logging Equipment

Three data loggers were used as part of the site investigation. The detailed site setups are further discussed in Section 3.5 but generally, Campbell Scientific CR300 and CR800 data loggers were used at the fixed site setups at the northern and southern abutments whereas an HBM QuantumX universal measurement amplifier was used for the moving site setups along the length of the bridge.

The CR300 is a multi-purpose, compact measurement and control data logger. The data logger is small and low-cost which has fast communication with relatively low power requirements. This data logger has excellent accuracy and resolution and is suitable for small scale applications which require continuous long term monitoring (Campbell Scientific, 2021).

Figure 3.20: Campbell Scientific CR300 Data Logger (Campbell Scientific, 2021)

The CR800 data logger is ideal for research grade data logging and is designed to operate in adverse and remote environments. This data logger is intended to accommodate smaller configurations with fewer sensors. As the sensors transmit data by means of a peripheral communication system, most sensor and telecommunication devices are compatible with the system. This data logger comprises various electronics, including an external keyboard, display screen and power supply, housed in a plastic casing. The CR800 data logger has the ability to operate for extended periods of time on a solar rechargeable battery. The data logger automatically suspends logging when the power drops below 9.6 V to avoid inaccurate measurements. The operating system uses a BASIC-like syntax programming language (CRBasic) which includes measurement, processing and output instructions. Both the CR300 and CR800 Campbell Scientific data loggers can be powered with a 12 V DC battery (Campbell Scientific, 2021).

Figure 3.21: Campbell Scientific CR800 Data Logger (Campbell Scientific, 2021)

The HBM Quantum X data acquisition system captures a variety of different physical quantities reliably. This system has the capability to acquire a large range of signals and sensors. The unit has the flexibility to be installed for permanent monitoring applications or be used for portable services. The HBM Quantum X data logger is compatible with CATman software for a simple plug and measure application. Depending on the sensor technology, accuracy classes of this system range from 0.05 to 0.10.

Figure 3.22: HBM QuantumX Data Logger with CATman software

3.5   SITE SETUP

The site investigations included fixed sites at the northern and southern abutments for continuous data logging as well as various moving site setups used to obtain ad-hoc data along the length of the bridge. The fixed setup at the southern abutment will be known as Site A whereas the fixed site at the northern abutment will be known as Site B. The purpose of Site A was to obtain continuous measurements of the bridge displacement at the bridge expansion joint, rail displacement at the rail expansion joint, bridge temperature (bridge deck surface only) and rail temperature.

Following the data analysis of the bridge deck surface temperature at Site A for the periods of March 2018 and September 2018, it was concluded that the bridge deck surface temperature was not an accurate representation of the effective bridge temperature, which was also supported by literature published by Emerson et al. (1976). Therefore, the purpose of Site B was to obtain continuous measurements of the cross-sectional bridge temperature to determine an effective bridge temperature as documented in Emerson et al. (1976) and discussed in Section 2.3.1. Campbell Scientific Data Loggers (either CR300 or CR800) were used to measure continuous data at Site A and Site B. Site A was setup for all three site investigations (March 2018, September 2018 and March 2019). Site B was setup for the site investigation in March 2019 only.

The moving site setups along the length of the bridge will be known as Site 1 to 5 with Site 1 at the southern end of the bridge and Site 5 at the northern end of the bridge. The purpose of Site 1 to 5 was to obtain change in rail strain and rail slip/creep along the length of the bridge with the aim of determining if rail creep/differential displacements increase linearly across the length of the bridge towards the rail expansion joint or creeps through each rail fastening system evenly. This will inform whether a "breathing length" occurs towards the REJ or if the "breathing length" is limited by the REJ longitudinal restraint.

To achieve this, the moving setups were required at relatively even intervals along the length of the bridge. Site 1 was placed 31 m north of Site A which is on the first panel of the fixed track slab, past the REJ. Site 2 to 5 were then placed at approximately 70 m intervals from Site 1. This setup ensures a relatively even distribution of rail slip/creep and strain measurements along the length of the bridge.

The HBM Quantum X data logger was used to measure the ad-hoc strain and rail slip/creep data at each location. Site 1 to 5 were setup at arbitrary times during the March 2018 and September 2018 testing periods. The moving setups did, however, coincide with the continuous data measurements

at Site A and, therefore, temperature and displacement data could be validated against the continuous data measurements. Figure 3.23 illustrates the positions and period of data logging for the various site investigations.
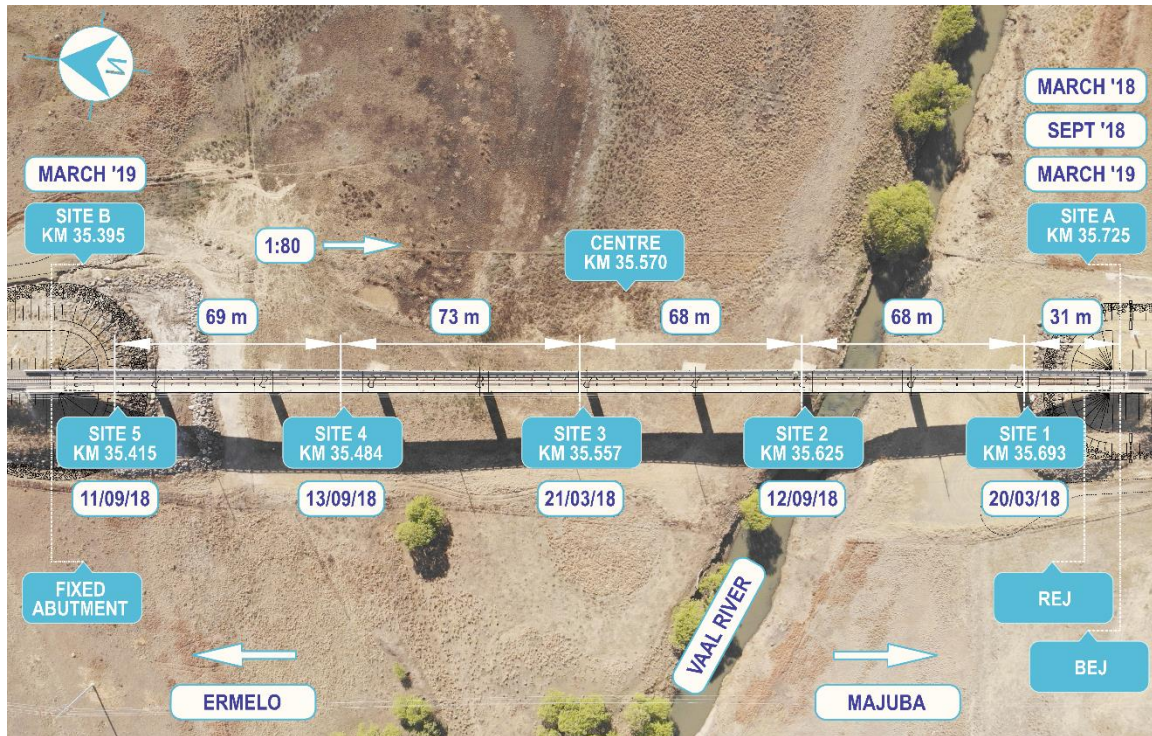
Figure 3.23: Vaal River Bridge Site Setups (March 2018, September 2018, March 2019)

3.6   SITE A – SOUTHERN ABUTMENT (~ KM 37.725)

As discussed in Section 3.5, Site A was located at the southern abutment with temperature and displacement instrumentation at the bridge expansion joint (BEJ) and rail expansion joint (REJ). This section discusses the site setup, testing procedure and typical results for Site A.

3.6.1 Site Setup

Site A was equipped with the following instrumentation:

- 2 no. 100 mm LVDT's to measure bridge displacement on the LHS and RHS of the bridge, next to the parapets.

- 2 no. 150 mm LVDT's to measure rail displacement at the REJ for the LHS and RHS rails.

- 4 no. 5 kΩ thermistors to measure bridge temperature on the LHS and RHS of the bridge, next to the track slab (inner) and LHS and RHS of the bridge next to the parapets (outer).

- 2 no. 5 kΩ thermistors to measure rail temperature for the LHS and RHS rails.

- METER Group ATMOS 41 weather station to measure ambient air temperature, solar radiation and precipitation (March 2018, September 2018).

- Campbell Scientific CR800 data logger (March 2018, September 2018) / Campbell Scientific CR300 data logger (March 2019). The Campbell Scientific data loggers recorded data at a 2-minute frequency.

To ensure stable and accurate displacement readings, the LVDT's were placed in mounting blocks that were designed in CAD and 3D printed specifically for this site investigation.
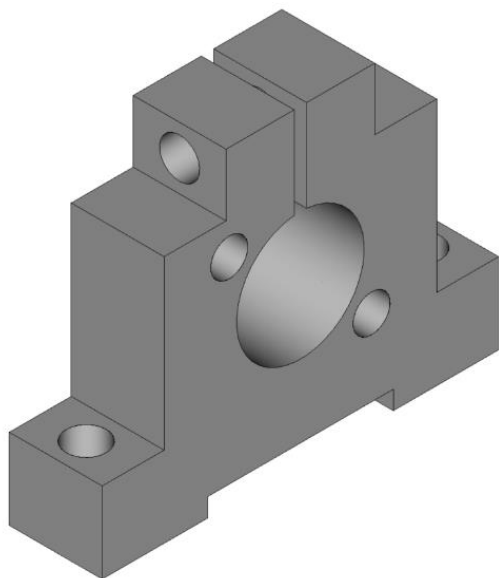
Figure 3.24: CAD Model for LVDT Mounting Blocks

The mounting blocks were fixed to the bridge deck by drilling and inserting concrete plugs/screws and were fixed to the rail web using a strong adhesive known as X60. The LVDT probe for the bridge displacement measurement was placed against a steel angle and bracket system which was fixed to the abutment with X60 adhesive. The LVDT probe for rail displacement was placed against the spliced rail web. The thermistors were placed on the surface of the bridge deck and the web of the rail (track side near the centroid) using thermal paste and duct tape to manage water ingress.
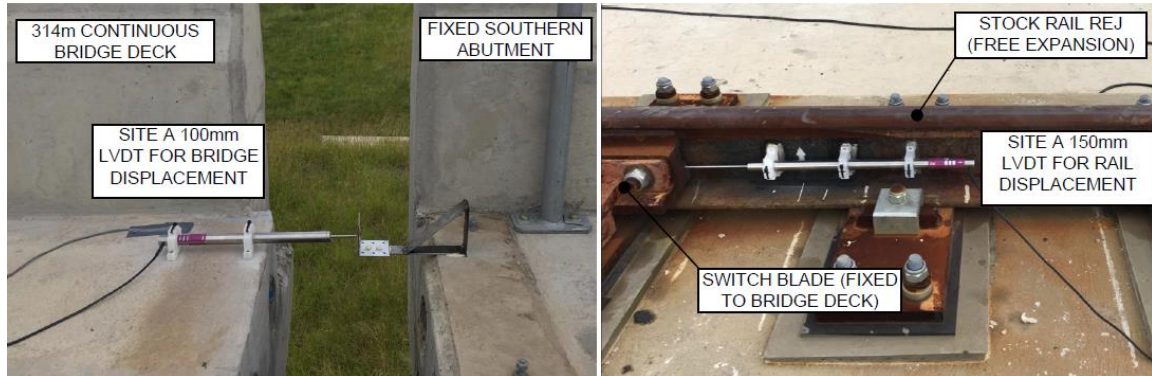
Figure 3.25: Site A LVDT and Thermistor Setup (March 2018, March 2019, September 2019)

The METER Group ATMOS 41 weather station was mounted to the bridge parapet at Site A (March 2019/September 2019) on a steel hollow circular tube, cross brace and hold down straps. It was then connected to the CR800 data logger where cables were secured to the bridge deck.

Figure 3.26: Site A - ATMOS 41 Weather Station (March 2018, September 2018)

3.6.2 Testing Methodology

The purpose of the test setup at Site A was to determine the total bridge and rail displacement (measured by the LVDT's) and correlate the displacement with measured bridge and rail temperature (measured by the thermistors). In addition, the weather station was used to measure the ambient air temperature, solar radiation and precipitation to understand the relationship between ambient air temperature and the rail/bridge material temperature and identify any irregularities in the data due to solar radiation or precipitation. In addition, the bridge and rail displacement readings were taken for both the LHS and RHS with the aim of determining if the position of the sun significantly influences the differential displacement between the LHS and RHS.

By measuring the total bridge and rail displacement individually, differential displacement between the bridge and rail could be determined to confirm and quantify the total rail creep as a function of bridge displacement for the REJ switch blade and rail creep from the conventional ballasted track (south of the abutment) for the REJ stock rail. The temperature and displacement data were used to calibrate the numerical model, further discussed in Section 5.2.
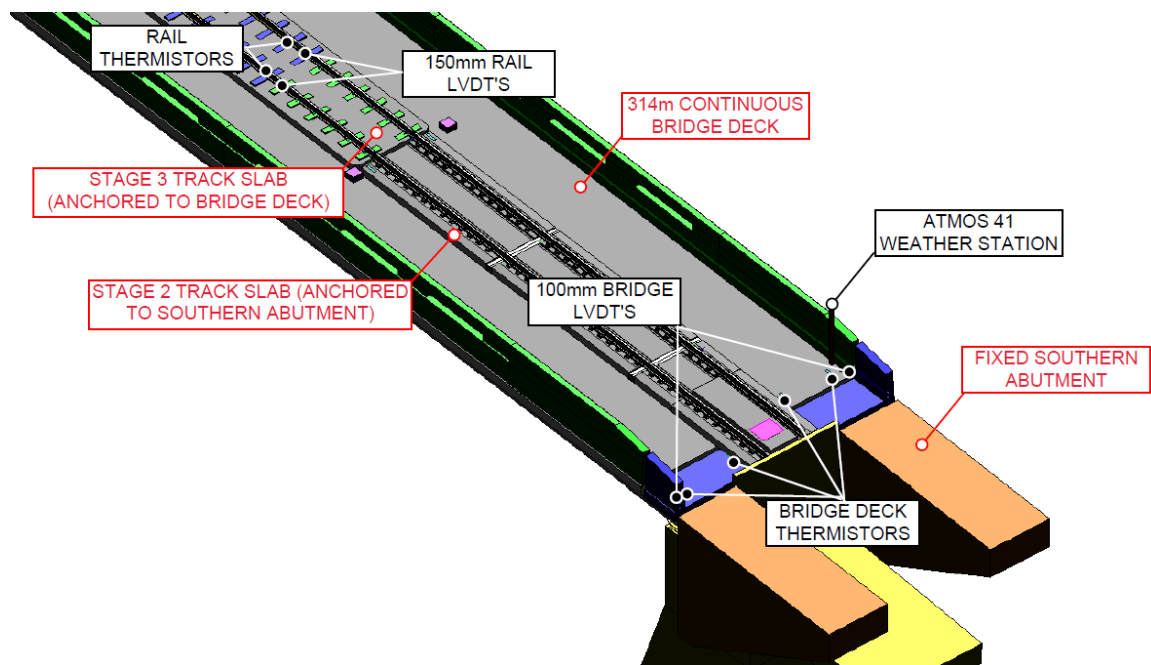
Figure 3.27: Indicative experimental setup for Site A

3.6.3 Bridge Temperature and Displacement Results

Bridge temperature and bridge displacement were measured at Site A over a 67 hour period in March 2018, 52 hour period in September 2018 and 86 hour period in March 2019 as per the setups discussed and illustrated in Section 3.6.1. To analyse the various peaks of the data, the time periods per site visit were further subdivided to capture AM peaks and PM peaks. Based on the data represented in Figure 3.28, a sensible distinction was to define the AM peaks occurring from 22:00 to 10:00 and PM peaks occurring from 10:00 to 22:00. Figure 3.28 illustrates typical results obtained from the LVDT's at the bridge expansion joint and the thermistors on the bridge deck. Results from the other site investigations are presented in Appendix B.

Figure 3.28: Site A - Bridge Temperature and Bridge Displacement in March 2019

Table 3.6 summarises the minimum AM peaks and maximum PM peaks and associated bridge displacement for the three site investigations.

Table 3.6: Site A - Bridge Temperature and Bridge Displacement

Period	Bridge Displacement (mm)	Minimum Temperature (°C)	Maximum Temperature (°C)
March 2018 - Day 1	7.5	16.5	26.1
March 2018 - Day 2	13.3	15.6	29.6
September 2018 - Day 1	16.8	6.1	27.6

September 2018 - Day 2	16.0	8.3	29.9
March 2019 - Day 1	19.4	16.1	43.2
March 2019 - Day 2	17.8	17.8	43.2
March 2019 - Day 3	11.4	19.4	40.4

3.6.4 Rail Temperature and Displacement Results

Rail temperature and rail displacement were measured at Site A over a 67 hour period in March 2018, 52 hour period in September 2018 and 86 hour period in March 2019 as per the setup discussed and illustrated in Section 3.6.1. To analyse the various peaks of the data, the time periods per site visit were further subdivided to capture AM peaks and PM peaks. Based on the data represented in Figure 3.29, a sensible distinction was to define the AM peaks occurring from 22:00 to 10:00 and PM peaks occurring from 10:00 to 22:00. Figure 3.29 illustrates typical results obtained from the LVDT's at the rail expansion joint and the thermistors on the rail web. Results from the other site investigations are presented in Appendix B.
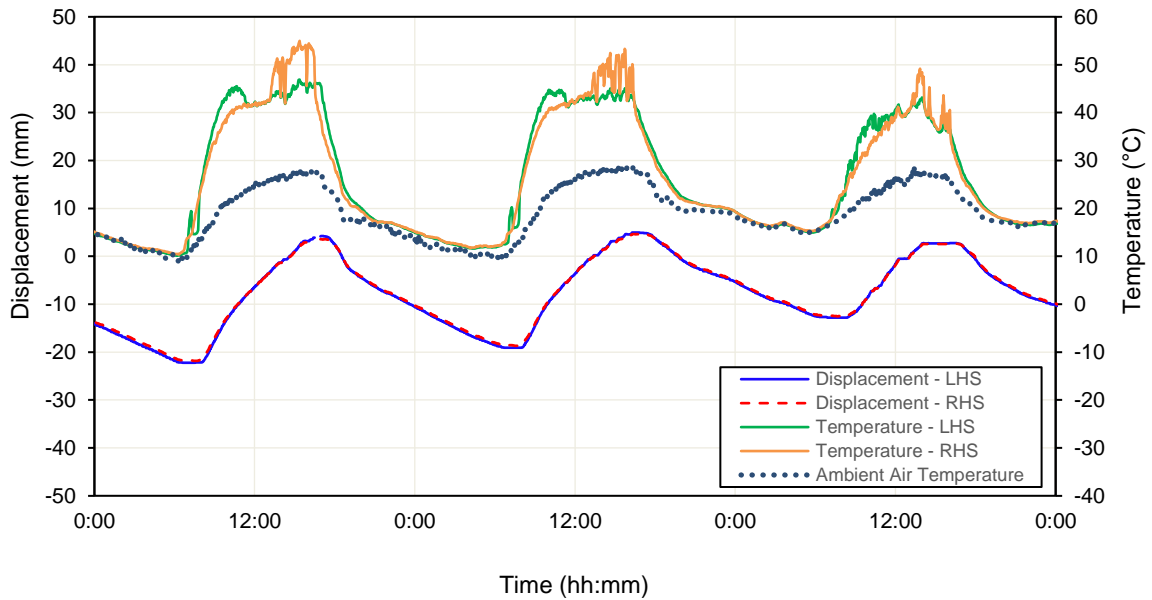
Figure 3.29: Site A - Rail Temperature and Rail Displacement in March 2019

Table 3.7 summarises the minimum AM peaks and maximum PM peaks and associated rail displacement for the three site investigations.

Table 3.7: Site A - Rail Temperature and Rail Displacement

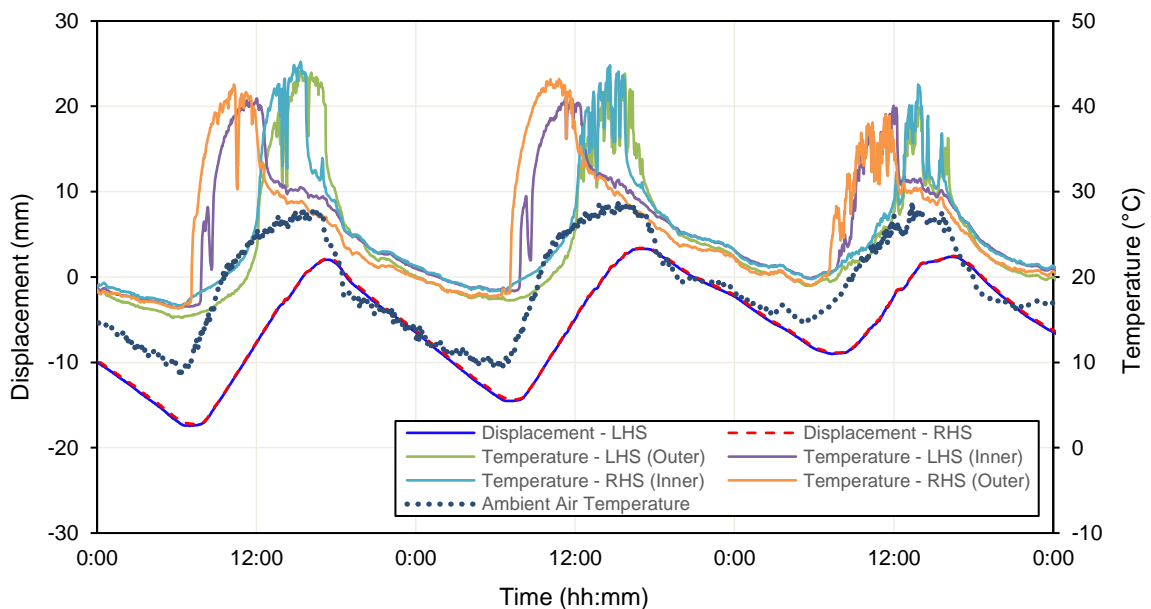| Period	Bridge Displacement (mm)	Minimum Temperature (°C)	Maximum Temperature (°C)
March 2018 - Day 1	11.2	13.5	39.6
March 2018 - Day 2	16.8	12.8	40.7
September 2018 - Day 1	20.4	0.8	35.5
September 2018 - Day 2	20.2	2.1	39.0
March 2019 - Day 1	25.9	10.3	50.9
March 2019 - Day 2	23.7	11.7	49.2
March 2019 - Day 3	15.4	15.1	46.2

3.7 SITE B – NORTHERN ABUTMENT (~ KM 35.395)

As discussed in Section 3.5, Site B is located at the northern abutment with temperature instrumentation placed throughout the cross-section of the bridge deck. This section discusses the site setup, testing procedure and typical results for Site B.

3.7.1 Site Setup

Site B was equipped with the following instrumentation:

- 20 no. 5 kΩ thermistors through the bridge deck cross-section, dividing the cross-section into 20 isotherms, to determine an effective bridge temperature.

- METER Group ATMOS 41 weather station to measure ambient air temperature, solar radiation and precipitation.

- Campbell Scientific CR800 data logger. The Campbell Scientific data logger recorded data at a 2 minute frequency.

The thermistors were distributed evenly throughout the cross-section of the bridge deck to best represent the effective bridge temperature. Similar to Site A, thermal paste and duct tape was used to manage water ingress.

Figure 3.30: Thermistors and Weather Station at Site B (external)
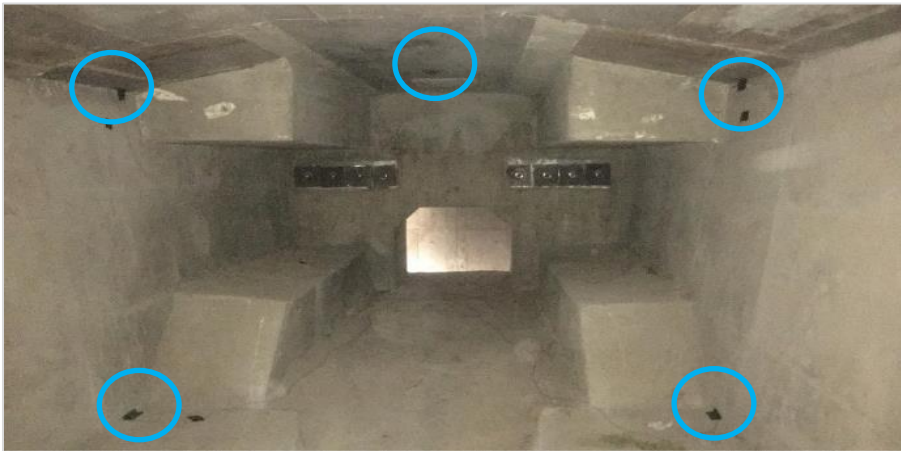
Figure 3.31: Thermistors at Site B (internal)

The METER Group ATMOS 41 weather station was mounted to the bridge parapet at Site B (March 2019) on a steel hollow circular tube, cross brace and hold down straps. It was then connected to the CR800 data logger where cables were secured to the bridge deck.

From the total 20 no. thermistors, 6 no. thermistors were placed on the bridge deck, 4 no. thermistors on the LHS of the bridge, 4 no. thermistors on the RHS of the bridge, 1 no. thermistor underneath the bridge and 5 no. thermistors inside the bridge, as illustrated in Figure 3.32.
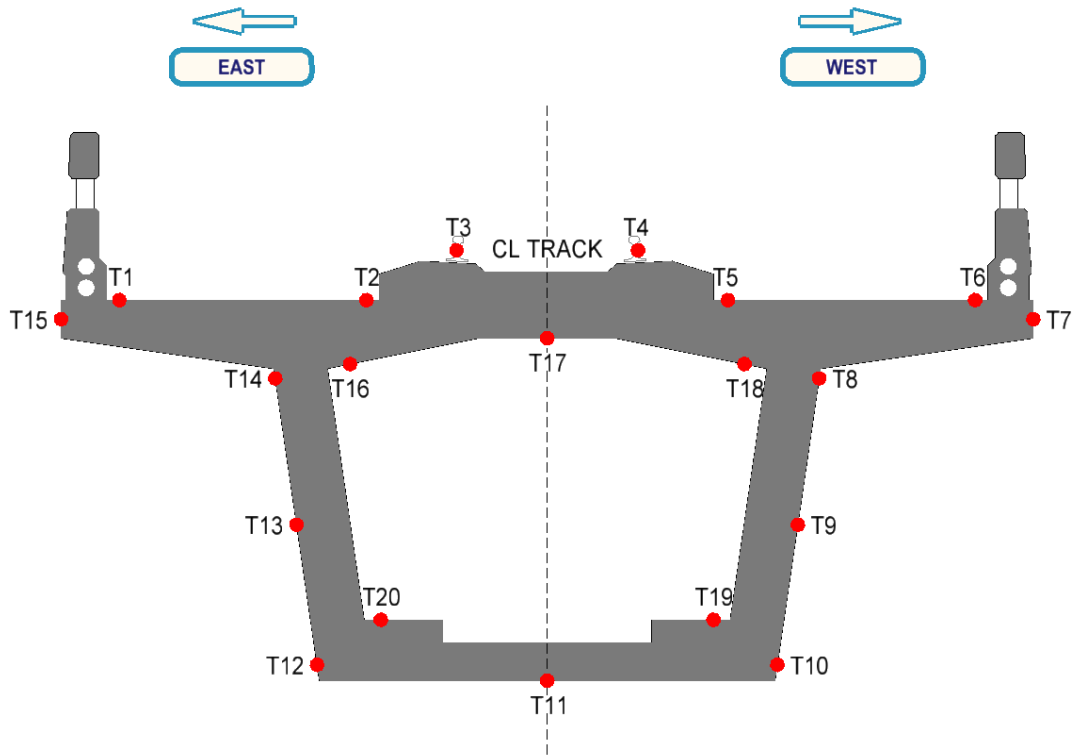
Figure 3.32: Position of Thermistors through bridge cross-section

3.7.2 Testing Methodology

The purpose of the test setup at Site B was to determine the effective material temperature through the cross-sectional area of the bridge. The bridge temperatures, recorded by the 20 no. thermistors, were continuously monitored and logged over a period 84 hours.

The effective temperature of a bridge is defined as the temperature which governs the longitudinal movement and can be derived from the sum of the products of areas between isotherms and their mean temperatures, divided by the total area of the cross-section of the bridge deck. In practice, it is difficult to locate isotherms but an approximation can be made by dividing the cross-section into temperature isotherm areas whereas the mean temperature per area can be determined by experimental measurement (Emerson et al., 1976).

For the determination of the effective bridge temperature, the bridge cross-section was divided into isotherms for each individual thermistor. The Thiessen Polygon Method was used to divide the cross-section. This method defines the zone of influence of each thermistor by drawing lines between pairs of thermistors and then bisecting the lines with perpendiculars. For the purpose of

determining the effective bridge temperature, it is assumed that the experimental measurement of the thermistor represents the temperature for a specific isotherm area, as discussed in Emerson et al. (1976).

Once an area is defined for each thermistor, the effective bridge temperature can be calculated by the sum of the products of areas between isotherms and their mean temperatures, divided by the total area of the cross-section of the bridge deck. Figure 3.33 illustrates the results of the thermistor isotherms as determined by the Thiessen Polygon Method.
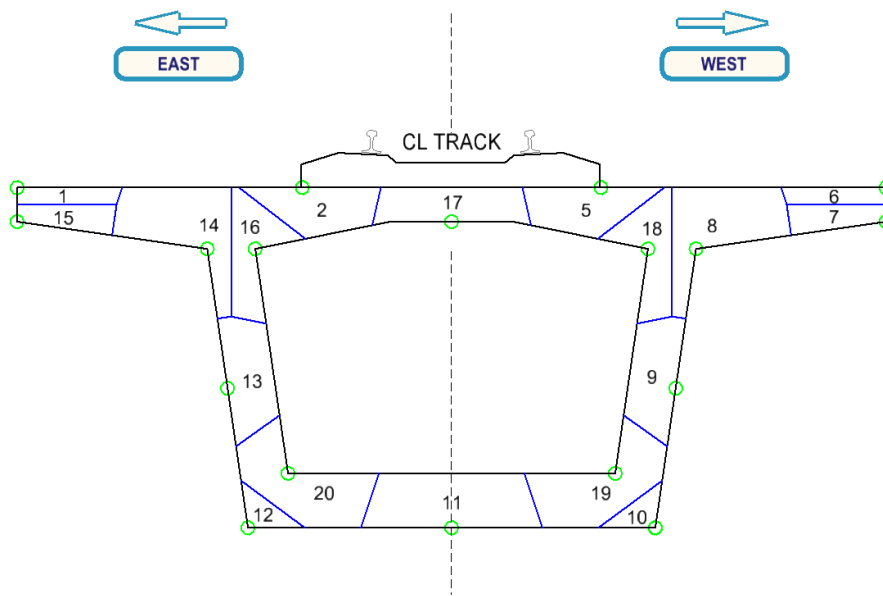
Figure 3.33: Thermistor isotherms determined by the Thiessen Polygon Method

3.7.3 Site B – March 2019

Temperature through the bridge deck cross-section was measured at Site B over an 84 hour period in March 2019 as per the setup discussed and illustrated in Section 3.7.1. The numeric label for each thermistor corresponds with the position of thermistor through the bridge deck cross-section as illustrated in Figure 3.32.

To analyse the temperature measurements of each thermistor, the thermistors were divided into four different areas, namely: (1) bridge top and bottom, (2) bridge left, (3) bridge right and (4) bridge inside. The individual areas are presented below and further discussed and analysed in Chapter 4.

The first areas analysed in the cross-section were the top and bottom of the bridge. The thermistors representing the top of the bridge were Thermistor 1, 2, 5 and 6 whereas the thermistor representing the bottom of the bridge deck was Thermistor 11, as illustrated in Figure 3.32. The temperature results of these thermistors are represented in Figure 3.34.
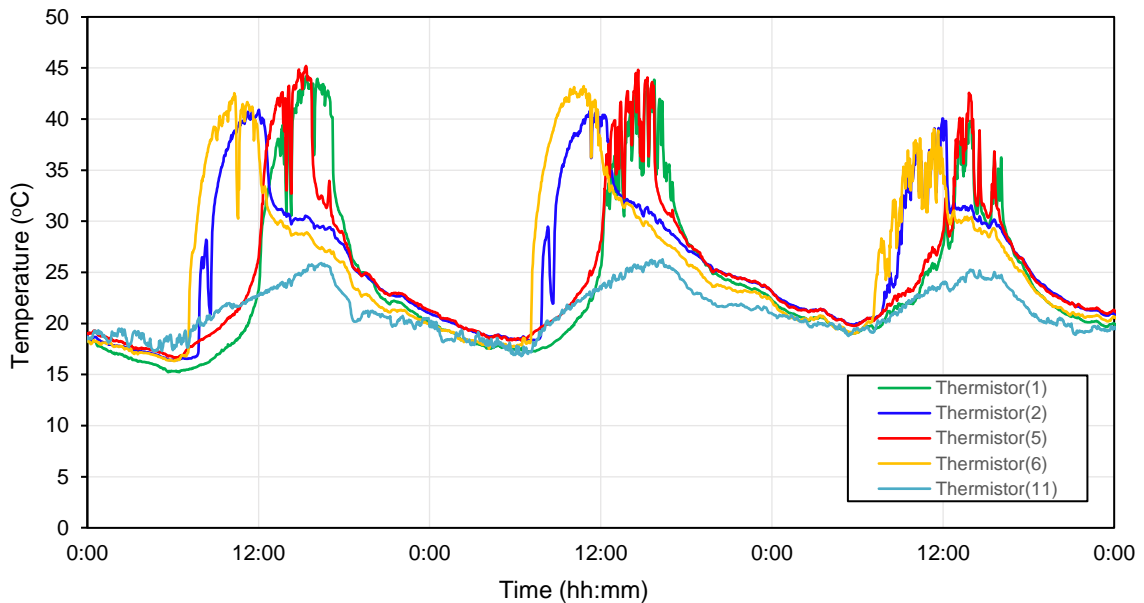
Figure 3.34: Site B – Bridge Temperature (Top and Bottom) in March 2019

The results of the thermistors located at the top of the bridge are similar to the results presented in Section 3.6 for Site A. It can be seen from Figure 3.34 that the time at which the minimum and maximum temperatures occurred varies significantly across the width of the bridge deck surface. During the day, Thermistor 6 (RHS Outer) and Thermistor 2 (LHS Inner) recorded maximum temperatures before midday whereas the Thermistor 5 (RHS Inner) and Thermistor 1 (LHS Outer) recorded maximum temperatures after midday. The large distribution of maximum bridge deck surface temperatures during the day can be explained by the position of the bridge thermistors in relation to the sun and is further discussed in Chapter 4.

Over the 84 hour period in March 2019, the top of bridge temperature varied significantly with a minimum and maximum temperature of 15.2 °C and 45.2 °C respectively. In contrast, the bottom of bridge temperature, represented by Thermistor 11, had less variation in temperature with a minimum and maximum temperature of 16.8 °C and 26.3 °C respectively and is attributed to its lack of exposure to solar radiation.

The second area analysed was the LHS of the bridge deck. The thermistors representing the LHS of the bridge were Thermistor 12, 13, 14 and 15 as illustrated in Figure 3.32. The temperature results of these thermistors are represented in Figure 3.35.
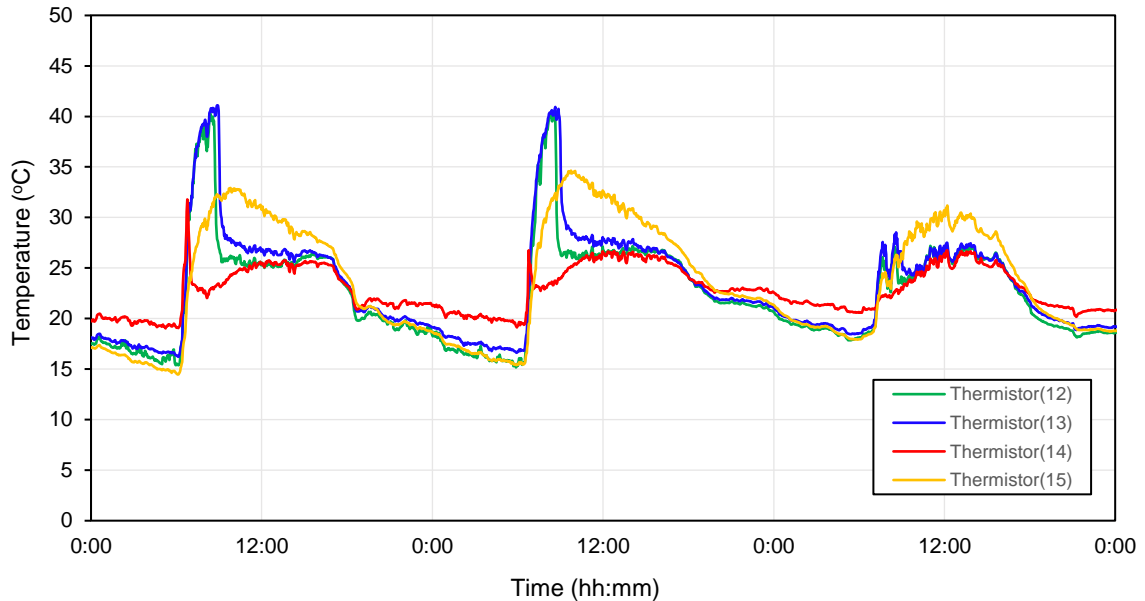
Figure 3.35: Site B – Bridge Temperature (LHS) in March 2019

From Figure 3.35, it can be seen that the temperature for Thermistor 12 and 13 increased rapidly until approximately mid morning before settling to a temperature similar to the other 2 thermistors at midday. Thermistor 14 also experienced a rapid increase in temperature in the morning, albeit for a much shorter duration. Conversely, Thermistor 15 experienced a gradual increase in temperature towards midday.

The varying temperature distributions between the various thermistors on the same side of the bridge can be explained by literature published by Dickinson (2003) that states that the angle between the direction of the sun and a specific surface is a key parameter in determining the magnitude of solar radiation on a given surface. If a surface is directly perpendicular to the sun, it receives a maximum amount of solar radiation. If the surface is angled to the sun, the solar radiation is reduced by the cosine angle between the direction of the sun and the perpendicular line the sun would take for maximum receipt of solar radiation.

In further investing the positions of the thermistors and referring to Figure 3.32, it can be seen that Thermistors 12, 13 and 14 would receive maximum amount of solar radiation as the sun starts rising, however, as the day progresses, the perpendicular angle between the sun and the LHS vertical face of the bridge decreases. As the day approaches noon, the bridge deck surface is perpendicular to the sun. Because the bridge deck is closer to the sun at noon in comparison to the morning, maximum temperatures are slightly higher at noon, as can be seen when comparing Figure 3.34 and Figure 3.35.

Figure 3.36 illustrates the effect of solar radiation on the bridge thermistor values. The temperature readings from Thermistor 13 (LHS of bridge in centre) are plotted for two separate days over a 2 hour period when the sun is rising (06:00 am – 08:00 am). On Day 1, solar radiaition increased rapidly and results in a rapid increase of Thermistor 13 temperature readings whereas on Day 3, solar radiation did not increase substantially for the first hour resulting in reduced temperature readings for Thermistor 13.
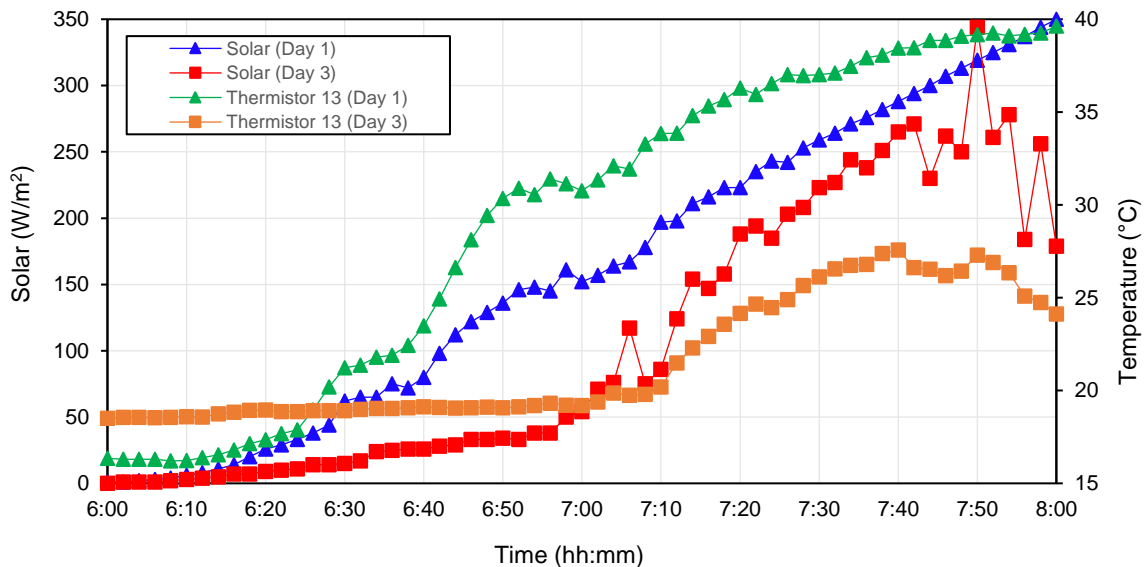
Figure 3.36: Effect of solar radiation on bridge temperature results

On the RHS of the bridge, Thermistor 7, which is closer to the bridge deck surface, is exposed to direct solar radiation whereas Thermistor 8, 9 and 10 are shaded by the box girder cantilever wings. This results in a significant difference in maximum temperature between Thermisor 7 and Thermistors 8, 9 and 10.
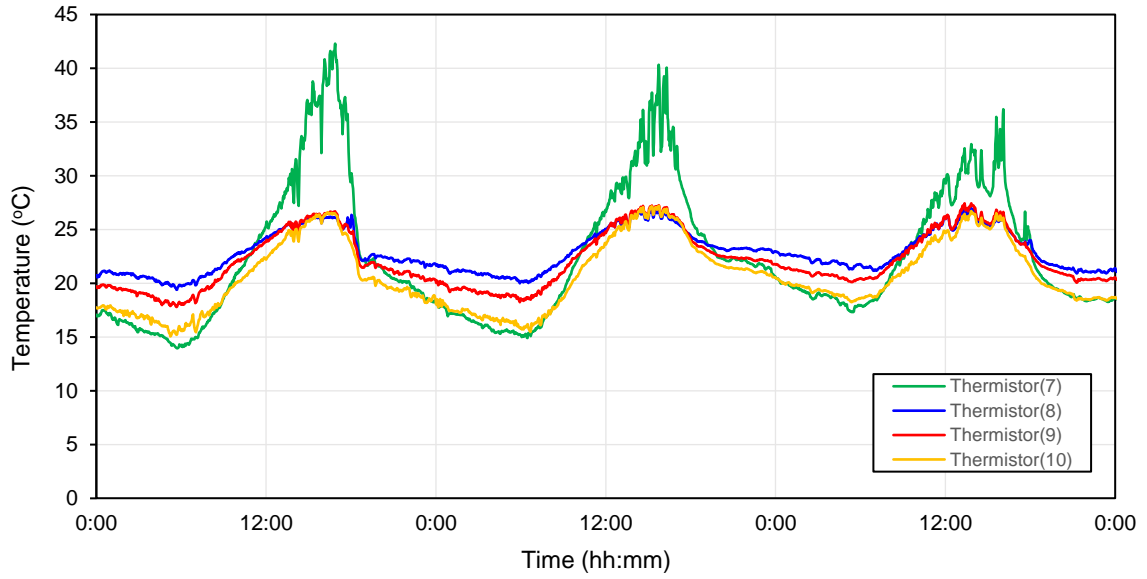
Figure 3.37: Site B – Bridge Temperature (LHS) in March 2019

Inside the box girder, where thermistors were not exposed to solar radiation, the temperature remained relatively constant over the 84 hour period and only varied by approximately 5 °C.
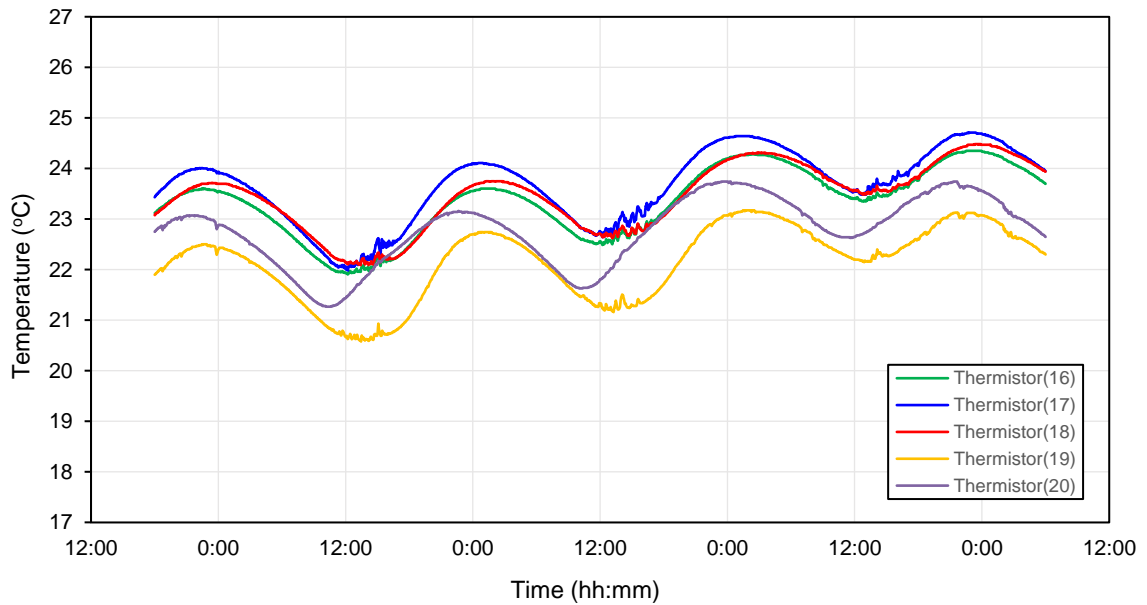
Figure 3.38: Site B – Bridge Temperature (Inside) in March 2019

The significant temperature variation between the 20 thermistors installed at Site B is attributed to a variety of factors and supports literature published by Krkoška & Moravčik (2015) which states

that temperature variations in a structure are a function of solar radiation, ambient air temperature, humidity and wind speed. Furthermore, temperature variations are affected by orientation of the structure, material of the structure, deck surface finishing layer, structure dimensions and cross-section geometry.

From the results presented in Section 3.7.3, it is evident that the bridge temperature varies significantly through the cross-section and limited material field measurements will not provide an accurate representation of the bridge temperature. Instead, an effective bridge temperature must be calculated from multiple temperature measurements distributed through the bridge cross-section.

The determination and analysis of the effective bridge temperature for this site is further discussed in Chapter 4.

3.8   SITE 1 TO 5 – MOVING SETUPS

This section discusses the site setup, testing procedure and results of Site 1 to 5.

3.8.1 Site Setup

Site 1 to 5 were equipped with the following instrumentation:

- 2 no. 10 mm LVDT's to measure rail displacement relative to the bridge deck (rail creep) on the LHS and RHS rails.

- 2 no. strain gauges to measure longitudinal strain in the LHS and RHS rail.

- 2 no. 5 kΩ thermistors to measure rail temperature for the LHS and RHS rails.

- HBM QuantumX data logger.

To ensure stable and accurate displacement readings, the LVDT's were placed in clamps that were fixed to the rail flange using X60 adhesive. The LVDT probe was placed against the PY track slab surface.

Before placing the longitudinal strain gauges, the rails were grinded to remove rust from the surface and various grades of sandpaper were applied to the rail web and bridge deck. Before applying X60 adhesive to the surfaces and strain gauges, the surfaces were cleaned with acetone to remove all fine particles.

The thermistors were placed on the surface of the bridge deck and the web of the rail (track side near the centroid) using thermal paste and duct tape to manage water ingress.
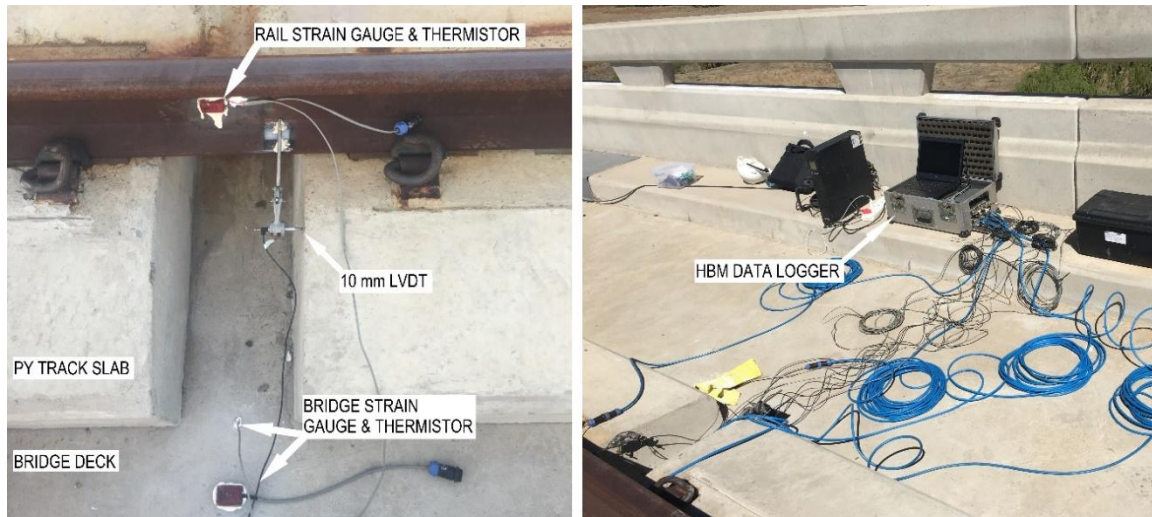
Figure 3.39: Site 1 to 5 Moving Site Setups

3.8.2 Testing Methodology

The purpose of Site 1 to 5 was to obtain rail strain and rail slip/creep along the length of the bridge with the aim of determining and quantifying the rail creep/differential profile along the length of the bridge towards the REJ.

As the switch blade was fixed to the bridge Slab Track by means of multiple high restraint fasteners, displacement of the switch blade was expected to be similar to the displacement of the bridge with the exception of minor creep through the fasteners and could be confirmed by the differential displacement measurements between the rail and Slab Track from the Site 1 to 5 moving setups.

The stock rail was expected to displace significantly more than the switch blade as it was fixed to the sliding Stage 2 PY Track Slab and was only connected by means of low restraint fasteners on the Stage 3 Flat Track Slab. As the total rail expansion at the REJ was measured at Site A at the same time the Site 1 to 5 measurements were taken, a distinction could be made between the displacement due to creep of the rail fixed on the bridge and the displacement due to the breathing length of the rail fixed on the rail embankment.

In addition to the displacement measurements obtained from the LVDT's, strain gauges were installed on the rail to understand the longitudinal stress profile along the length of the bridge.

3.8.3 Site 1 to 5 Typical Data

Figure 3.40 and Figure 3.41 represents typical rail slip/creep and rail temperature as well as strain gauge results for the rail and bridge respectively.

Site 1, represented below as an example, which included rail temperature, rail creep and change in rail strain measurements, was setup from 8:30 am to 12:16 pm on the 20th of March 2018. According to the continuous rail temperature data, recorded at Site A, the maximum rail temperature on this day occurred at 11:42 am, therefore, maximum rail temperature was achieved for the Site 1 setup. Similar results are presented in Appendix C for Site 2 to 5.
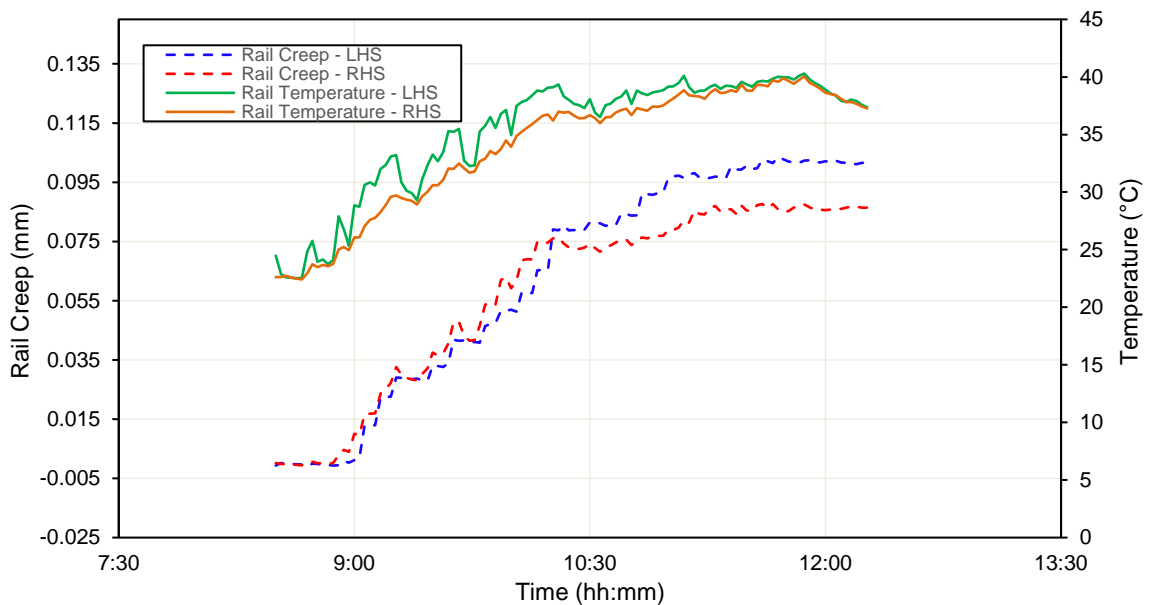
Figure 3.40: Site 1 - Rail Temperature and Rail Creep at km 35.693

Figure 3.41 represents the strain gauge results for the rail and bridge at Site 1. During this period, the LHS and RHS rail strain increased by 111 µm/m and 106 µm/m respectively whereas the bridge strain only increased by 17 µm/m. The change in rail stress was calculated by assuming an Elastic Modulus of 210 GPa for the rail section. The increase in longitudinal rail stress at Site 1 was 23.31 MPa for the LHS rail and 22.26 MPa for the RHS rail.

During this period, the LHS and RHS rail temperature increased by 17.8 °C and 17.6 °C respectively. The rail slip results indicate a very low amount of creep for both the LHS and RHS rail of 0.10 mm and 0.09 mm respectively.
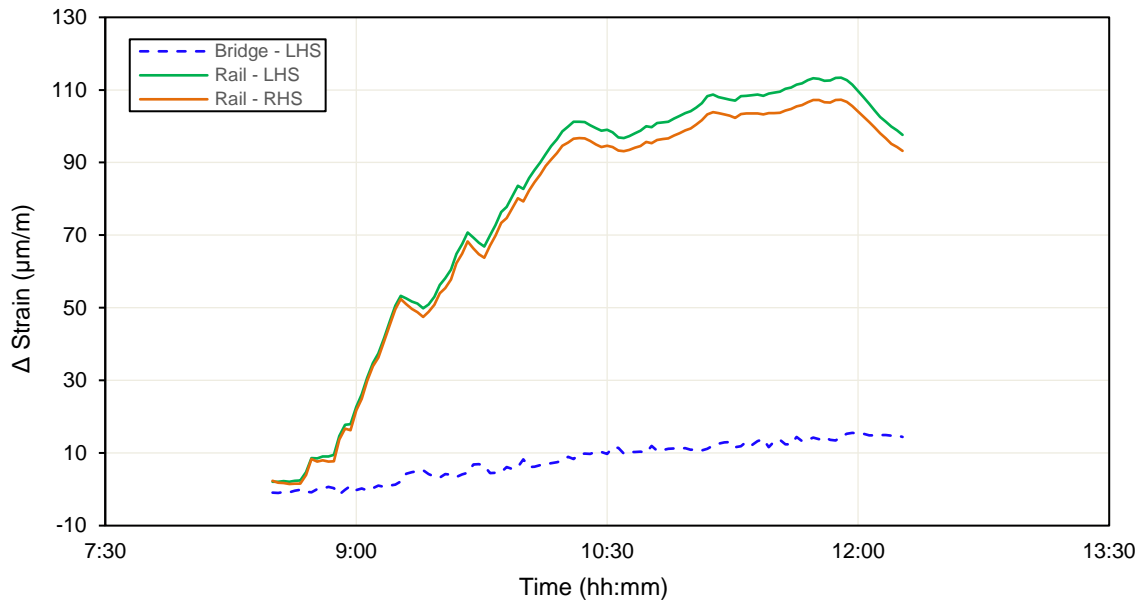
Figure 3.41: Site 1 – Rail and Bridge Strain at km 35.693

Results from the other site investigations are presented in Appendix C with minimum and maximum data summarised in Table 3.8.

Table 3.8: Site 1 to 5 - Rail Temperature and Rail Displacement

Period	Δ Rail Strain (µm/m)	Δ Rail Temperature (°C)	Rail Creep (mm)
Site 1 - LHS	111	17.8	0.10
Site 1 - RHS	106	17.6	0.09
Site 2 -LHS	214	14.7	0.09
Site 2 -RHS	219	23.2	0.07
Site 3 - LHS	118	18.6	0.05
Site 3 - RHS	124	20.2	0.08
Site 4 - LHS	187	16.15	0.04
Site 4 - RHS	198	33.52	0.04
Site 5 - LHS	110	13.4	0.06
Site 5 - RHS	67	19.0	0.06

3.9   DISCUSSION

The purpose of the site investigation undertaken at the Majuba Rail Bridge was to obtain data of parameters that influence the track-bridge interaction phenomenon. These data sets included bridge and rail temperature, bridge and rail displacement, ambient air temperature and rail slip/creep. In addition, this chapter provided a site description with detailed explanation of the various components and discussed the various data logging equipment and testing methodology. The data obtained during the site investigation include temperature measurements through the cross-section of the bridge which enables a comparison with the Emerson et al. (1976) method to calculate effective bridge temperature. In addition, total bridge and rail displacement data enables a differentiation between rail displacement due to the bridge and rail displacement due to the rail "breathing length". Rail creep measurements, from Site 1 to 5, further enables the determination of rail "breathing length" between the bridge rail section and embankment rail section. Finally, rail stress data provides an additional parameter to aid in the calibration of a numerical model.

4 ANALYSIS OF SITE INVESTIGATION DATA

Chapter 4 provides an interpretation of the results obtained during the various site investigations as described in Chapter 3. The purpose of this chapter is to critically analyse the site investigation data in accordance with the objectives of this study, discussed in Section 1.2. This chapter is broadly subdivided into five main sections where the theme of each section aims to interpret data, form a conclusion and serve as input into the calibration of a numerical model in Chapter 5. The data analysis in this chapter aims to:

- Evaluate the accuracy of the proposed method by Emerson et al. (1976) used to determine an effective bridge temperature;

- Quantify the total bridge and rail displacement as a function of effective bridge temperature and rail temperature, to serve as input into the calibration of a numerical model;

- Quantify the amount of rail creep at the REJ due to (1) high fixity switch blade and (2) low restraint stock rail, to serve as input into the calibration of a numerical model;

- Analyse the track longitudinal stiffness characteristics of the fastening system and compare the longitudinal stiffness profile with recommendations in UIC Code 774-3R (2001);

- Confirm if the additional rail compressive stress is constant and linear on the bridge deck when an REJ is installed, similar to literature discussed by Mirković et al. (2017).

4.1 BRIDGE TEMPERATURE/DISPLACEMENT & EFFECTIVE BRIDGE TEMPERATURE

4.1.1 Bridge Temperature/Displacement

Bridge temperature and bridge displacement were measured over a total period of approximately 205 hours. Bridge temperature results indicate that the maximum temperatures across the width of the bridge deck surface occurred at ad-hoc times during the day.

Although the minimum and maximum bridge temperature varied across the width of the bridge deck surface, the differential displacement between the LHS and RHS of the bridge varied by a maximum of 0.23 mm only. The 0.23 mm differential displacement confirms that the bridge deck expands uniformly with minimal displacement difference between the LHS and RHS of the bridge as a result of the position of the sun and solar radiation effects.

It can be seen from Figure 4.1 that the time at which the minimum and maximum temperatures occurred varies significantly across the width of the bridge deck surface. During the day, the RHS (Outer) and LHS (Inner) thermistors recorded maximum temperatures before midday whereas the RHS (Inner) and LHS (Outer) recorded maximum temperatures after midday. In addition, the maximum bridge deck surface temperatures did not correlate well with the maximum bridge displacements recorded by the LVDT's. The large distribution of maximum bridge deck surface temperatures during the day can be explained by the position of the bridge thermistors in relation to the sun.
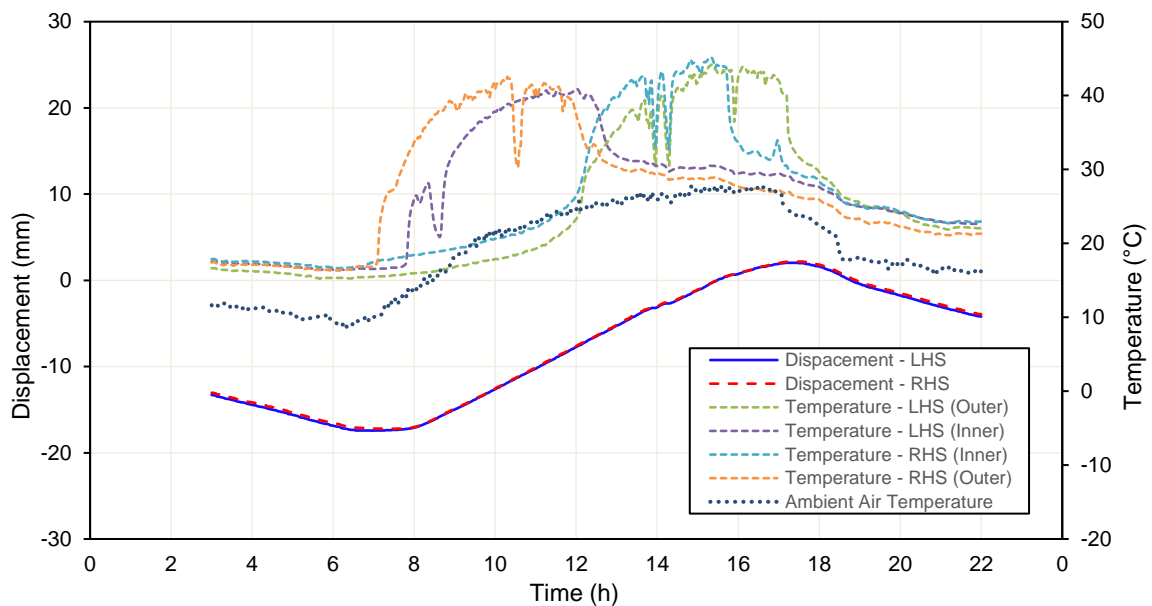
Figure 4.1: Site A - Bridge Temperature and Bridge Displacement for a 19 hour period

It can be seen from Figure 4.1 that the minimum temperature remains relatively constant during the night which further supports the effects of solar radiation on the bridge deck surface.

With the large distribution of maximum bridge deck surface temperatures, there is no correlation between the occurrence of maximum bridge deck surface temperature and maximum bridge displacement. Figure 4.2 provides a summary of the time at which the various maximum bridge deck surface temperatures were recorded and the time at which the maximum bridge displacement was recorded.
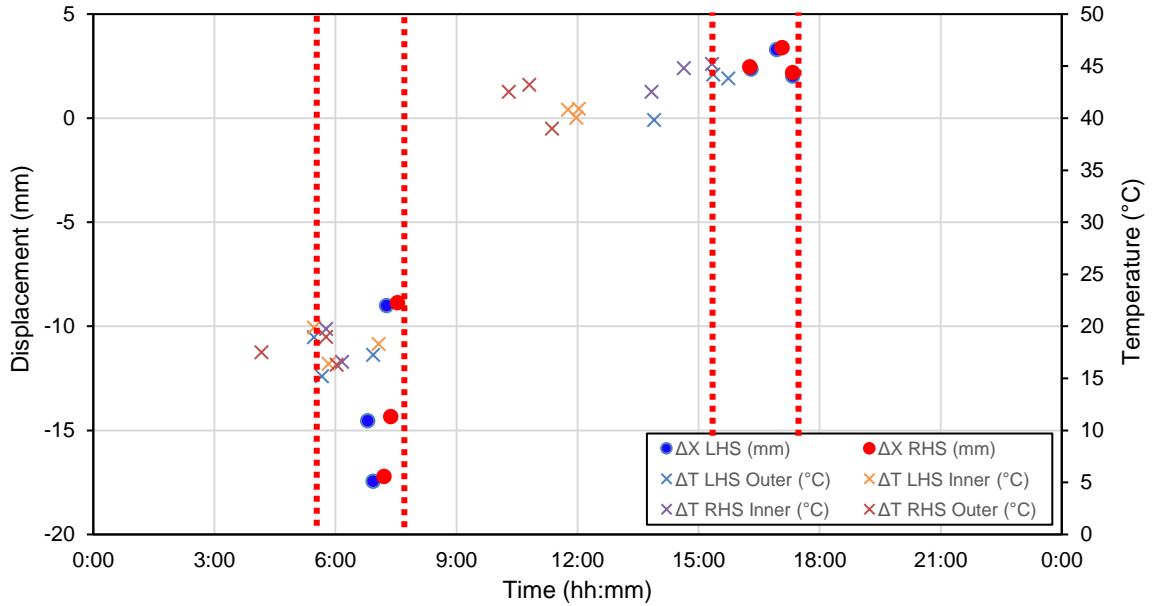
Figure 4.2: Comparison between min. & max. displacement as a function of time

It can be seen from Figure 4.2 that the minimum and maximum LHS and RHS bridge displacements, measured by the LVDT's, occur at similar times irrespective of solar radiation. The AM Peak (minimum displacement) corresponds closely with the minimum temperatures and generally occur within a 2 hour period between 5:30 am and 7:30 am. The PM Peak (maximum displacement), however, varies significantly during the day with a lag between maximum temperature and maximum displacement ranging from 2 to 6 hours.

Due to the significant lag between maximum displacement and maximum temperature, it can be concluded that an average bridge deck surface temperature for the four thermistors does not correlate well with the maximum bridge displacement, as illustrated in Figure 4.3.

From Figure 4.3, it can be seen that the minimum displacement and minimum average bridge deck temperature occur at similar times, however, there is still a lag between the maximum displacement and maximum average bridge deck temperature of approximately 2 hours.
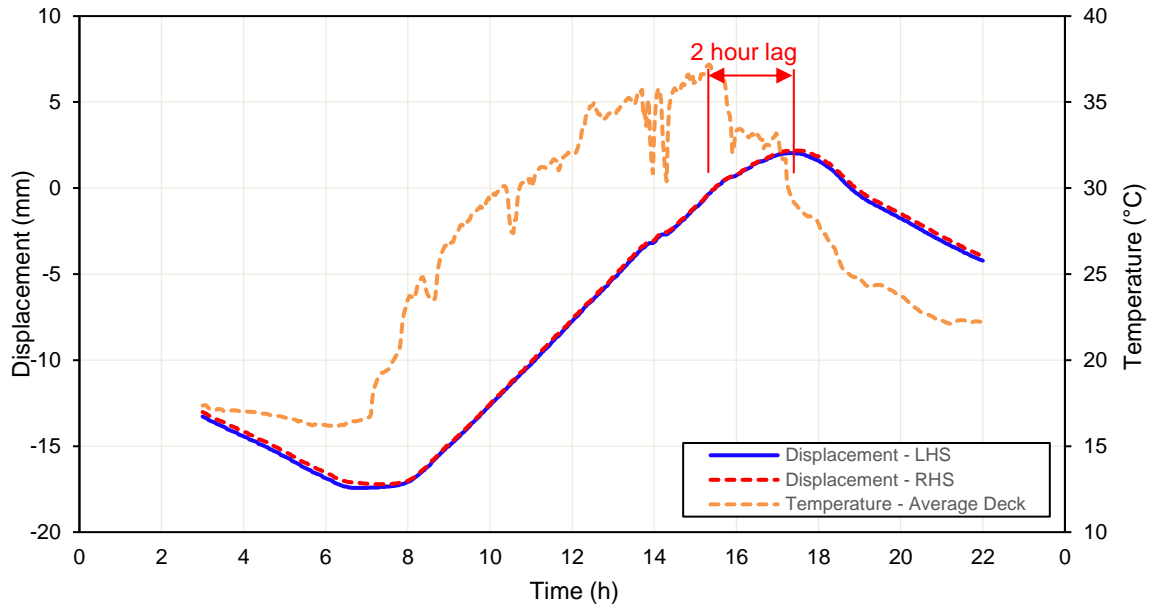
Figure 4.3: Site A – Average Bridge Temperature and Bridge Displacement

From the data analysis of the bridge temperature and displacement results, it can be concluded that the individual or average bridge deck temperature is not an accurate representation of the total bridge temperature due to the effect of solar radiation on the bridge deck. Although the bridge surface (top and sides) experience large temperature exposure as a result of direct sunlight, the temperature throughout the rest of the bridge cross-section will experience significantly less temperature exposure as uniform bridge temperature is a function of radiation, convection and conduction heat flow (Roeder, 2002). This supports a notion that an effective bridge temperature cannot be limited to a few ad-hoc temperature readings. Instead, continuous material temperature monitoring is required throughout the cross-section of the bridge. The concept of an effective bridge temperature is supported by literature published by Emerson et al. (1976).

4.1.2 Effective Bridge Temperature

The effective temperature of a bridge is defined as the temperature which governs the longitudinal movement and can be derived from the sum of the products of areas between isotherms and their mean temperatures, divided by the total area of the cross-section of the bridge deck. In practice, it is difficult to locate isotherms but an approximation can be made by dividing the cross-sections in temperature isotherms whereas the mean temperature per area can be determined by experimental measurement (Emerson et al., 1976).

The equation for determining effective bridge temperature is derived by considering two adjacent bridge sections of unit length. One section being concrete and the other steel. The derivation for the effective bridge temperature is discussed in Appendix A.

For the determination of the effective bridge temperature, the bridge cross-section was divided into isotherms for each individual thermistor. The Thiessen Polygon Method was used to divide the cross-section. This method defines the zone of influence of each thermistor by drawing lines between pairs of thermistors, bisecting the lines with perpendiculars. For the purpose of determining the effective bridge temperature, it is assumed that the experimental measurement of the thermistor represents the temperature for a specific isotherm area, as discussed in Emerson et al. (1976).

Figure 4.4 illustrates the result of the thermistor isotherms as determined by the Thiessen Polygon Method.
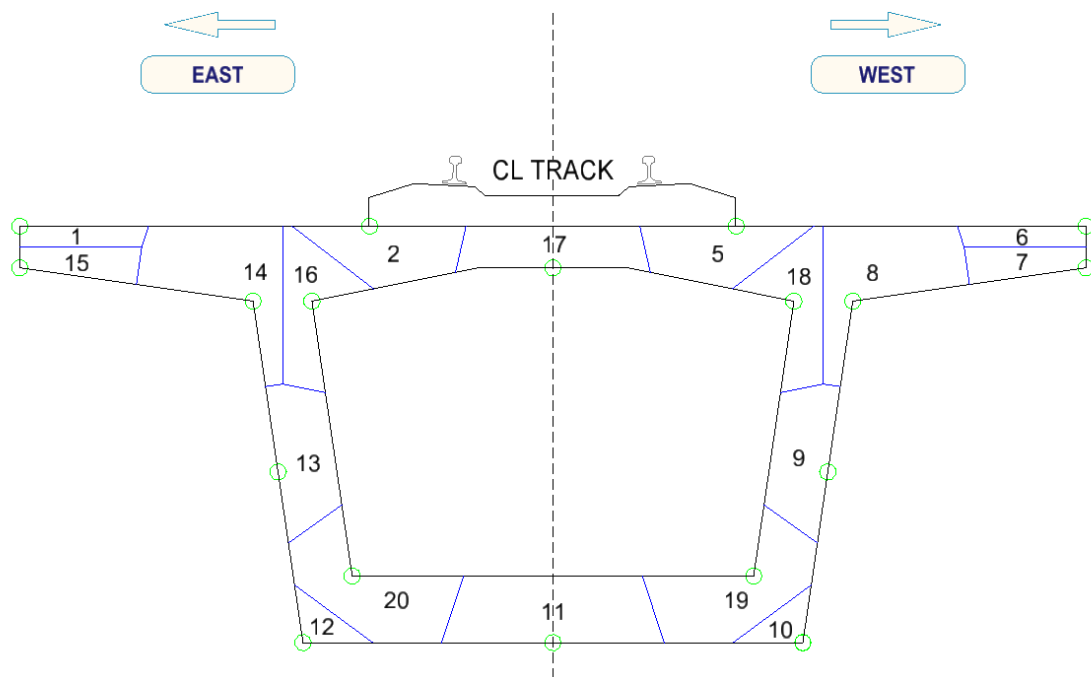
Figure 4.4: Thermistor isotherms determined by the Thiessen Polygon Method

Once an area is defined for each thermistor, the effective bridge temperature can be calculated by the sum of the products of areas between isotherms and their mean temperatures, divided by the

total area of the cross-section of the bridge deck. The individual isotherm areas were measured in CAD Software (MicroStation).

An example of the calculated effective temperature over an 18 hour period is illustrated in Figure 4.5. The calculated effective temperature is plotted with the average temperatures of the individual isotherms for comparison. It can be seen from Figure 4.5 that the distribution of the calculated effective temperature varies significantly from the individual isotherms, supporting the theory that multiple temperature readings through a bridge cross-section are required to calculate the resultant bridge displacement.
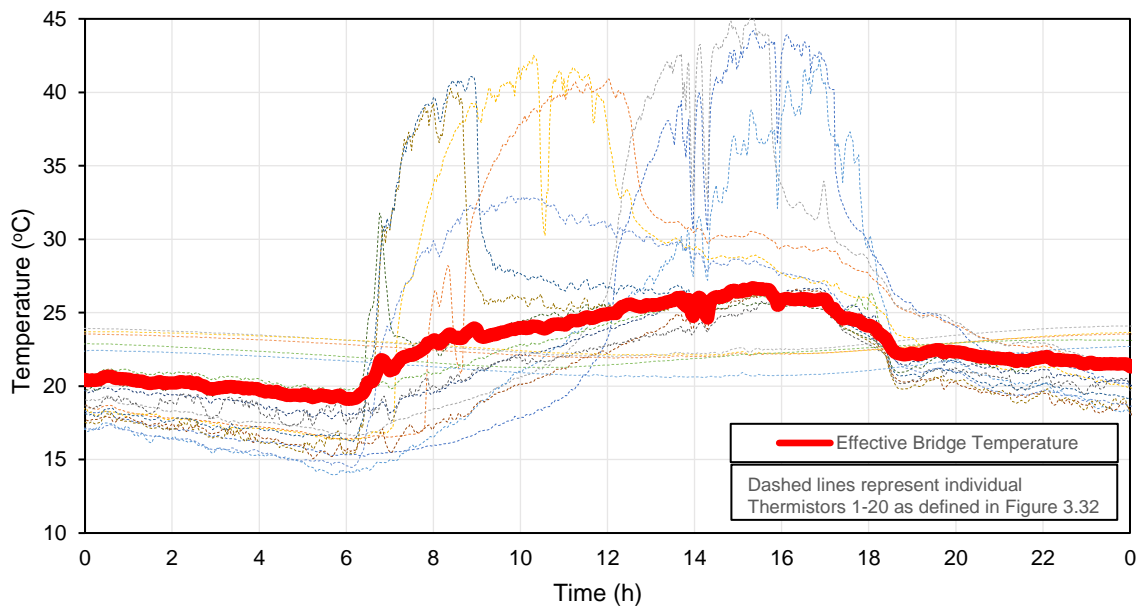
Figure 4.5: Comparison between isotherm and effective bridge temperatures

As discussed in Section 4.1.1, the average bridge deck surface temperature does not provide an accurate indication of the bridge temperature and there is a significant lag of up to 2 hours between the maximum average bridge temperature and maximum displacement. In addition, the bridge temperature results suggest a much larger overall longitudinal displacement in comparison to the displacement recorded by the LVDT's at the BEJ. Assuming a thermal expansion coefficient (α) of 10×10^{-6} /°C and using the recorded bridge displacement presented in Figure 4.3, the expected temperature variation for Site A can be calculated and compared with the actual temperature variation for Site A. From Figure 4.3 it can be seen that the minimum and maximum displacements recorded was -17.20 mm and 2.01 mm respectively resulting in an overall bridge displacement of

19.21 mm. By applying Equation 2-1, the expected temperature variation in the bridge is expected to be approximately 6.1 °C, however, the recorded variation in bridge deck surface temperature was approximately 20.9 °C.

It is worth noting that the rail displacement can be determined using compatibility methods, however, for this study rail displacement was computed using a calibrated numerical model as presented in Chapter 5.

To analyse the accuracy of an effective bridge temperature through the cross-section, in comparison to a bridge deck surface temperature, the calculated effective bridge temperature is plotted against the bridge displacement results recorded at the BEJ, see Figure 4.6:
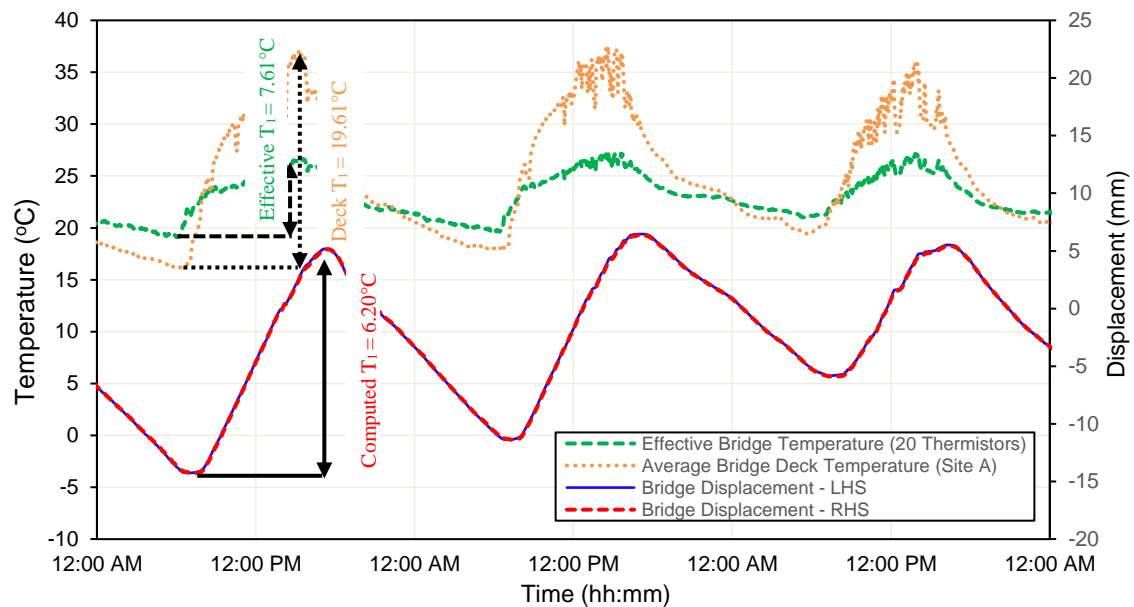
Figure 4.6: Site B – Effective Bridge Temperature and Bridge Displacement (March 2019)

To analyse the accuracy of the calculated effective bridge temperature, the expected temperature variation per day, computed from LVDT displacement readings, can be calculated and compared with the actual temperature variation, measured from thermistors.

If we compare the results of the average bridge deck surface temperature and the effective bridge temperature through the cross-section it can be seen that for the effective bridge temperature, the actual temperature results correlated well with the computed temperature results, whereas there was

a significant difference between the actual temperature results and the computed temperature results for bridge deck surface measurements.

It is understood that increasing the number of thermistors throughout the bridge deck cross-section will further refine the computed effective bridge temperature as it converges to the actual effective bridge temperature. In further analysing the isotherms used to compute the effective bridge temperature, illustrated in Figure 4.4, it can be seen that isotherm 2, 5, 9, 11 and 13 are only represented by thermistors on the exterior of the bridge deck with no thermistors inside the bridge deck.

From the temperature results presented in Figure 3.38, it is understood that the temperature within the bridge deck remains relatively constant in comparison to temperature on the exterior which is affected by solar radiation. It is, therefore, considered important that isotherms in the bridge cross-section are represented by a thermistor on the inside and outside of the bridge (with the exception of the box girder cantilever wings).

Due to the relatively constant temperature of the bridge deck interior, it is deemed acceptable to increase the density of the isotherm readings within the bridge deck by taking an average at the mid-point of two consecutive isotherms, eliminating the need for further site investigations. For example, an additional thermistor reading can be calculated by taking the average between Thermistor 16 and 17. The revised isotherm arrangement is illustrated in .
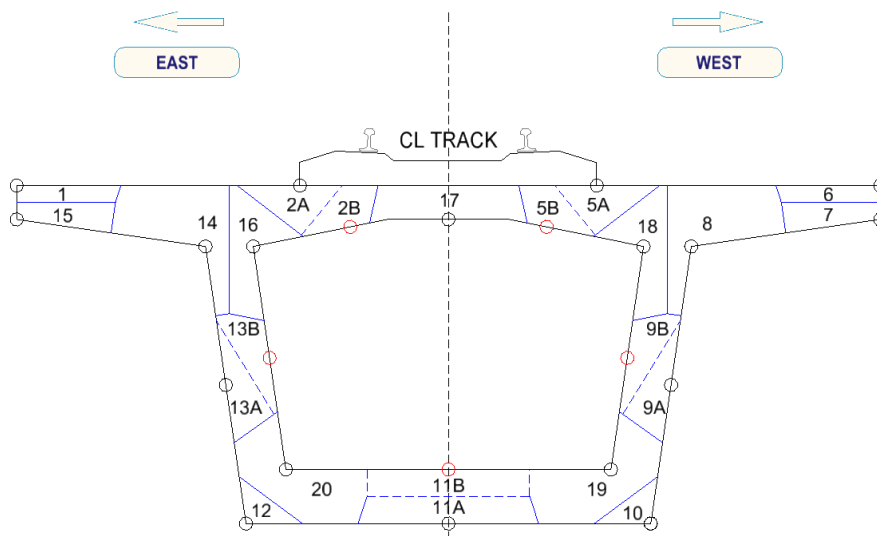
Figure 4.7: Revised isotherms with additional thermistor positions

Increasing the density of the thermistors and, therefore, the temperature readings will improve the accuracy of the computed effective temperature as it converges to the actual effective bridge temperature. It can be seen from Figure 4.8 that the computed maximum effective bridge temperature has reduced and the computed minimum effective bridge temperature has increased, resulting in a decrease in the effective bridge temperature variation.
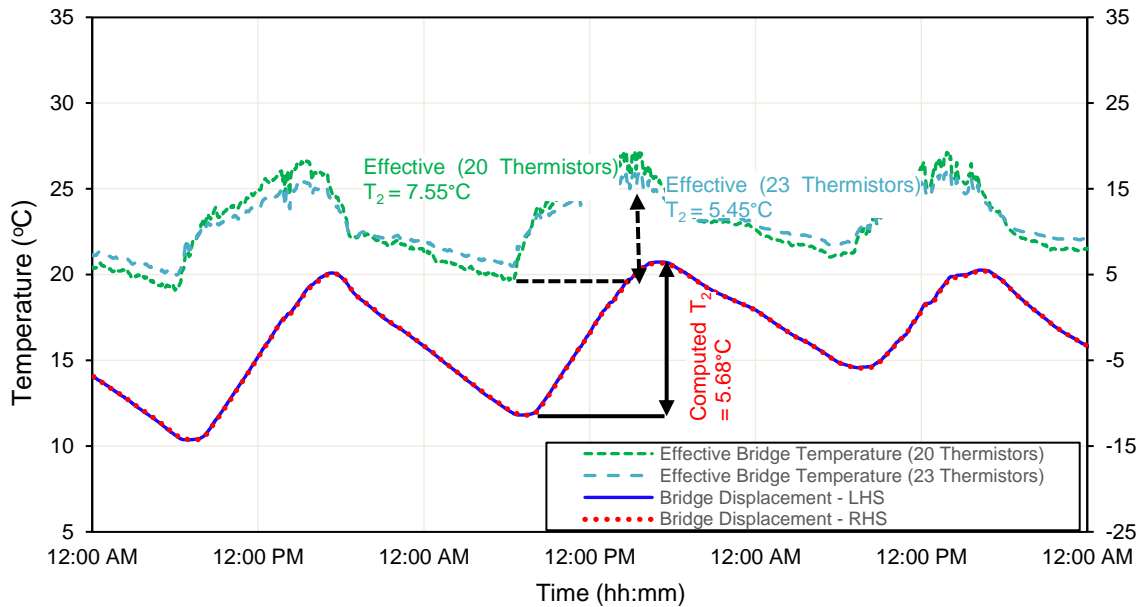
Figure 4.8: Site B – Effective Bridge Temperature and Bridge Displacement (23 thermistors) (March 2019)

From Figure 4.8 it can be seen that the actual effective bridge temperature variation for 23 thermistors, at 5.45 °C, has converged closer to the computed effective bridge temperature, at 5.68 °C. The results of the revised effective bridge temperature for 23 thermistors confirms the importance of providing sufficient temperature readings throughout the cross-section of the bridge to represent the bridge temperature. In addition, due to the large variations in temperature between the bridge deck surface and inside of the bridge deck, it is important to strategically place temperature probes/thermistors to obtain sufficient coverage and distribution throughout the bridge deck.

4.2   TRACK-BRIDGE INTERACTION

By reviewing the principles of CWR on an embankment, discussed in Section 1.1.1 of UIC Code 774-3R (2001), it is understood that CWR is subject to thermal and traffic loading as the rails are restrained from free movement. In addition to the track forces, thermal and traffic loading can contribute to rail creep. A major consequence of rail creep is increased longitudinal stress as the rail slips towards a localised position resulting in increased track forces and ultimately track buckling. An investigation by Gräbe & Jacobs (2015) found that rail creep/slip due to reduced fastening strength can result in variation of stree free temperature which further limits the ability to monitor longitudinal rail stress in CWR.

As discussed in Section 1.1.2 of UIC Code 774-3R (2001), introducing a bridge under CWR track effectively means the CWR track is resting on a surface subject to deformation and movement, adding an additional load case to the buckling analysis.

In summary, CWR track on a bridge structure is subject to the following load effects as a minimum:

- **Thermal:**
    - Thermal expansion of the deck and rail when an REJ is present.
    - Thermal expansion of the deck only when no REJ is present.
- **Braking:**
    - Horizontal braking and acceleration forces.
- **Bending:**
    - Rotation of the bridge deck subject to vertical traffic loading.
    - Deformation of the bridge deck due to creep/shrinkage.
        - Longitudinal displacement of supports due to thermal gradient.
        - Deformation of the structure due to vertical temperature gradient.

It should be noted that the site investigations undertaken at the Majuba Rail Bridge did not have traffic present which provided the opportunity to isolate the effects due to thermal loading only and ignore the effects due to vertical bending and braking/acceleration effects.

It is understood from Section 1.5.2 of UIC Code 774-3R (2001) that the total maximum permissible rail stress is a combination of these three load effects (thermal/braking/bending). However, according to Lee et al. (2015), the effect related to temperature load accounts for 50~70% of the

total additional axial force whereas 20~40% is related to traction/braking and 5~10% is related to vertical load.

The analysis for this dissertation will, therefore, reduce the additional permissible rail stress recommended in UIC Code 774-3R (2001) by 30% percent for the purpose of evaluating thermal loading only. As described above, there are two conditions for thermal loading, namely, (1) with REJ, (2) without REJ.

The site data obtained and analysis thereof is based on condition (1) with REJ. This will, therefore, become the base case to calibrate a numerical model in Section 5.2. Condition (2) without REJ will then be a scenario used in the numerical model to determine certain objectives, defined in Section 1.2, such as determining the need for an REJ, analysing the effect of fastening strength on track-bridge interaction and determining the maximum allowable bridge expansion length that results in permissible additional compressive rail stress.

4.2.1 Total Bridge and Rail Displacement

As described in Section 3.3.1, the Majuba Rail Bridge is a continuous concrete bridge girder with a total expansion length of 314 m.

From the site investigations undertaken, a maximum bridge expansion length of 19.4 mm was recorded.

By considering Equation 2-1, the theoretical change in bridge temperature required to cause an expansion of 19.4 mm is 6.2 °C (assuming a thermal expansion coefficient (α) of 10 x 10^{-6}/°C). The theoretical temperature correlates well with the effective temperature of 5.4 °C determined from multiple thermistor measurements a per results in Section 4.1.2.

It is, however, worth noting that although a thermal expansion coefficient (α) of 10 x 10^{-6}/°C is a good average for structural concrete, a range of 7 x 10^{-6}/°C to 12 x 10^{-6}/°C has been observed. Assuming a thermal expansion coefficient (α) of 11.5 x 10^{-6}/°C results in an effective temperature of 5.4 °C for the measured total displacement of 19.4 °C.

It should be noted that the ambient air temperature for this day varied by 18 °C and although the ambient air temperature profile correlated well with the effective bridge temperature profile, the bridge temperature was approximately a third of the ambient air temperature.
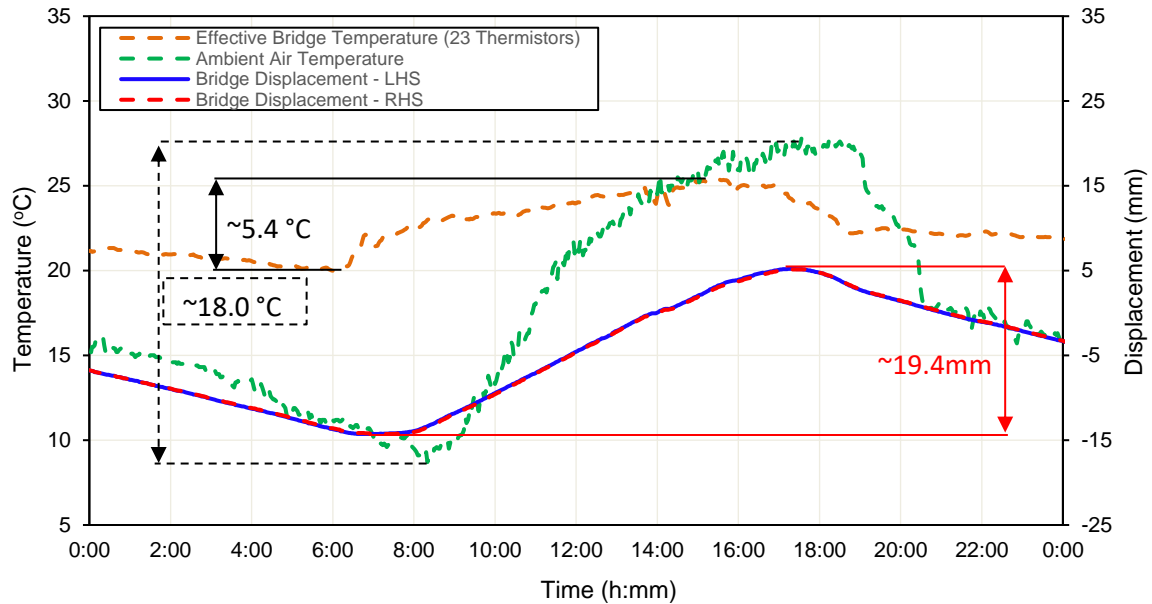
Figure 4.9: Maximum bridge displacement recorded (March 2019)

To further understand the track-bridge interaction phenomenon, a comparison is required between the total bridge displacement, measured at the BEJ and the total rail displacement, measured at the REJ.

From the three site investigations undertaken, a maximum rail expansion of 25.9 mm occurred on the same day as the maximum bridge displacement was recorded. It is worth noting that the minimum and maximum rail displacement at the REJ occurred within minutes of the minimum and maximum bridge displacement at the BEJ. Although the total rail expansion cannot be calculated from rail temperature alone, as it is a function of bridge expansion, the minimum and maximum rail temperature recorded on this day were 10.2 °C and 50.9 °C respectively with a change in temperature of 40.6 °C.

It should be noted that the difference in bridge temperature (~5.4 °C) was determined using a method published in Emerson et al. (1976). This temperature has also been confirmed by back calculation from real-time displacement data obtained by LVDT measurements. Therefore, there is a reasonable level of confidence related to the effective bridge temparature required to cause the measured displacement of 19.4 mm. In addition, the rail temperature readings have been obtained from using two different site setups with separate data loggers and, therefore, there is a high level of confidence in the rail temperature measurements.

The change in temperature and displacement for both the bridge (at the BEJ) and rail (at the REJ) are summarised in Table 4.1.

Table 4.1: Change in bridge and rail temperature/displacement

Description	Bridge (at BEJ)	Rail (at REJ)
Maximum change in temperature (°C)	+5.4	+40.6
Maximum change in displacement (mm)	+19.4	+25.9

The displacement results indicate that although the rail is fastened directly to the bridge deck by means of elastic fastenings, a differential displacement of up to 6.5 mm occurred between the bridge deck and rail. This is understood to be as a result of rail creep and "breathing length" associated with thermal loading. This phenomenon will be further analysed and discussed in Section 4.2.2 and 4.2.3.

4.2.2 Differential Bridge and Rail Displacement

As discussed in Section 3.6, continuous rail and bridge displacement measurements were taken during all three site investigations. This provided an opportunity to investigate the displacement of the rail relative to the bridge. It is understood that the bridge will push and pull the rail as it expands, however, additional rail displacement is also expected due to rail creep and "breathing length" at the rail expansion devices.

Figure 4.10 represents the continuous bridge and rail displacement results recorded at the BEJ over 7 days during the three site investigations.
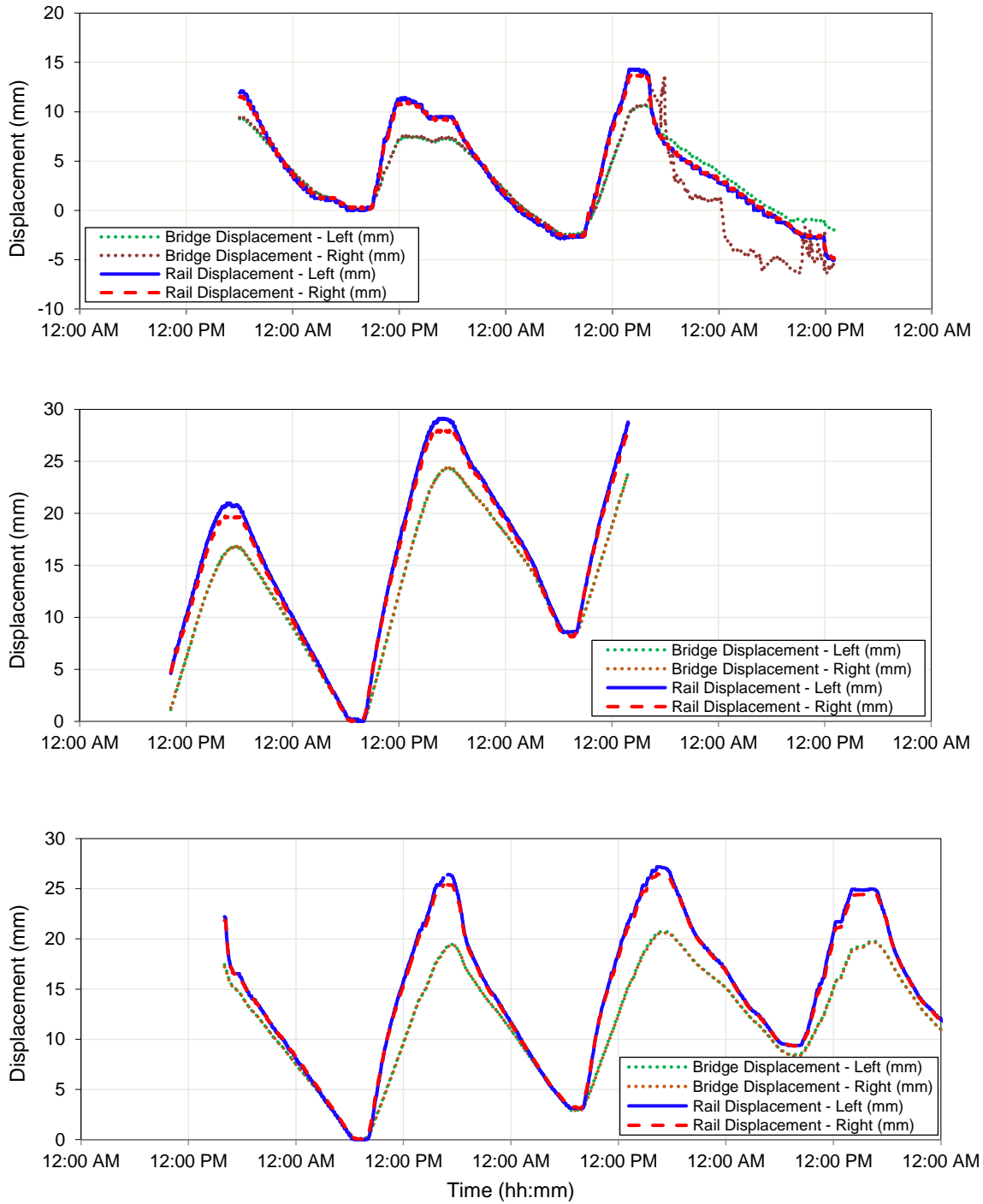
Figure 4.10: Continuous Bridge and Rail Displacement recorded at the BEJ and REJ

To analyse the displacement of the rail relative to the bridge, the bridge and rail displacement measurements were set to zero at the minimum displacement readings for the first AM peak which generally occurs between 06:30 am and 07:30 am. This method was proposed as it is understood that the bridge and rail move into a similar position, without differential displacement, in the evenings and early mornings. This is confirmed by the results presented in Figure 4.10.

The graphs in Figure 4.10 clearly indicate that there is a differential displacement between the bridge and rail during the PM Peak. In all cases, the rail displaces more than the bridge as temperature increases. Figure 4.11 summarises the maximum differential displacement between the bridge and rail.
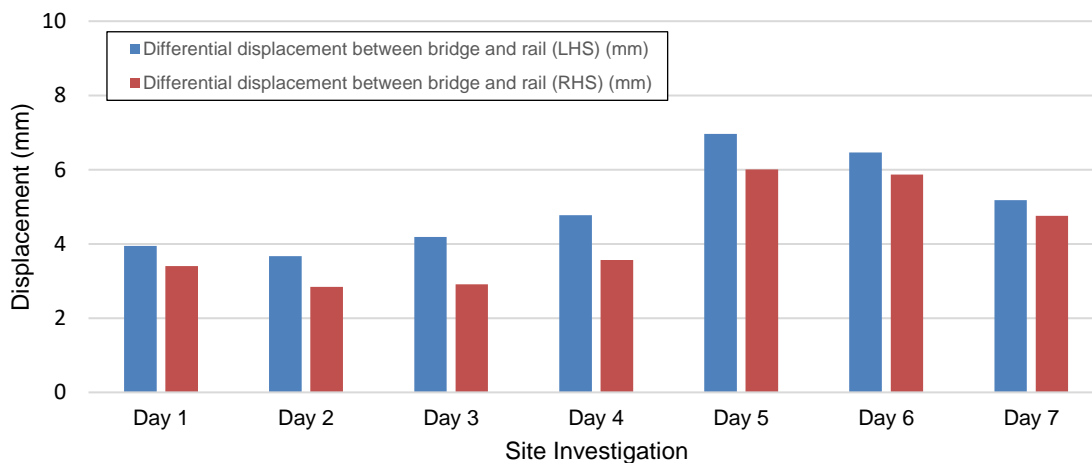
Figure 4.11: Differential displacement between bridge and rail recorded at the BEJ (March 2019)

The results, illustrated in Figure 4.11, indicate that on average the LHS rail displaced 33% more than the LHS bridge whereas the RHS rail displaced 26% more than the RHS bridge. On average, the LHS rail displaced 25% more than the RHS rail. This is likely due to the position of the sun, rising on the LHS of the bridge and the increased solar radiation before midday.

As these site investigations did not include any traffic loading, the differential displacement was due to thermal loading only. Actions due to thermal loading occur due to differences in temperature between the deck and the rails in the case of track with an expansion device. As demonstrated in Section 4.1.2, bridge temperature must be represented by an effective bridge temperature calculated as a weighted average of thermal readings through the entire bridge cross-section. Effective bridge

temperature results were obtained for Day 5, 6 and 7. The analysis of differential displacement due to thermal loading is, therefore, limited to results from this period.
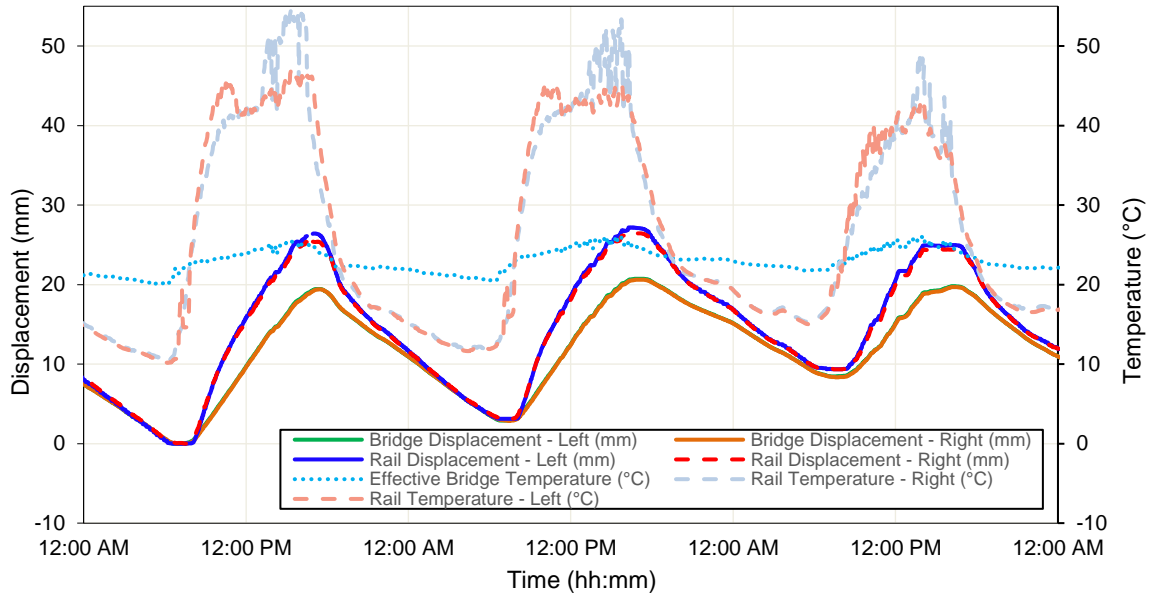
Figure 4.12: Bridge and rail differential displacement / temperature (March 2019)
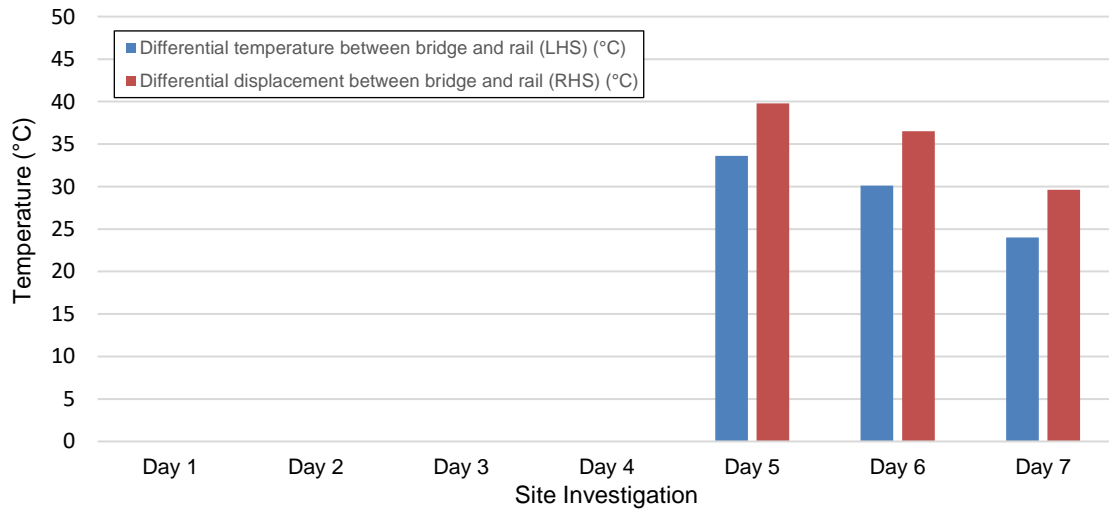
Figure 4.13: Differential temperature between bridge and rail recorded at the BEJ and REJ (March 2019)

An interesting observation can be made by comparing the differential displacement results with the differential temperature results. From Figure 4.11 it can be seen that the LHS differential

displacement between the rail and the bridge is approximately 25% higher than the RHS, however, the LHS differential temperature is approximately 20% lower than the RHS. It is understood that the rapid increase in rail temperature between approximately 06:00 am and 10:30 am accounts for a large proportion, approximately 80%, of the rail force required to overcome the fastening system longitudinal restraint and causes uncontrolled slip of the rail.

In further analysing the data, it can be seen that the rapid increase in rail temperature between 06:00 am and 10:30 am is the reason the rail displacement is greater than the bridge displacement on a given day, however, it can be seen that the rail and bridge displacement profiles generally correlate better with ambient air temperature as compared to either rail or bridge temperature. This is supported in literature for a study undertaken at the Olifants River Bridge by Maree (1987) that states "with a knowledge of daily fluctuations in air temperature the interaction forces for similar decks can be predicted".
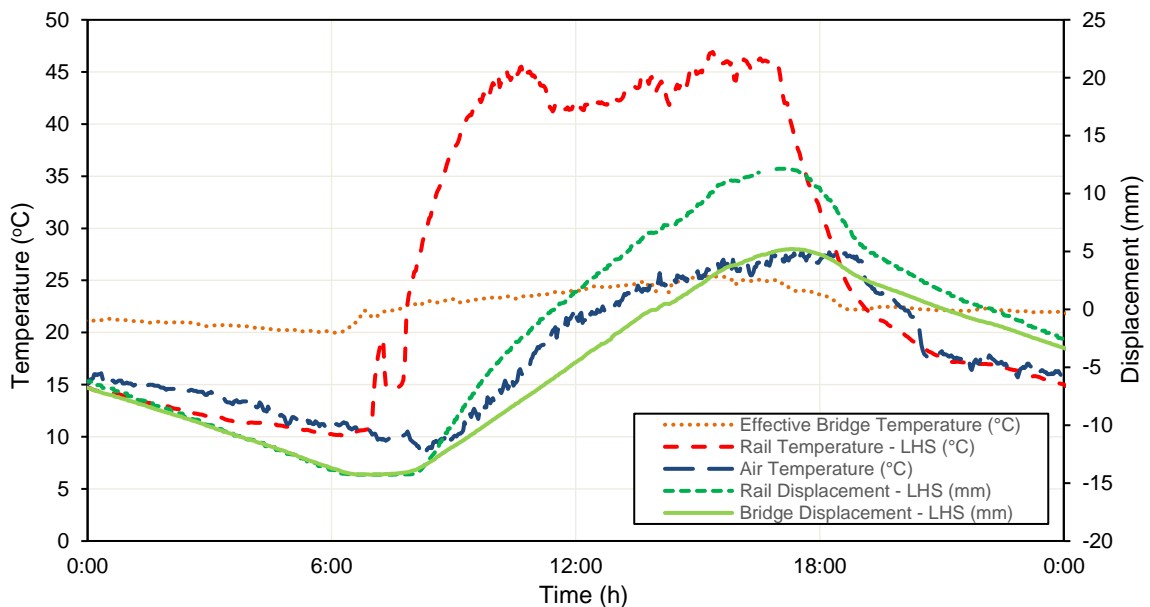
Figure 4.14: Bridge and rail comparison (March 2019)

4.2.3 Rail Creep / Slip

As stated in UIC Code 774-3R (2001), introducing a bridge under a CWR track means, effectively, that the track is resting on a surface subject to deformation and movements, hence causing displacement of the track and inducing additional track forces.

However, in addition to track displacement due to the bridge, results presented in Section 4.2.1 and 4.2.2 indicate that in addition to the rail displacing as the bridge expands, additional rail displacement occurs and is likely due to rail creep. To further analyse the rail creep distribution, the total bridge displacement, measured at the BEJ, was subtracted from the total rail displacement, measured at the REJ, with the resultant data being the rail creep.

When analysing the rail creep, it is important to consider the track structure system which includes the fastening systems for the plain line ballasted track on the embankment, PY Track Slab on the bridge and the rail expansion joint arrangement. It is believed that the REJ setup will significantly impact the rail creep from the Slab Track on the bridge and the ballasted track on the embankment. As described in Section 3.3.5, the REJ comprises a switch blade, fixed to the bridge deck and stock rail, anchored to the abutment/embankment. The switch blade, which does not facilitate sliding, is anchored by means of various high toe load fasteners which include a combination of K-clip KP60-306/307 fastening clips and switch blade rail support buttresses which facilitate fastening to the base plate and the switch blade web resulting in high fixity fasteners. The stock rail, which does facilitate sliding, is guided on the Stage 3 Flat Track Slab by a combination of low restraint fasteners which include a combination of K-clip KP60-309 fastening clips and stock rail support buttresses that are only fastened to the baseplate and are not fastened to the stock rail.

Due to the arrangement of the REJ switch blade and stock rail respectively, it is understood that the longitudinal restraint of the switch blade, on the bridge, is very high and will result in minimal if not zero rail creep whereas the longitudinal restraint of the stock rail, on the embankment, is low and will allow the majority of rail creep due to the "breathing length" at the REJ. To confirm this hypothesis, data from Site A (embankment stock rail) and Site 1 (bridge switch blade) was used, presented in Figure 4.15.
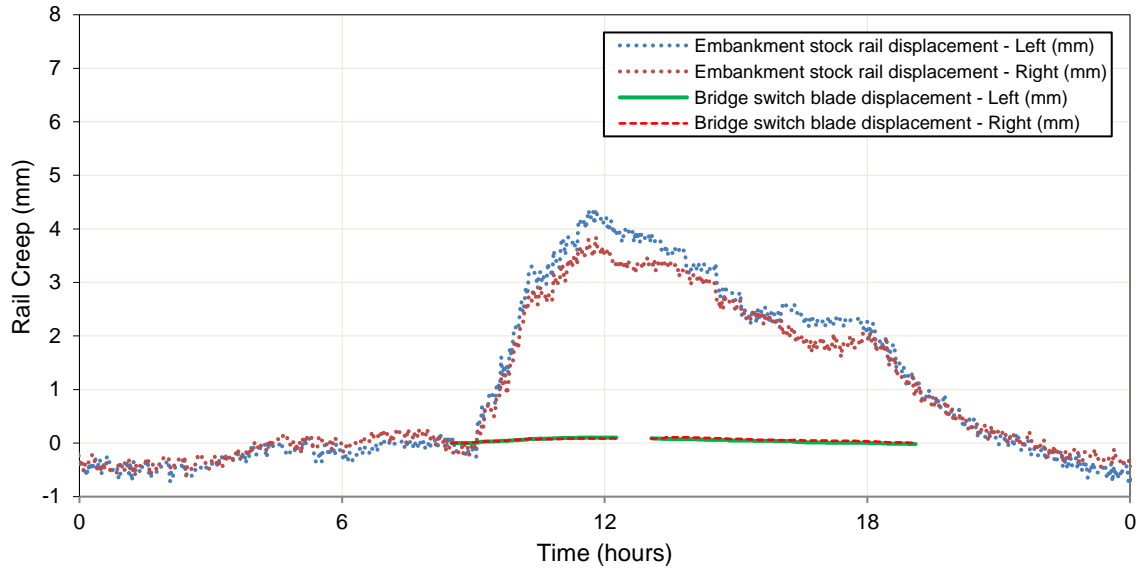
Figure 4.15: Comparison of rail creep due to stock rail and switch blade (March 2019)

From the data presented in Figure 4.15, it can be seen that rail creep of up to 7 mm can be expected at the REJ. Rail creep for the high fixity switch blade on the bridge, however, had a negligible rail creep with all values less than 0.1 mm taken during the period of maximum total rail creep and temperature increase, irrespective of position along the length of the bridge.

It can, therefore, be concluded that total rail expansion is due to the bridge pulling the rail as it expands and rail creep due to the "breathing length" of the low fixity stock rail on the ballasted embankment with rail creep on the bridge negligible due to the high fixity switch blade.

Figure 4.16 represents the two components that make up total rail expansion, namely, expansion due to the bridge pulling the rail and expansion due to rail creep or "breathing length" from the ballasted track on the embankment. It can be concluded that of the total rail expansion measured at the REJ, approximately 78% of the displacement is due to the high fixity Slab Track rail being pulled by the bridge and the remaining 22% is due to the ballasted rail track on the embankment "breathing" towards the discontinuity at the REJ where rail creep of the high fixity Slab Track is negligible. Further validation of these results can be confirmed using testing methods described in BS EN 13146-1 (2012) and is recommended as further scope to this study.

Figure 4.16: Rail displacement due to bridge expansion and rail creep (March 2019)

4.2.4 Longitudinal Track Stiffness

As discussed in Section 4.2.3, rail displacement measured at the REJ is due to the bridge pulling the high fixity switch blade rail and the "breathing" of the stock rail from the ballasted embankment. Rail creep from the high fixity switch blade is negligible whereas the majority of the rail creep is due to the stock rail only.

As described in UIC Code 774-3R (2001), track resistance (k) to longitudinal displacement (u) is a function of the rail displacement relative to its supporting structure. At low displacement, the resistance increases rapidly, however, once a certain displacement (u) is reached, the rail slips and longitudinal resistance (k) remains virtually constant (UIC Code 774-3R, 2001). It is generally accepted that this non-linear relationship between longitudinal track resistance (k) and displacement (u) is simplified to a bi-linear function as represented in Figure 4.17.
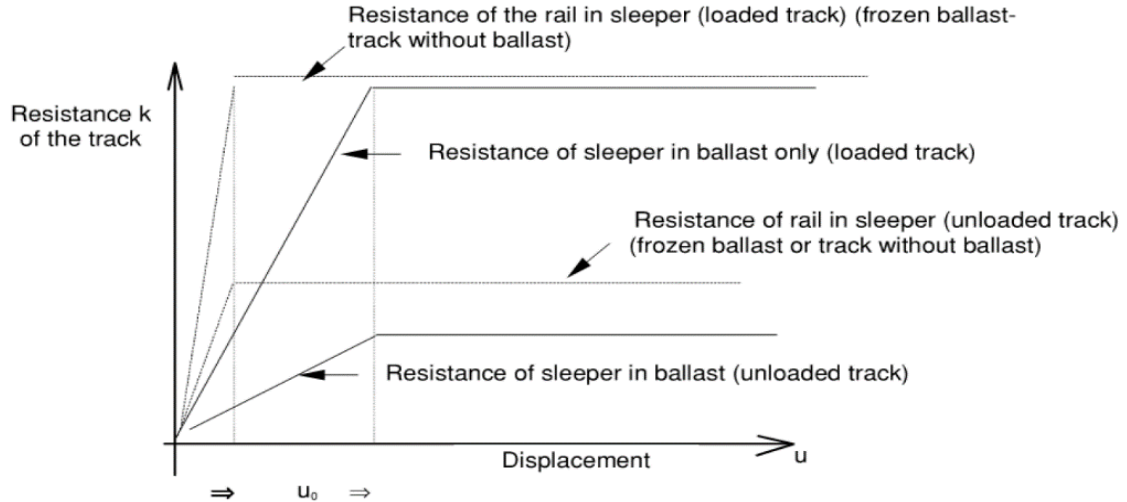
Figure 4.17: Longitudinal resistance (k) per unit length as a function of displacement (u)

During the site investigation, both rail temperature and rail creep of the stock rail from the ballasted embankment were recorded. By plotting the rail creep as a function of temperature, the temperature at which "uncontrolled" rail creep occurs can be determined. This "uncontrolled" rail creep/slip is more generally known as the "plastic zone", where the rail has moved past the "elastic zone" associated with the properties of the elastic fastening and rail pad. It should be noted that even though the bi-linear function is plotted against resistance, when considering thermal loading only, the measured temperature is representative of force, which can be calculated if the stress free temperature for a particular site is known.

Figure 4.18 represents the creep associated with the ballasted embankment stock rail as a function of temperature. Some interesting observations, marked up on the graph below, indicate that "uncontrolled slip" / "plastic zone" generally occurs at temperatures greater than 25 °C. In addition, short term drift of the rail displacement occurs, however, is limited to less than 1 mm and the rail generally returns to its initial position.
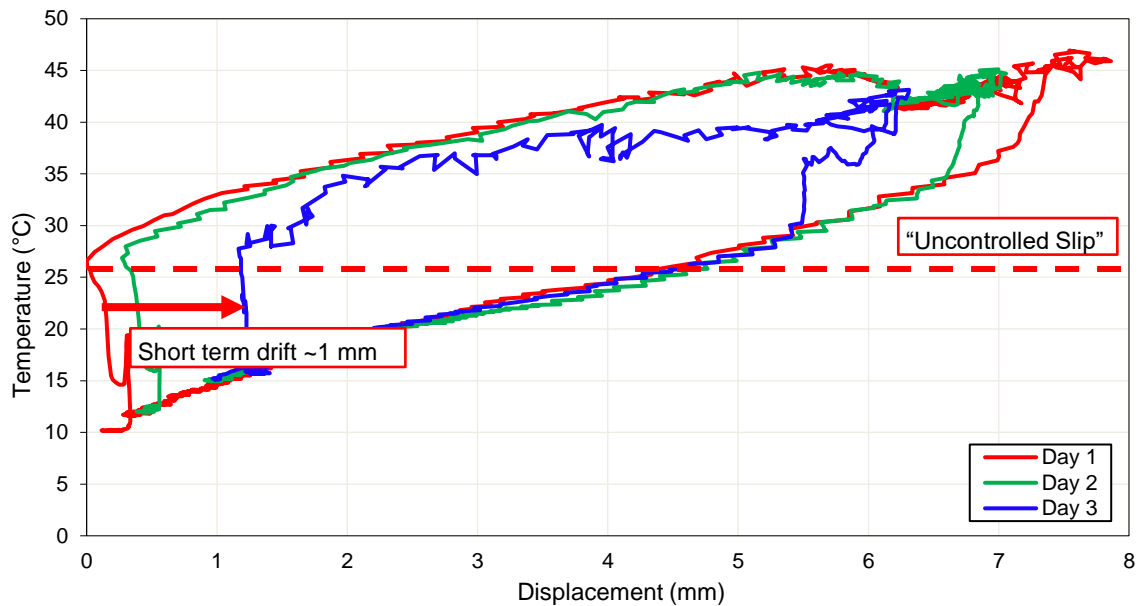
Figure 4.18: Rail creep as a function of temperature (track resistance)

As discussed earlier, it should be noted that even though the bi-linear function is plotted against resistance, when considering thermal loading only, the measured temperature is representative of force, which can be calculated if the stress free temperature for a particular site is known. It must, however, be noted that "uncontrolled slip" is expected to occur at a much lower temperature or force increase due to the presence of the REJ and the "breathing length" phenomenon. A much larger force will be required to cause "uncontrolled slip" with the resistance provided by CWR.

4.2.5 Rail Stress Profile on the Bridge

As the Majuba Rail Bridge has an REJ installed at the southern abutment, a similar strain profile to the profile represented in Figure 2.14 is expected for the rail fixed to the bridge deck. The site data, obtained from the setups from Site 1 to 4 includes continuous rail temperature and strain. Figure 4.19 represents typical rail temperature and strain for Site 2, with data from other sites represented in Appendix C.
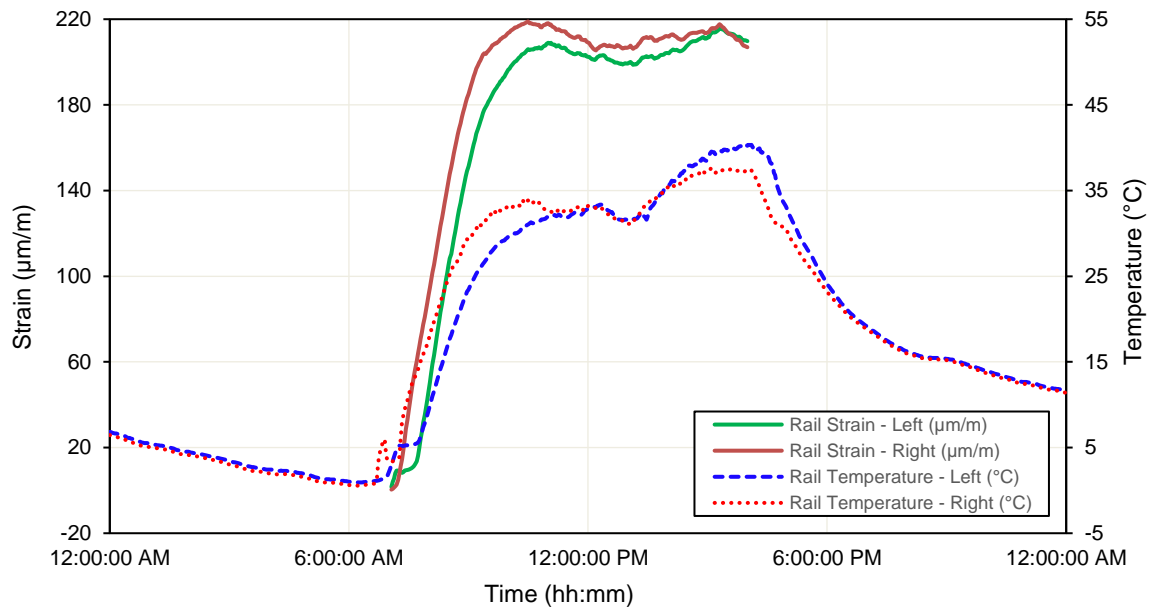
Figure 4.19: Rail strain and temperature – Site 2

As rail strain was recorded for the period that the rail experienced the greatest increase in temperature, the rail strain can be plotted as a function of rail temperature which can then be used to compare the rail stress profile/distribution at different locations along the length of the bridge.

It can be seen from Figure 4.20 that the rail strain generally follows a similar linear trend irrespective of the position on the bridge, from Site 1 to 4. This confirms that when an REJ is installed on a continuous bridge, the additional stress in the rail generally follows a uniform linear trend, similar to the profile represented in Figure 2.14.
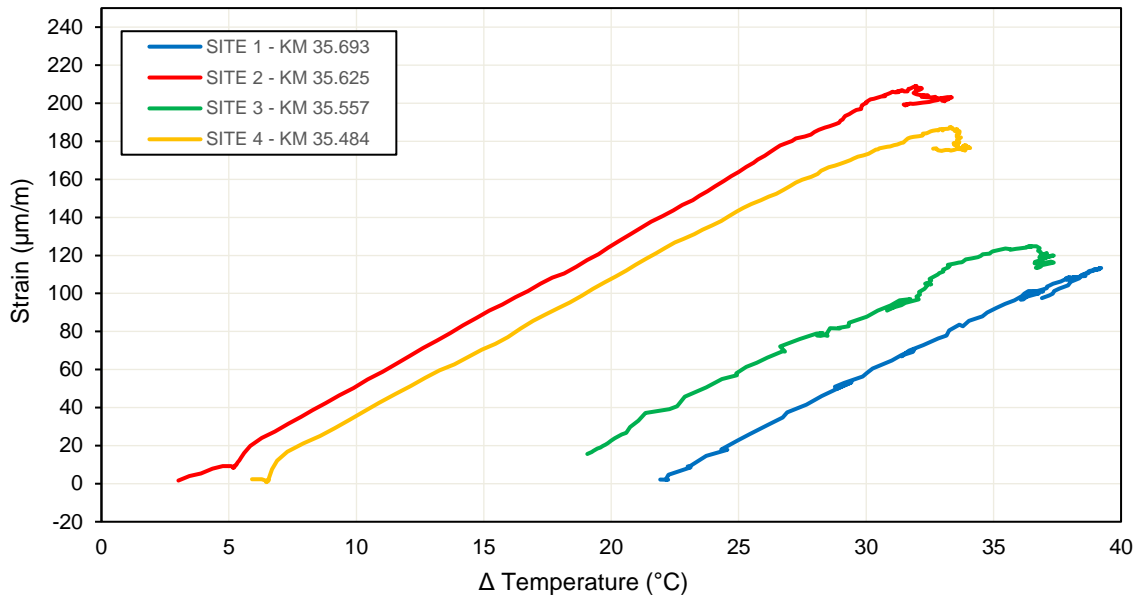
Figure 4.20: Rail strain as a function of rail temperature (Sites 1 to 4)

The site data presented in Figure 4.20 provides the opportunity to further define the relationship between rail temperature increase and rail strain as measured on the Majuba Bridge from Site 1 to 4. It can be seen from Figure 4.20 that Site 2 and 4 commenced at temperatures as low as 3 and 6 °C whereas Site 1 and 3 commenced at temperatures of 19 and 22 °C. A logical temperature to select as the "zero" strain point would be at the point of assumed SFT, thus resulting in all negative strains representing longitudinal rail tension and all positive strains representing longitudinal rail compression, presented in .
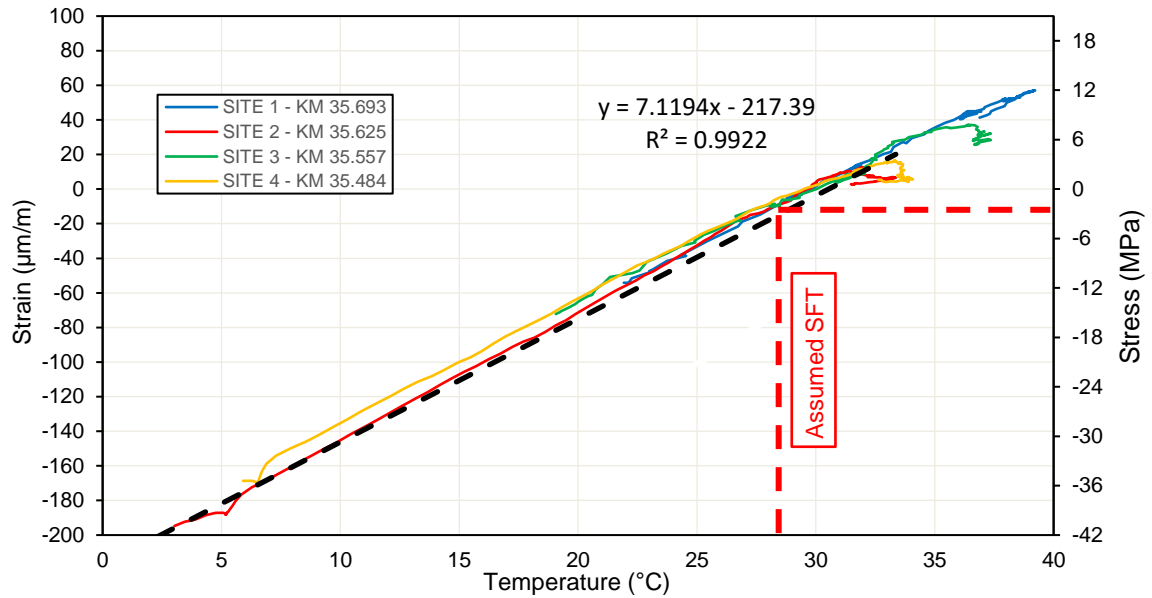
Figure 4.21: Rail strain as a function of rail temperature set to assumed SFT (Site 1 to 4)

The data represented in demonstrates the strong linear relationship between rail temperature and rail stress/strain. The following linear relationship was derived from which provides the opportunity to determine the rail stress/strain with a known rail temperature:

$$\sigma_{\text{ADD. RAIL}} = (7.1194\,\Delta T - 217.39)\,E \qquad\qquad\qquad (\text{Eq. 4-1})$$

Where:

$\sigma_{\text{ADD. RAIL}} = $ Additional rail stress (m^2)
$E = $ Elastic Modulus of rail of 210 (GPa)
$\Delta T = $ Change in temperature (SFT $-$ Actual) (°C)

Although the SFT was not measured as part of the various site investigations, the construction data books for the Majuba Rail Bridge were available during this study. These data books included destressing and thermit weld data sheets. From the data available it was confirmed that the rail was generally destressed using the tensor method and fixed at the mid-point of the A-range for Ermelo, which is between 20 °C to 40 °C. The welds in the vicinity of the REJ, at km 35.677 and km 35.702 were destressed and welded at approximately 28 °C.

The data presented in Chapter 3 and further analysed in Chapter 4 provides valuable insight into various key parameters and relationships including:

- Total bridge and rail displacement;

- Effective bridge and rail temperature;

- Rail creep/slip;

- Longitudinal track stiffness;

- Rail stress profile.

These results and the specific relationships serve as input to the calibration of a numerical model, presented in Chapter 5, which has been further analysed to confirm objectives related to the relationship between fastening strength, expansion length and the track-bridge interaction phenomenon. Chapter 5 provides insight into the numerical modelling software, describes the process to calibrate the model and presents results and analysis of key parameters associated with the track-bridge interaction phenomenon.

5 TRACK-BRIDGE INTERACTION NUMERICAL MODELLING

Midas Civil 2021 was used for numerical modelling. The finite element analysis software has a built in "Rail Structure Interaction (RSI) Wizard". A key feature of the RSI Wizard is to generate model files considering various parameters automatically for checking stress and displacement results.

The RSI Wizard receives simple layout input values for rail, bridge superstructure, bridge substructure and embankment model. A set of sections, material, boundary conditions and load cases (thermal/vehicle) are assigned to the layout. The RSI Wizard then provides three modelling methods including simplified separate analysis, modelling for moving load analysis and modelling for stage analysis. The post-processing features provide a final summary sheet with key parameters based on UIC Code 774-3R (2001) recommended values including individual rail stress, rail and deck relative displacements and absolute deck displacements.

Although a relatively new feature, there are several examples of the Midas Civil RSI Wizard being adopted in industry. In addition, UIC Code 774-3R (2001) Section 1.7.3 provides recommendations for numerical analysis and several test cases to calibrate numerical models. A case study (Choi, 2020) involving rail structure interaction analysis confirmed that the Midas Civil RSI Wizard produced satisfactory results for the UIC Code 774-3R (2001) Test Case No. 1.

	Load Case	Deck Type	Span	Direction	Quantity	Unit	T^0 rail	T^0 deck	Braking	End Rotation	Sum
UIC 774-3	E1-3	1	60	1 (Fixed to free support)	Rail stress	MPa	-126	-30.67	-16.42	-16.98	-64.07
	E1-3	1	60	1	Absolute Displacement	m	0	-1.69E-03	1.36E-03	3.77E-03	3.44E-03

	Load Case	Deck Type	Span	Direction	Quantity	Unit	T^0 rail	T^0 deck	Braking	End Rotation	Sum
MIDAS Civil	E1-3	1	60	1 (Fixed to free support)	Rail stress	MPa	-119.7	-30.64	-17.76	-17.96	-66.36
	E1-3	1	60	1	Absolute Displacement	m	0	-1.7E-03	1.59E-03	4.05E-03	3.94E-03

Figure 5.1: Midas Civil RSI Wizard / UIC 774-3R Test Case Comparison (Choi, 2020)

5.1   RAIL TRACK ANALYSIS MODEL WIZARD

The Midas Civil Rail Structure Interaction Wizard comprises the following five input tabs, which are described in further detail:

- Layout;
- Section;
- Boundary;
- Load;
- Wizard Option.

5.1.1 Layout

The layout tab presents the bridge and track arrangements. Key input parameters include bridge length, number of spans, material type, length of embankment, support types and section of rail. Additional rails checks are also available within this tab that enable the user to model rail expansion joints or zero longitudinal restraints. The ZLR's are simply modelled by setting the bi-linear elastic link stiffness to 0 kN/m.
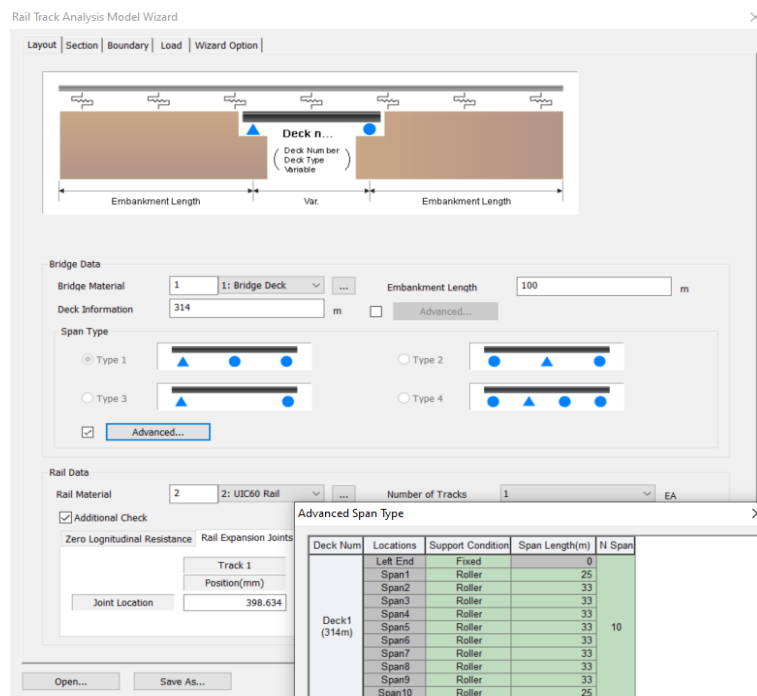
Figure 5.2: Midas Civil – User Defined Properties – Track / Bridge Layout

5.1.2 Section

In the Section tab, the user can define the geometry section of a box girder and a rail. The Section tab has a user friendly function to input key section parameters to develop the bridge cross-section. The exact cross-section of the Majuba Rail Bridge was simply developed using this functionality. The RSI Wizard has a rail profile library which includes a UIC60 rail. It is important to note that any rail related inputs represent a complete track and not individual rails.
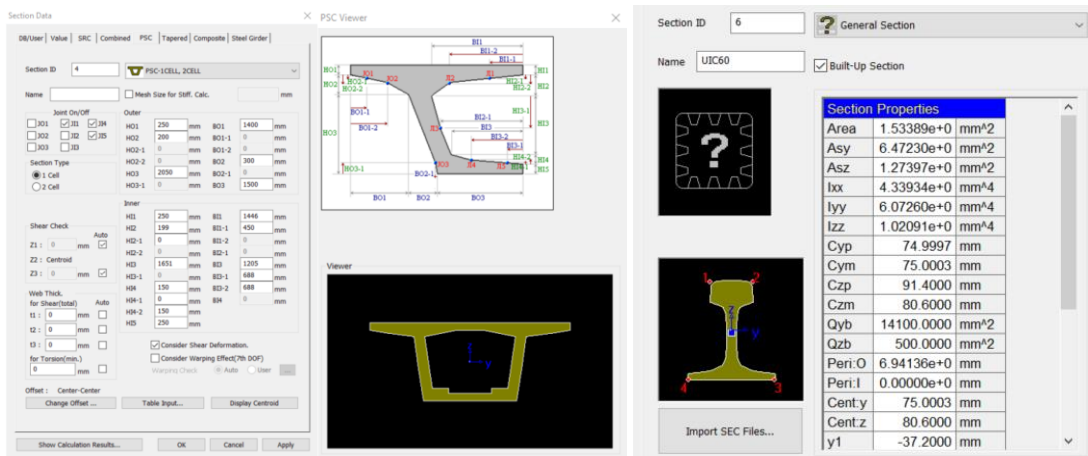
Figure 5.3: Midas Civil – Bridge and Rails Sections
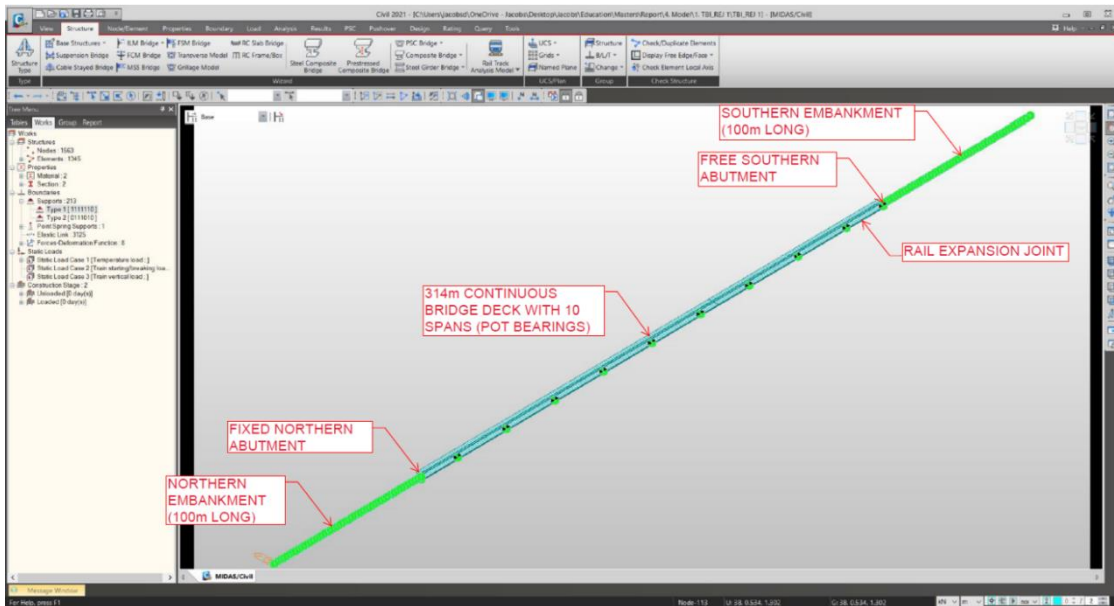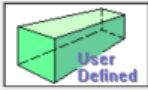
Figure 5.4: Midas Civil – Track / Bridge Layout – Majuba Rail Bridge

Material properties are then assigned to a particular section. Material properties functionality includes a library of steel or concrete materials, however, also has the capability for user defined material inputs.
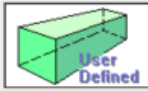
Figure 5.5: Midas Civil – User Defined Properties – Rail (adopted from Shaw et al. (2007))

Figure 5.6: Midas Civil – User Defined Properties – 50 MPa Concrete Deck

5.1.3 Boundary Conditions

The RSI Wizard provides the functionality to input the bi-linear functions as recommended in UIC Code 774-3R (2001) for track resistance. The boundary condition tab allows longitudinal track resistance values for ballasted or Slab Track. It also facilitates a combination of ballasted and Slab Track in the "Advanced Wizard".
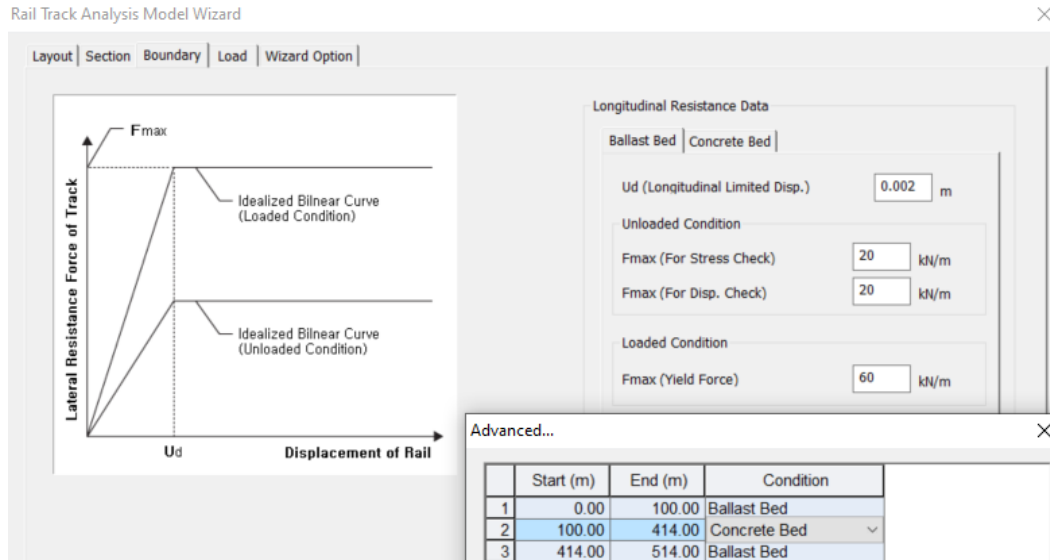
Figure 5.7: Midas Civil – Ballasted Longitudinal Resistance (adopted from UIC 774-3R)
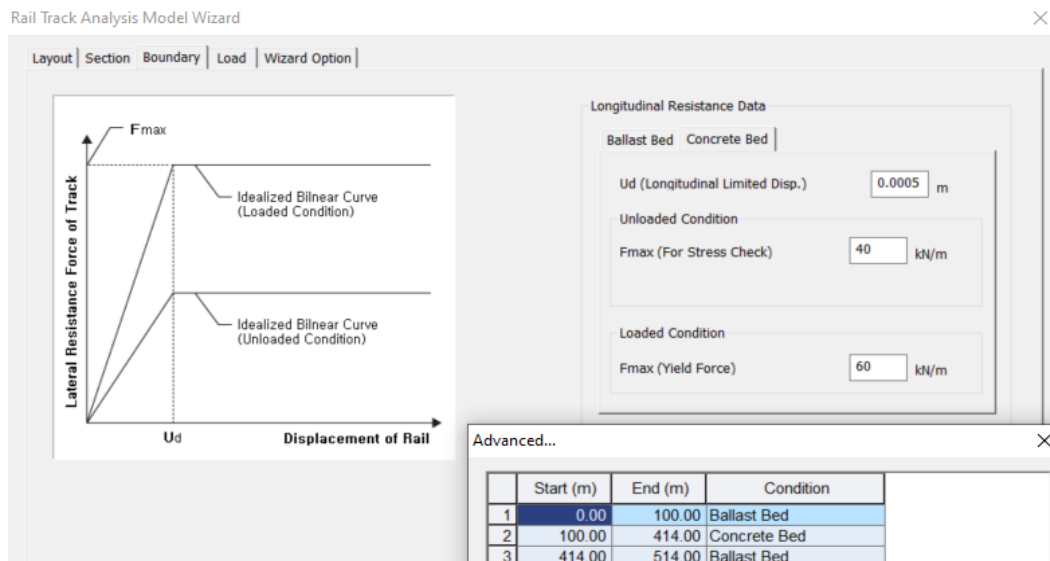
Figure 5.8: Midas Civil – Slab Track Longitudinal Resistance (adopted from UIC 774-3R)

The boundary option defines the boundary conditions of element models. It provides "Spring" and "Bearing" types. The essential input for both is horizontal stiffness. The "Guide" option shows the difference between the types. The user can also check the other boundary conditions in advance (Midas Civil, 2021).

If the "Spring" type is selected, the decks support will be considered as a point spring type. In the same manner, the "Advanced" option allows setting different stiffnesses at each point spring.
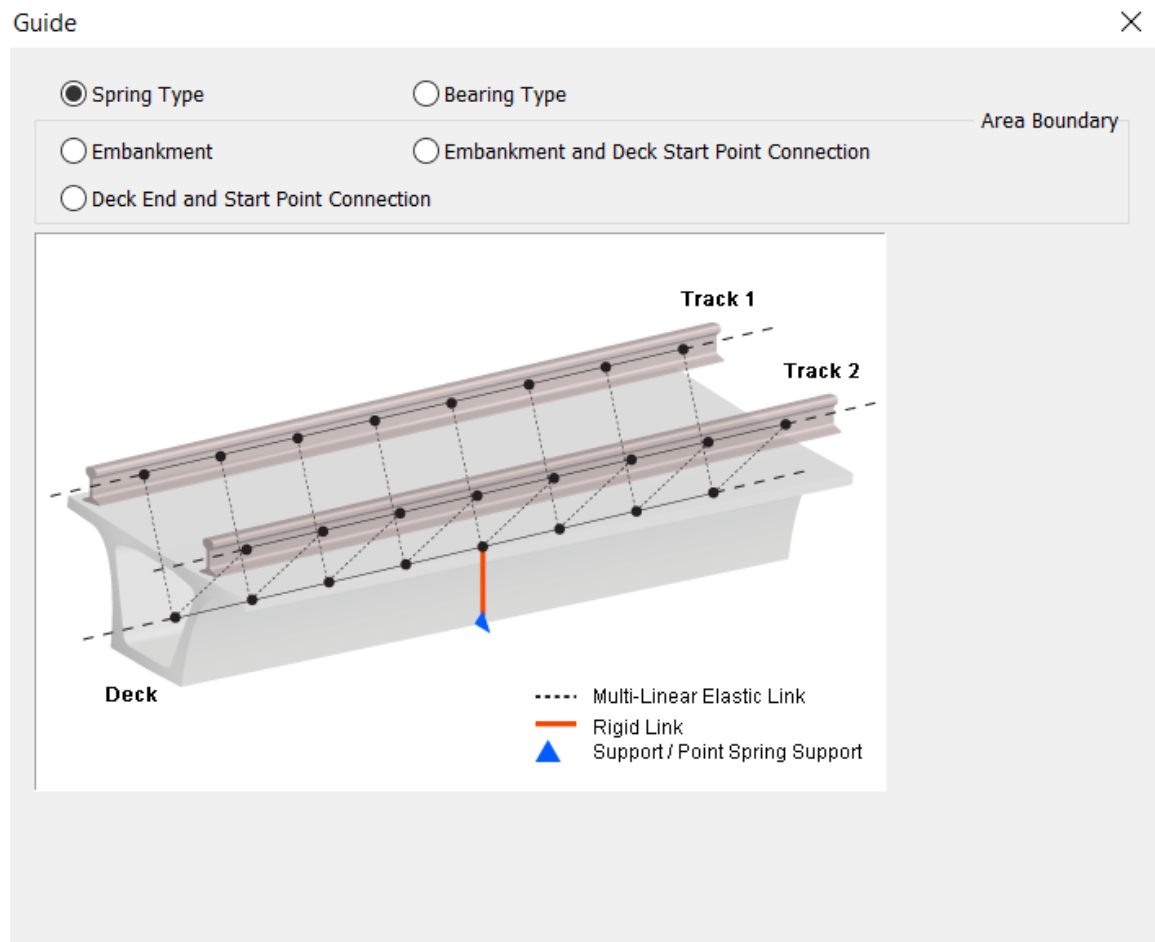
Figure 5.9: Midas Civil – Spring Type Boundary Conditions (Midas Civil, 2021)

5.2   MODEL CALIBRATION

5.2.1 UIC 774-3R (2001) Boundary Conditions (Model 0A)

The initial model calibration will be known as "Model 0A" where "0" denotes models associated with calibration and "A" denotes the revision of the model. Initial calibration was undertaken using the maximum displacement and temperature variations of the site data, as represented in Table 4.1.

As discussed in Section 2.5.3, an important parameter to determine the effect of track-bridge interaction is longitudinal track resistance. The longitudinal track resistance is generally defined by the idealised bi-linear relationship as represented in Figure 5 of UIC Code 774-3R (2001). Longitudinal resistance parameters for ballasted and Slab Track were used as a starting point for calibration, however, is is noted that these values are provided as a guide only and do not take into account increased sleeper spacing and high fixity fasteners associated with the Majuba Rail Bridge and REJ. Initial paramters adopted for model calibration are summarised in Table 5.1.

Table 5.1: Track-Bridge Interaction – Model 0A

Description	Value	Comment
Embankment Length (m)	100	Length of ballasted track on low chainage end of northern abutment and high chainage end of southern abutment
Bridge Deck Length (m)	314	Total length from fixed northern abutment to bridge expansion joint (expansion length over 10 spans)
REJ Position (m)	298.634	Position of REJ measured from northern fixed abutment based on information presented in Table 3.2
ZLR Position (mm)	N/A	ZLR not applicable for model calibration
Δ Bridge Temperature (°C)	5.4	Input load case for thermal load effect analysis based on data from Table 4.1
Δ Rail Temperature (°C)	40.7	Input load case for thermal load effect analysis based on data from Table 4.1
Ballast Resistance Unloaded (kN/m)	20	Unloaded ballasted track (good maintenance) / loaded track not applicable for thermal loading analysis (UIC 774-3R)
PY Track Slab Resistance Unloaded (kN/m)	40	Unloaded Slab Track / loaded track not applicable for thermal loading analysis (UIC 774-3R)
Δ Model Bridge Displacement (mm)	19.4	Expected output at BEJ based on data from Table 4.1
Δ Model Rail Displacement (mm)	25.9	Expected output at REJ based on data from Table 4.1
Differential (Bridge/Rail) (mm)	6.5	Expected differential displacement between bridge and rail based on data from Figure 4.11

The static analysis of Calibration Model 0A performed as expected with stress and displacement results consistent for a continuous bridge deck with an REJ installed. A typical output of the displacement and stress results are illustrated in Figure 5.10 and Figure 5.11.
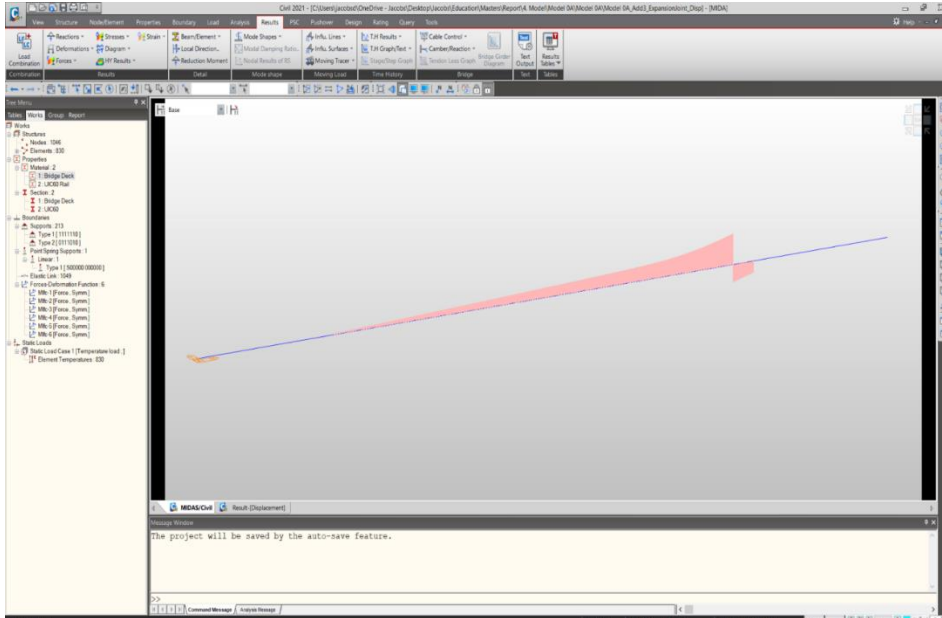
Figure 5.10: Midas Civil – Typical Track Displacement Output
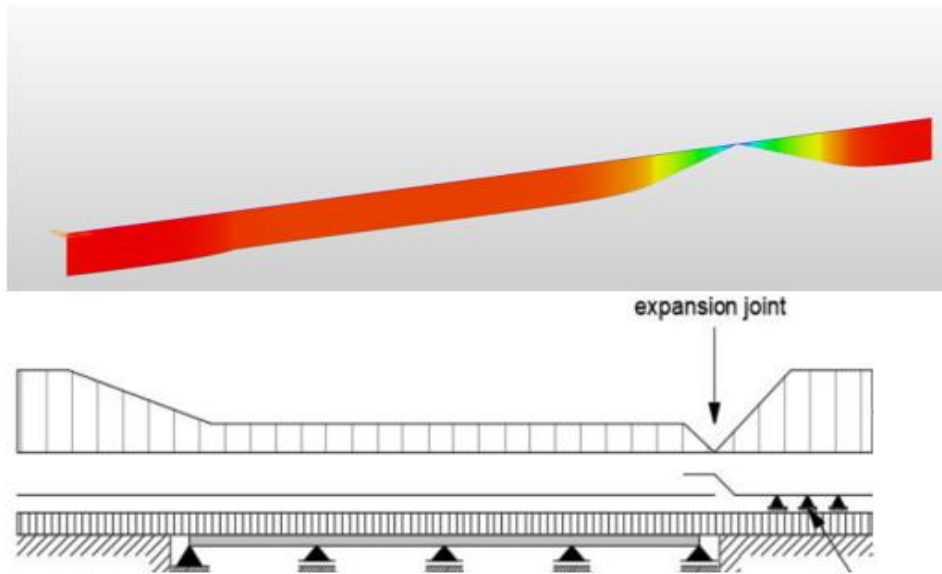
Figure 5.11: Midas Civil – Typical Track Stress Output / Comparison to UIC 774-3R

In order to compare the Model 0A results with the site data in Table 5.1, the rail displacement, bridge displacement and rail stress were plotted against the bridge position as illustrated in Figure 5.12.
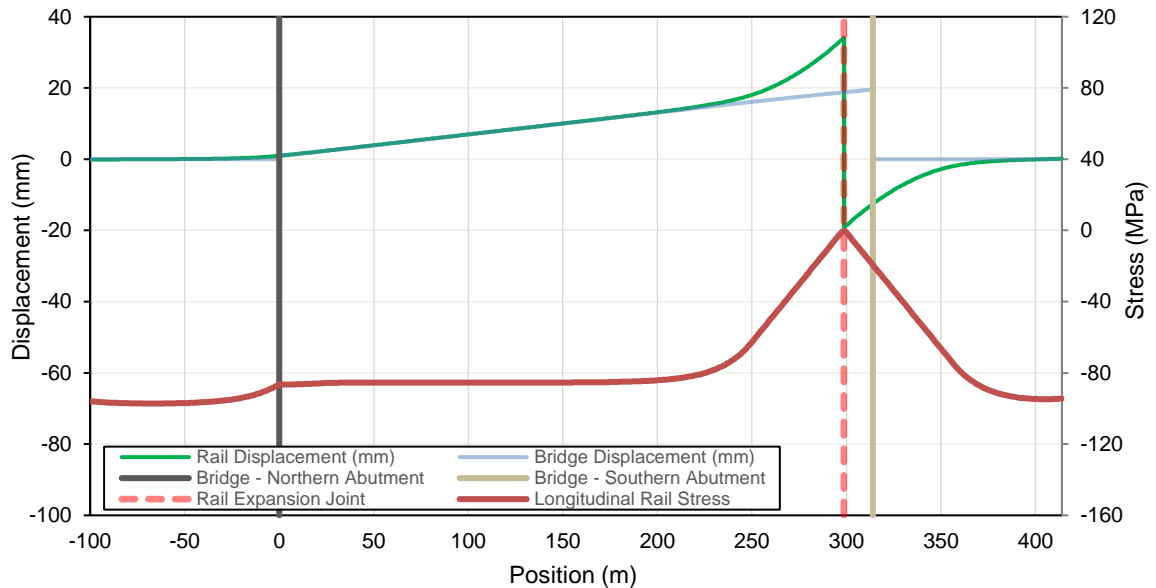
Figure 5.12: Midas Civil – Model 0A Calibration

Figure 5.12 demonstrates that track displacement is negligible on the embankment and then increases linearly as the bridge expands towards the right (south). Approximately 100m from the REJ, the rail displacement increases exponentially and is understood to be due to the track "breathing length" as described in Section 2.5.3 and Figure 1 of UIC Code 774-3R (2001). This "breathing length" results in differential displacement between the bridge and the rail at the REJ.

Rail axial stress results were also as expected with constant linear stress on the rail embankments slightly higher than rail axial stress on the bridge. The rail axial stress on the bridge, in compression, then decreases to zero at the REJ. On the southern embankment, again the rail is in maximum compression stress on the embankment which then decreases to zero at the REJ. The decrease in rail axial stress on the bridge deck is due to the increased fixity fastenings transferring additional load to the PY Track Slab.

The maximum displacement results from calibration Model 0A are summarised and compared to maximum site data results in Table 5.1.

Table 5.2: Model 0A calibration results compared with field data results

Description	Model 0A	Site Data
Maximum Rail Displacement (mm)	53.4 [(+34.1 rail slip north of REJ) - (-19.3 rail slip from south of REJ)]	25.9
Maximum Bridge Displacement (mm)	19.6	19.4

When comparing the calibration Model 0A data with the site investigation data (input temperature of 5.4 °C and 40.7 °C for bridge and rail respectively), it can be seen that the maximum bridge displacement from Model 0A (19.6 mm) compares well with the site data (19.4 mm) and further calibration of the bridge data is, therefore, not required.

In contrast, the maximum rail displacement for the calibration Model 0A was significantly higher than the maximum rail displacement for the site data results. This, however, was expected for this calibration case and can be explained as follows:

- Total rail expansion at the REJ is calculated as the sum of bridge expansion, rail displacement on the bridge, rail displacement from the northern abutment and rail displacement from the southern abutment.

- Bridge expansion results from the calibrated model are satisfactory and do not need further calibration. Rail displacement results from the calibration Model 0A are due to the longitudinal track resistance values adopted from UIC Code 774-3R (2001).

- UIC Code 774-3R (2001) longitudinal track resistance assumes constant stiffness for all sections of ballasted or Slab Track.

- Due to the high fixity fastening associated with the REJ switch blade (described in Table 3.2), differential displacement (rail slip) between the bridge and the rail north of the REJ is practically zero.

- From the calibration Model 0A data, rail slip to the north of the REJ was approximately 34.1 mm. The model, therefore, needs to be re-calibrated introducing high fixity fastenings at the REJ. Conversely, all rail slip is expected from the rail south of the REJ, which had

site data results of 25.9 mm in comparison to Model 0A results of 19.3 mm confirming low restraint fastenings must, therefore, be added to the model for the Stage 2 PY Track Slab.

5.2.2 Revised Boundary Conditions (Model 0B)

The large difference in rail displacement results between the calibration Model 0A and site investigation prompted the need for a second calibration iteration which incorporates high fixity fastenings on the north of the REJ and low restraint fastenings on the south of the REJ, as detailed in the description of the REJ, Section 3.3.5. Parameters adopted for Model 0B calibration are summarised in Table 5.3.

Table 5.3: Track-Bridge Interaction – Model 0B

Description	Value	Comment
Embankment Length (m)	100	Length of ballasted track on low chainage end of northern abutment and high chainage end of southern abutment
Bridge Deck Length (m)	314	Total length from fixed northern abutment to bridge expansion joint (expansion length over 10 spans)
REJ Position (m)	298.634	Position of REJ measured from northern fixed abutment based on data presented in Table 3.2
ZLR Position (mm)	N/A	ZLR not applicable for model calibration
Δ Bridge Temperature (°C)	5.4	Input load case for thermal load effect analysis based on data from Table 4.1
Δ Rail Temperature (°C)	40.7	Input load case for thermal load effect analysis based on data from Table 4.1
Ballast Resistance Unloaded (kN/m)	20	Unloaded ballasted track (good maintenance) / loaded track not applicable for thermal loading analysis (UIC 774-3R)
PY Track Slab Resistance Unloaded (kN/m)	40	Unloaded Slab Track / loaded track not applicable for thermal loading analysis (UIC 774-3R) including Stage 2 PY Track
PY Track Slab Stage 3 REJ Resistance Unloaded (kN/m)	∞	Infinite stiffness assigned over 12m at Stage 3 PY Track Slab REJ to simulate high fixity fasteners / web buttress supports
Δ Bridge Displacement (mm)	19.4	Expected output at BEJ based on data from Table 4.1
Δ Rail Displacement (mm)	25.9	Expected output at REJ based on data from Table 4.1
Differential (Bridge/Rail) (mm)	6.5	Expected differential displacement between bridge and rail based on data from Figure 4.11

For the Stage 1 PY Track Slab, the Slab Track longitudinal resistance as recommended by UIC Code 774-3R (2001) was adopted, namely, 40 kN/m for unloaded track. For the Stage 3 PY Track

Slab, the longitudinal track resistance was increased to an infinite stiffness to simulate the high fixity rail fastening (bolted) with fixed web clamped buttress supports that are bolted to the web of the switch blade REJ. The Slab Track longitudinal resistance of 40 kN/m for unloaded track was continued on the Stage 2 PY Track Slab at the southern abutment. This setup limits the ability for differential displacement between the switch blade REJ and the bridge, as demonstrated and discussed in Section 4.2.3.

With the high fixity restraint associated with the PY Track Slab Stage 3 REJ, longitudinal axial stress will increase as rail displacement is restrained. On the low restraint REJ stock rail, however, the rail south of the REJ is free to breathe and, therefore, experiences zero stress at the REJ.

The maximum rail stress experienced at the rail embankment and high fixity Stage 3 REJ is 97.25 MPa which is consistent with a restrained UIC60 rail section subject to a rail temperature of 40.7 °C (site input data).

In order to compare the Model 0B results with the site data in Table 5.3, the rail displacement, bridge displacement and rail stress were plotted against the bridge position:
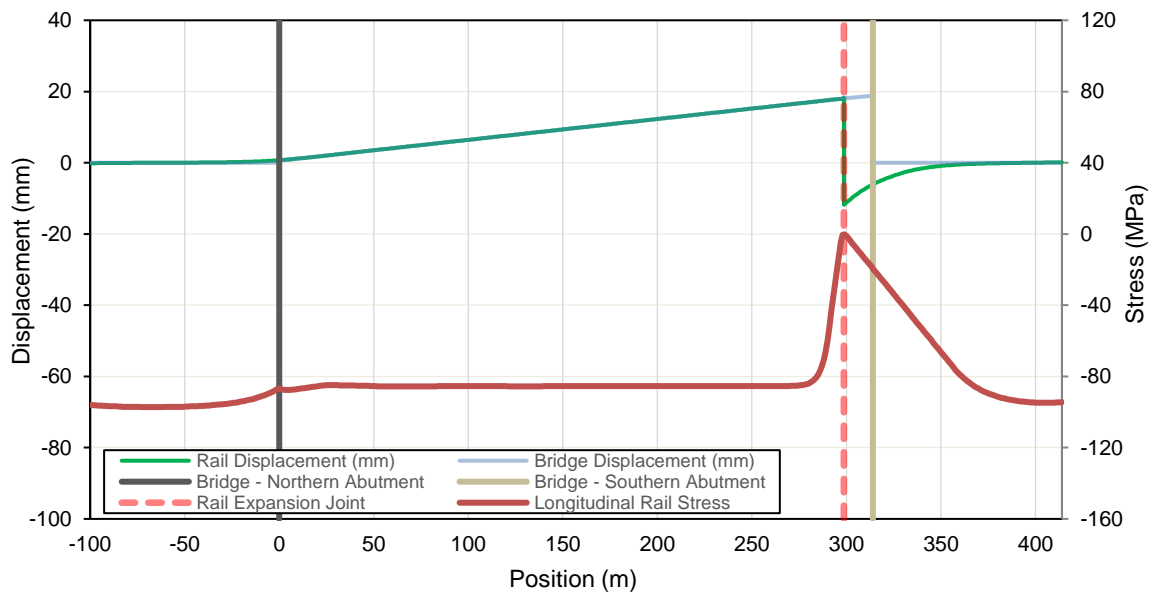

Figure 5.13: Midas Civil – Model 0B Calibration

The maximum displacement results from calibration Model 0B are summarised and compared to maximum site data results in Table 5.4.

Table 5.4: Model 0A calibration results compared with field data results

Description	Model 0B	Site Data
Maximum Rail Displacement (mm)	30.0 [(+18.2 rail slip north of REJ) - (-11.8 rail slip south of REJ)]	25.9
Maximum Bridge Displacement (mm)	18.6	19.4

When comparing the calibration Model 0B data with the site investigation data (input temperature of 5.4 °C and 40.7 °C for bridge and rail respectively), it can be seen that the maximum bridge displacement from Model 0B (18.6 mm) compares well with the site data (19.4 mm) and further calibration of the bridge data is, therefore, not required. It is, however, worth noting that the maximum bridge displacement decreased by ~1 mm between Model 0A and 0B. This result is expected and is due to the track with REJ interacting with the bridge as the stiffness between the bridge and rail increases at the fixed REJ section, as supported by Section 1.4.1 of UIC Code 774-3R (2001).

When comparing the calibration Model 0B data with the site investigation data (input temperature of 5.4 °C and 40.7 °C for bridge and rail respectively), it can be seen that the maximum rail displacement from Model 0B (30.0 mm) compares relatively well with the site data (25.9 mm). This is mainly attributed to the infinite stiffness applied to the PY Track Slab Stage 3 REJ.

5.3 TRACK-BRIDGE INTERACTION MODELLING SCENARIOS

5.3.1 Confirming the need for an REJ (Model 1A)

As discussed in Section 1.2, an objective of this study was to confirm the need for a rail expansion joint. The following method is proposed to confirm the need for an REJ at the Majuba Rail Bridge:

- Use the calibrated model developed in Section 5.2.2 for numerical analysis, noting that the longitudinal track resistance parameters as adopted from UIC Code 774-3R produced satisfactory results, with the exception of the adjusted high fixity restraints at the REJ switch blade.

- Remove the REJ from the model and baseline the maximum longitudinal rail stress as a result of thermal loading only, removing the additional stress due to bridge expansion by setting the bridge temperature variation to zero.

- With a baseline longitudinal rail stress (representing an embankment with Slab Track), add and quantify the effect of bridge expansion in addition to the baseline stress.

- Compare the additional rail stress with the **"maximum permissible additional compressive rail stress"** as recommended by UIC Code 774-3R (2001). It should be noted that the maximum permissible rail stress is 72 MPa and considers loading due to temperature, braking/acceleration and vertical load bending. This value was reduced by 30% on the basis that thermal loading may account for up to 70% of track-bridge interaction loading (Lee et al., 2015). Therefore, a maximum **additional** permissible rail stress of 50 MPa was used for ballasted track.

- It is worth noting that the 72 MPa **"maximum permissible additional compressive rail stress"**, as recommended by UIC Code 774-3R (2001), is derived from lateral buckling analysis of ballasted track. The lateral buckling of a Slab Track system will occur at a much higher rail stress. The 72 MPa adopted from UIC Code 774-3R (2001) serves as a "worst case scenario" considering the track transitions from Slab Track to ballasted track at each abutment. To further analyse the numerical modelling results, a **"maximum permissible additional compressive rail stress"** for Slab Track of 112 MPa (as recommended in CEN/TR17231:2017) was plotted on the rail stress graphs. Once again, this value was reduced by 30% on the basis that thermal loading may account for up to 70% of track-bridge interaction loading (Lee et al., 2015). Therefore, a maximum **additional** permissible rail stress of 78 MPa was used for Slab Track. The 72 MPa adopted from UIC Code 774-3R (2001) for ballasted track is a necessary failure mode due to the proximity of the ballasted track to the southern abutment and bridge expansion joint.

As described in Section 1.4.2 of UIC Code 774-3R (2001), the bridge and rail temperature do not deviate from their reference (neutral temperature) by more than 35 °C and 50 °C respectively.

Firstly, the load case was set to a zero bridge temperature variation with the rail temperature increasing by 50 °C. Without an REJ installed and without an increase in bridge temperature/ displacement, the CWR does not displace over the length of the bridge. A 50 °C increase in the CWR temperature results in 120 MPa compressive stress in the track [$E = 20$ GPa $/ \alpha = 1.2*10^{-5} / \Delta T = 50$ °C]. The 120 MPa compressive stress will be known as the "baseline stress" and represents CWR on an embankment, without the influence of bridge interaction.

Figure 5.14 represents the track displacement for the "baseline" case. The displacement profile represents the typical arrangement for CWR on an embankment as represented in Figure 1 in UIC Code 774-3R (2001) where zero displacement and maximum compressive force is expected in the middle section and displacement increases toward the end of the CWR (such as a fish plate or REJ) to zero stress. It can be seen from Figure 5.14 that when modelling the track-bridge interaction phenomenon, it is important to ensure that the embankment length is sufficient to avoid rail displacements on the embankment influencing the peak stress expected on the bridge deck. It is worth noting that Figure 5.14 is illustrative and exaggerated for discussion purposes and the maximum displacement at the end of the CWR in this figure is less than 0.2 mm.
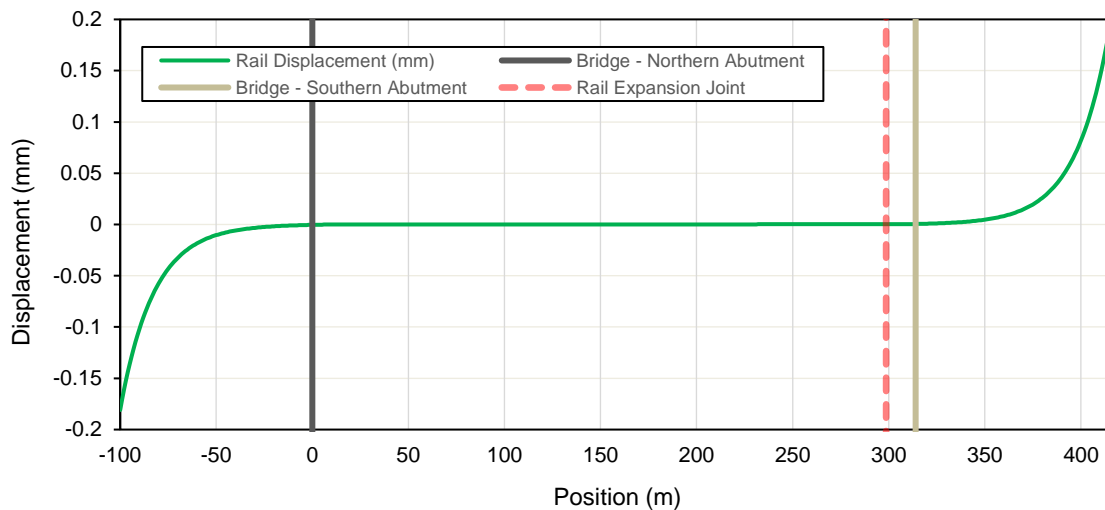
Figure 5.14: Midas Civil – Model 1A Displacement Output (T$_{BRIDGE}$ = 0 °C / T$_{RAIL}$ = 50 °C)

Following the determination of the 120 MPa "baseline stress" at T$_{BRIDGE}$ = 0 °C, the bridge temperature was increased to 35 °C, as prescribed in UIC Code 774-3R (2001), to determine the "additional peak stress" due to track-bridge interaction. The rail displacement and rail axial stress results are presented in Figure 5.15 and Figure 5.16 respectively. It can be seen that when the bridge breaths towards the southern abutment, it causes additional displacement in the rail towards the BEJ. The rail displacement on the bridge, however, is then opposed by the rail fixed to the southern embankment where displacement then decreases to zero at the end of the 100 m long embankment.
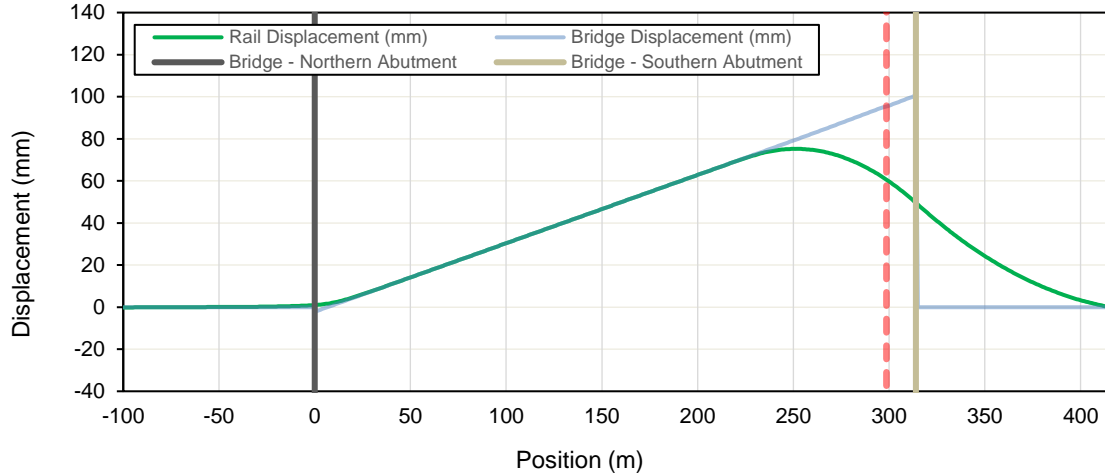
Figure 5.15: Midas Civil – Model 1A Displacement Output (T$_{BRIDGE}$ = 35 °C / T$_{RAIL}$ = 50 °C)

As the rail is restrained on the bridge deck, any movement of the bridge deck induces a movement of the CWR track and, therefore, additional rail stress.

Figure 5.16 represents the maximum compressive rail stress as a function of bridge position for Model 1A [No REJ / Slab / T$_{BRIDGE}$ = 35 °C / T$_{RAIL}$ = 50 °C]. It can be seen from Figure 5.16 that removing the REJ has major implications on the additional rail stress at the southern abutment BEJ where rail stress increases to a maximum of 283 MPa. Three limits are plotted on the stress profile diagram, namely, (1) maximum plain line rail stress representing expected rail stress on embankment sections, (2) 70% of the maximum permissible **additional** compressive stress (72 MPa for ballasted track) as recommended by UIC Code 774-3R (2001) Section 1.7.2 representing the thermal loading contribution only and (3) 70% of the maximum permissible **additional** compressive stress (112 MPa for Slab Track) as recommended by BS PD CEN/TR 17231 (2017) representing the thermal loading contribution only.
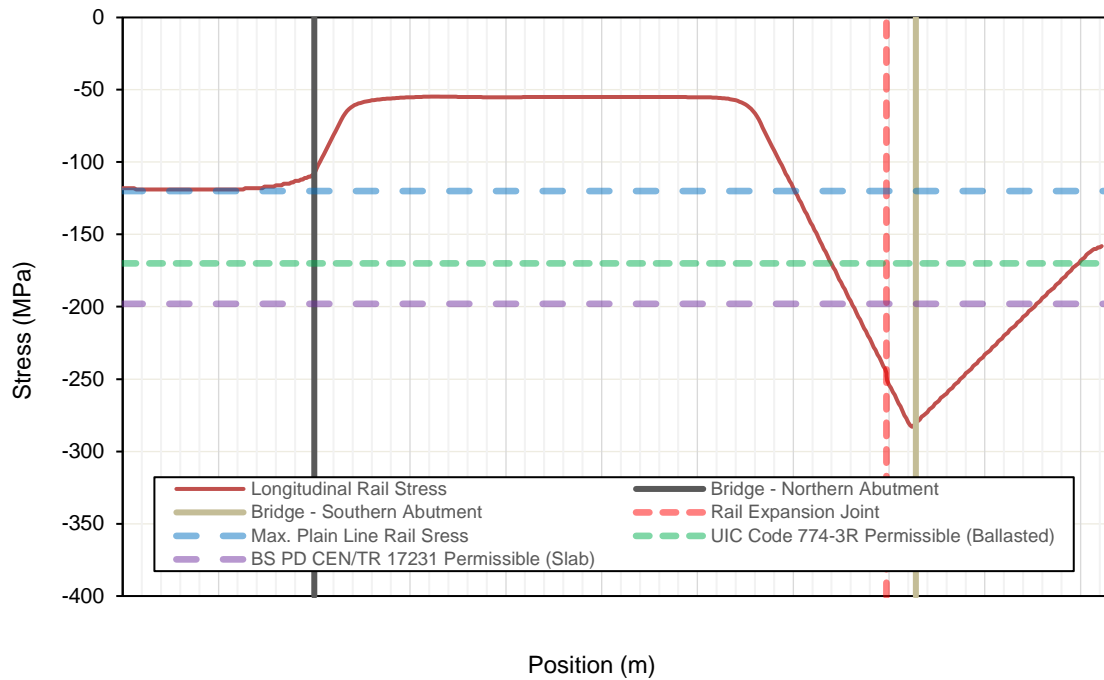
Figure 5.16: Midas Civil – Model 1A [No REJ / Slab / T$_{\text{BRIDGE}}$ = 35 °C / T$_{\text{RAIL}}$ = 50 °C]

It can be concluded that the need for a rail expansion joint on the Majuba Bridge is justified and high compressive rail stresses resulting in lateral buckling can be expected in the absence of an REJ for both ballasted track (UIC Code 774-3R (2001)) and Slab Track (BS PD CEN/TR 17231 (2017)). This is demonstrated in the photograph taken at the southern abutment of the bridge during permanent way construction (prior to the delivery and installation of the REJ) circa December 2016.

Figure 5.17: Lateral Buckling during Permanent Way Construction (prior to REJ installation)

Although the calibrated model is conclusive about the high compressive rail stress generated at the southern bridge abutment (BEJ), it has not yet been confirmed whether there is an alternative means to manage the additional rail stress due to track-bridge interaction. The following two additional models are, therefore, recommended to investigate the alternatives to an REJ:

- CWR with ballasted trackform (Model 2A)

- CWR with Slab Track and Zero Longitudinal Restraints (Model 2B)

5.3.2 CWR with Ballasted Trackform (Model 2A)

Figure 5.18 represents the maximum compressive rail stress as a function of bridge position for Model 2A [No REJ / Ballast / $T_{BRIDGE} = 35\ ^{\circ}C$ / $T_{RAIL} = 50\ ^{\circ}C$]. It can be seen from Figure 5.18 that although the use of ballasted trackform reduced the maximum compressive rail stress by approximately 16% (283 MPa to 244 MPa), the rail stress is still significantly higher than the maximum permissible **additional** compressive stress as recommended by UIC Code 774-3R (2001) Section 1.7.2 for ballasted track.

It is important to note that although the implementation of ballasted trackform on a long-span bridge may provide a reduction of additional compressive stress, as the ballast bed may provide a level of discontinuity between an expanding bridge and CWR, the implementation of a ballasted trackform as opposed to Slab Track may have significant impacts on the bridge structural design due to additional dead load. In addition, track-bridge interaction can result in excessive relative displacement between ballast and sleepers impacting the stability of the track (Esveld et al., 1995). Further investigation into the use of ballasted trackform on long-span bridges is, therefore, recommended.

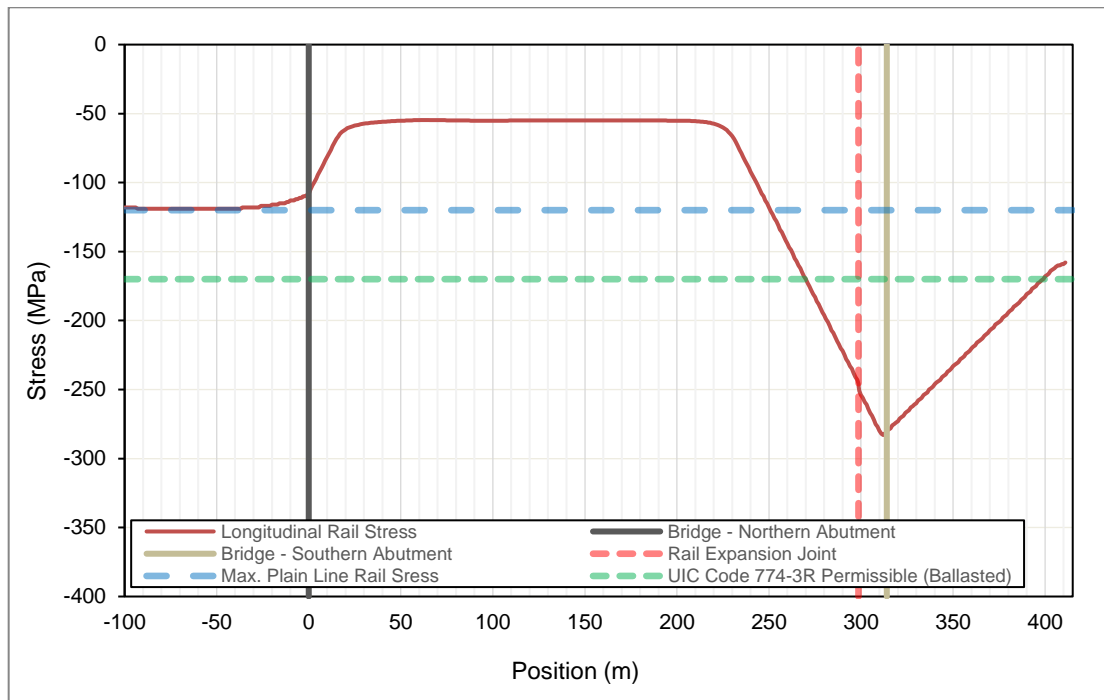**Figure 5.18: Midas Civil – Model 2A [No REJ / Ballast / TBRIDGE = 35 $^{\circ}$C / TRAIL = 50 $^{\circ}$C]**

5.3.3 CWR with Slab Track and Zero Longitudinal Restraints (Model 2B)

The alternative track-bridge interaction mitigation measure, using ZLR's, has successfully been implemented on several long-span ballasted bridges, for example, the Olifants River Bridge (South Africa) and a bridge on a high-speed line between Brussels – Lille on the junction for London/Paris (Esveld et al., 1995). The use of ZLR on Slab Track, however, has been limited in new railway projects due to lack of confidence in the design procedure and the non-availability of a dedicated design standard for Slab Track (Rhodes & Baxter, 2016). On the Bangkok MRTA Green Line, the design consultant worked with Pandrol to analyse additional rail stresses on continuous structures to justify the use of CWR with ZLR at peak stress locations as opposed to installing an REJ. Another example of an alternative to REJ's on long-span bridges was the use of low longitudinal resistance fastening systems on either side of pier locations on the Caulfield to Dandenong Level Crossing Removal Project in Melbourne, Australia (McManus et al., 2017). Refer to Section 2.1.2 and 2.5.2 for a comprehensive literature review of ZLR's.

The use of ZLR's can be incorporated into a numerical model by setting the bi-linear elastic link resistance to 0 kN/m. Based on the comprehensive literature review undertaken in Section 2.5.2, it can be concluded that common practice is to install ZLR's at key locations of a bridge structure, such as piers and abutments, with the aim of reducing peak rail stress in these locations. A similar approach was adopted in the Majuba Rail Bridge model where ZLR's were installed over a length of 10 m either side of the southern abutment BEJ (20 m total).
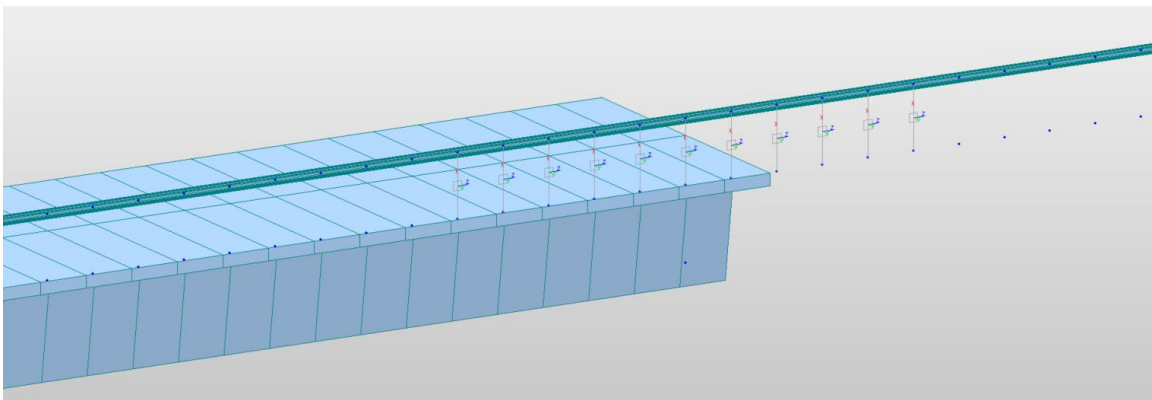
Figure 5.19: ZLR's installed at the Majuba Rail Bridge southern abutment

Figure 5.20 represents the maximum compressive rail stress as a function of bridge position for Model 2B [No REJ / ZLR's / $T_{BRIDGE} = 35\ °C$ / $T_{RAIL} = 50\ °C$].
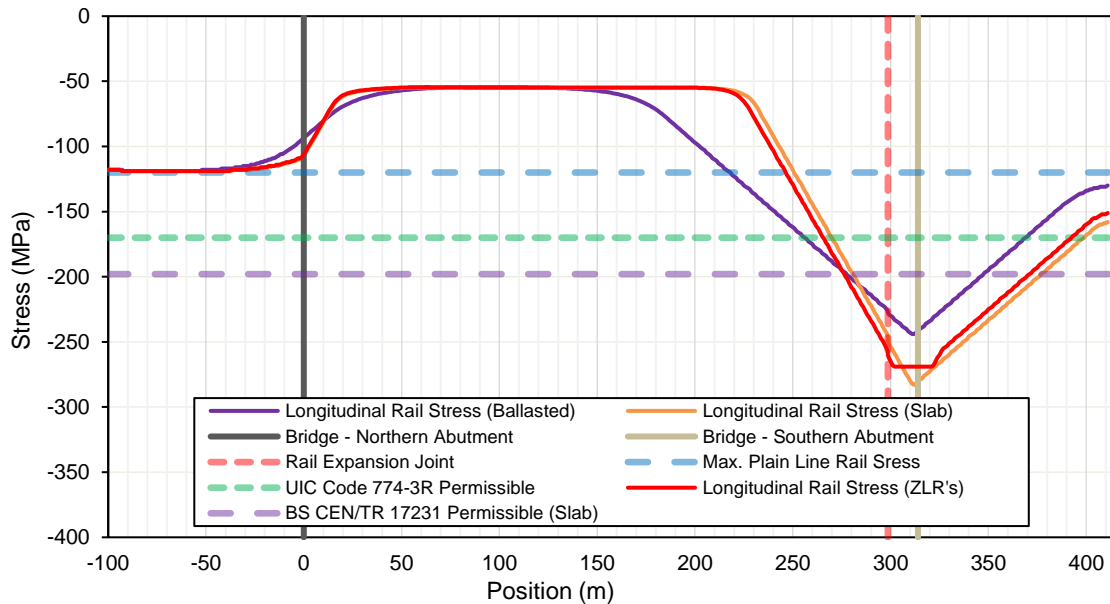
Figure 5.20: Midas Civil – Model 2B [No REJ / ZLR's / $T_{BRIDGE} = 35\ °C$ / $T_{RAIL} = 50\ °C$]

It can be seen from Figure 5.20 that the installation of ZLR's over a length of 20 m results in a very minor reduction in peak compressive rail stress for both ballasted track (UIC Code 774-3R (2017)) and Slab Track (BS PD CEN/TR 17231 (2017)) and can be deemed ineffective on the Majuba long-span bridge.

Although there has been several examples of the successful implementation of ZLR's on both freight and high speed lines (Esveld et al., 1995; Rhodes & Baxter, 2016; McManus et al., 2017), the bridge expansion lengths did not exceed 120 m in all three cases. Further consideration of bridge expansion length is, thus, discussed in Section 5.4.

The numerical analyses undertaken in Midas Civil Model 2B and the supporting literature listed above thus confirm that the use of ZLR's is not a feasible alternative to an REJ on the Majuba Rail Bridge.

5.4 THE EFFECT OF BRIDGE EXPANSION LENGTH (MODEL 3A)

Section 2.5.2 and UIC Code 774-3R (2001) Section 1.1.3.1 discuss the importance of bridge expansion length as a parameter in the track-bridge interaction phenomenon. The following key observations (in order of increasing expansion length) have been made with regard to bridge expansion length from the detailed literature review undertaken in Chapter 2:

- Network Rail in the UK limits the bridge expansion length to 30 m (Rhodes & Baxter, 2016).

- For a single bridge deck carrying CWR without alternative methods to reduce additional rail stress (such as a rail expansion device), it is generally accepted that the maximum expansion length will be 90 m for steel / concrete structures with concrete slab carrying ballasted track (UIC Code 774-3R, 2001).

- A bridge on a high-speed line between Brussels – Lille on the junction for London/Paris had a maximum span (expansion length) of 120 m (Esveld et al., 1995).

- A project in South East Asia included a 225 metre long balanced cantilever viaduct with two bridge expansion joints (reducing expansion length in half), supporting a double track railway with ballastless track (Rhodes & Baxter, 2016).

- The Caulfield to Dandenong Level Crossing Removal Project in Melbourne, Australia, considered low longitudinal resistance fastening systems on three elevated railway structures with maximum continuous spans (expansion lengths) of 120 m (McManus et al., 2017).

- The South African Railways (now Transnet) limited the use of ballasted CWR track to a maximum expansion length of 200 m where winged sleepers and ballast kerbs are recommended for expansion lengths greater than 100 m. For bridge expansion lengths greater than 200 m, the SAR recommended concrete Slab Track with an REJ (De Wet, 1989).

- The 1035 m long Olifants River Bridge with 495 m continuous sections are the longest known sections supporting CWR in the world (De Wet, 1989). On September 24th, 1982, a derailment occurred on the Olifants River Bridge due to a compression kick-out associated with track-bridge interaction forces and the absence of an REJ. Although an REJ was considered shortly after the derailment, a monitor/alarm system was recommended

instead due to the large movements and unique REJ required as well as a weak point being created in the track.

- Transnet Freight Rail released a "User Requirement Specification for Rail Expansion Joints (BBG2478)" (Meyer & Mistry, 2014). This specification states that REJ's are required on ballasted and Slab Track bridges for long-span bridges with a deck length of 500 m. There is no evidence that site investigations or numerical modelling were undertaken to support the 500 m length stated in specification BBG2478.

The research listed above shows a large variation in recommended or adopted parameters from 30 m for Network Rail, 90 m for UIC Code 774-3R (2001) to a maximum of 200 m recommended by SAR in the 1980's.

Extensive review of literature related to the Olifants River Bridge derailment in 1982 revealed that the Olifants River Bridge still operates with 495 m of CWR and monitors the exceedance of rail stresses, which occurs 3 times a year according to De Wet (1989). Although the restrictive operations and risk profile associated with the Olifants River Bridge expansion length may be deemed unacceptable in modern railways, the vast difference between this expansion length (495 m) and the examples quoted by Network Rail (30 m) and UIC Code 774-3R (90 m) is questionable.

A further numerical analysis was, therefore, undertaken in Midas Civil 2021 to confirm the maximum expansion length that can be accommodated before the maximum permissible **additional** compressive stress, as recommended by UIC Code 774-3R (2001) Section 1.7.2 (Ballasted Track) and BS PD CEN/TR 17231 (2017) (Slab Track), is exceeded.

Figure 5.21 represents the maximum compressive rail stress as a function of bridge position for Model 3A [No REJ / Slab Track / T_{BRIDGE} = 35 °C / T_{RAIL} = 50 °C].
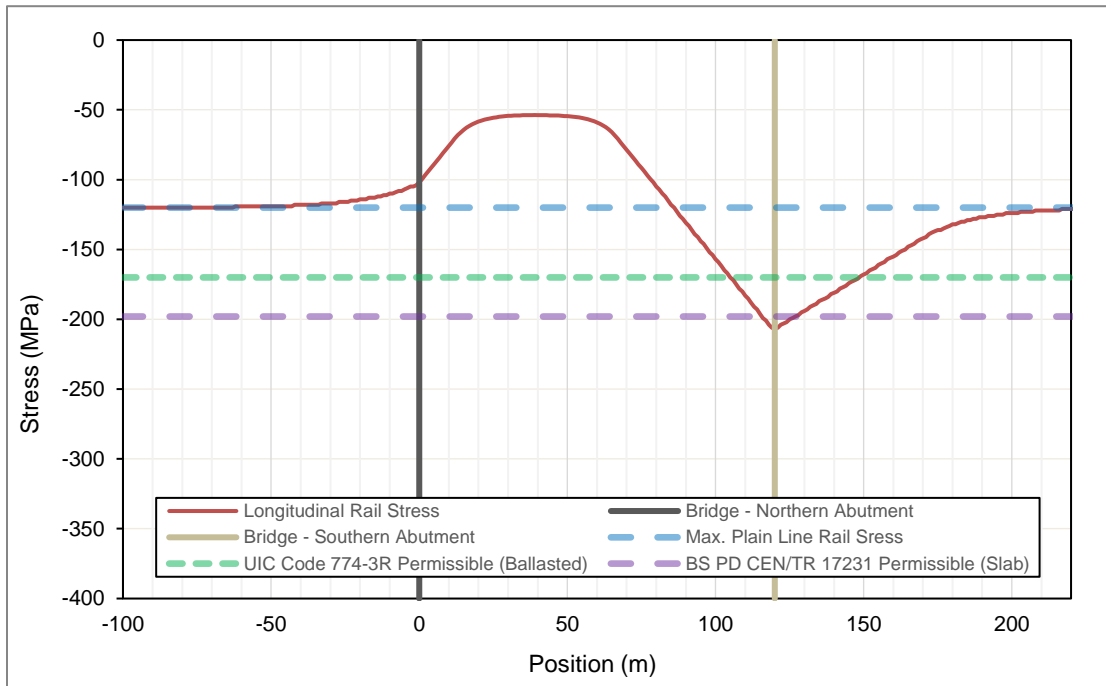
Figure 5.21: Midas Civil – Model 3A with reduced expansion length (120 m)

The results from Model 3A demonstrate that **additional** compressive rail stress can be reduced to permissible values, as per BS PD CEN/TR 17231 (2017) (Slab Track), by reducing the total Majuba Rail Bridge expansion length from 314 m to 120 m. However, the installation of ZLR's at the southern abutment will be required noting that the permissible **additional** compressive rail stress is exceeded by a minor 9 MPa.

Noting that the required bridge length of 314 m for the Majuba Rail Bridge is a function of typography, flood hydrology and geometric constraints, it is recommended that bridges of a similar length reduce expansion lengths by revising the static arrangement of the bridge by introducing bridge expansion joints.

As previously discussed, research shows a large variation in recommended parameters from 30 m for Network Rail, 90 m for UIC Code 774-3R (2001) to a maximum of 200 m recommended by SAR in the 1980's. The evaluation of the Majuba Rail Bridge indicates that expansion lengths recommended in various academic publications and standards can be further challenged. The vast difference in recommended values, ranging from 30 m to 200 m, supports the need for further evaluation of track-bridge interaction due to total bridge expansion length.

An interesting observation can be made from the results in Figure 5.21 noting that the recommended maximum bridge expansion length of 120 m compares well with results obtained

from Esveld et al. (1995), Rhodes & Baxter (2016), McManus et al. (2017) which adopted similar expansion lengths and further supports the need to challenge current permissible bridge expansion lengths across various codes and standards. These results also highlight that recommendations for a bridge expansion lengths of up to 200 m (SAR's in the 1980's) and the 495 m bridge expansion lengths on the Olifants River Bridge may result in unacceptable risk to most rail operators.

The numerical analysis also confirms that a bridge expansion length of up to 500 m without an REJ, as stated in the Transnet Freight Rail "User Requirement Specification for Rail Expansion Joints (BBG2478)", is unlikely and further review of the specification is recommended.

6   CONCLUSIONS AND RECOMMENDATIONS

The conclusions and recommendations from this dissertation study, related to the track-bridge interaction phenomenon, are discussed in this chapter.

6.1   CONCLUSIONS

The objectives and associated conclusions can be broadly defined into the following categories:

(1) Analysis of effective bridge temperature;

(2) Total bridge and rail displacement;

(3) Differential displacement and rail creep/slip;

(4) Longitudinal track stiffness and rail stress profile;

(5) Model calibration and the need for an REJ;

(6) Alternative methods to manage the track-bridge interaction phenomenon;

(7) The effect of bridge expansion length.

The following sections provide conclusions to the objective categories listed above.

6.1.1   Analysis of Effective Bridge Temperature

- Bridge temperature determination cannot be limited to a few ad-hoc temperature readings, for instance on the bridge deck only. Instead, a range of temperature readings are required through a bridge cross-section, including readings in the box girder.

- The concept of an effective bridge temperature, supported by literature published by Emerson et al. (1976), is an effective means of defining the uniform bridge deck temperature. Calculated effective bridge temperature results correlated well with bridge displacement measurements.

- Due to the large variations in temperature between the bridge deck surface and inside of the bridge deck, it is important to strategically place temperature probes/thermistors to obtain sufficient coverage and distribution throughout the bridge deck. Increasing the density of temperature readings increases the accuracy of a uniform effective bridge temperature.

- Although the bridge surface (top and sides) experience large temperature exposure as a result of direct sunlight, the temperature throughout the rest of the bridge cross-sectional area will experience significantly less temperature exposure as uniform bridge temperature

is a function of radiation, convection and conduction heat flow (Roeder, 2002). This supports a notion that an effective bridge temperature cannot be limited to a few ad-hoc temperature readings. Instead, continuous material temperature monitoring is required throughout the cross-section of the bridge.

6.1.2 Total Bridge and Rail Displacement

- On average, the LHS rail displaced approximately 25% more than the RHS and is likely attributed to the position of the sun, rising on the LHS of the bridge and the increased solar radiation before midday.

- Rapid increase in rail temperature occurs between approximately 06:00 am and 10:30 am and accounts for a large proportion, approximately 80%, of the rail force required to overcome the fastening system longitudinal restraint and cause uncontrolled slip of the rail.

- The rail and bridge displacement profiles generally correlate better with ambient air temperature as compared to either rail or bridge temperature. This is supported by literature for a study undertaken at the Olifants River Bridge by Maree (1987) that states "with a knowledge of daily fluctuations in air temperature the interaction forces for similar decks can be predicted".

6.1.3 Differential Displacement and Rail Creep/Slip

- Rail creep for the high fixity switch blade on the bridge accounted for less than 2% of the total rail creep and less than 0.5% of the total rail expansion. Rail creep due to the high fixity switch blade on the bridge is, therefore, negligible. Rail creep is, therefore, only a function of "breathing length" from the ballasted track on the embankment for this bridge and rail expansion joint configuration.

- Approximately 78% of the displacement at the REJ is due to the high fixity Slab Track rail being pulled by the bridge and the remaining 22% is due to the ballasted track on the embankment "breathing" towards the discontinuity at the REJ. Rail creep of the high fixity Slab Track is negligible.

- Uncontrolled slip of the ballasted embankment stock rail occurred at approximately 25 °C.

6.1.4 Longitudinal Track Stiffness and Rail Stress Profile

- The rail strain generally follows a similar uniform linear trend irrespective of the position on the bridge. This confirms that when an REJ is installed on a continuous bridge, the additional stress in the rail generally follows a linear trend, similar to the profile presented by Mirković et al. (2017).

- The maximum bridge displacement from the numerical model compares well with the site data for the input site temperature. This further supports the use of the effective bridge calculation method by Emerson (1976) for multiple temperature readings through a bridge cross-section.

- Rail axial stress profile results for the numerical model compared well with stress profiles presented by Mirković et al. (2017). For a continuous bridge with an REJ installed on one end, rail axial compression is generally higher on the rail embankment, decreasing towards the bridge deck and remaining constant on the bridge deck. The rail axial compression then decreases to zero at the REJ.

- The decrease in rail axial stress on the bridge deck is due to the increased fixity fasteners transferring additional load to the PY Track Slab. This supports the idea that peak axial rail stress due to track-bridge interaction can be managed by means of varying the fastening strength in strategic locations.

6.1.5 Model Calibration and the need for an REJ

- UIC Code 774-3R (2001) longitudinal track resistance values provide a reasonable initial calibration input, however, do not consider additional aspects of the site or REJ installation such as high or low fixity restraints in the proximity of an REJ.

- The high fixity rail fastening (bolted) with fixed web clamped buttress supports was successfully simulated by applying an infinite stiffness which limited the ability for differential displacement between the switch blade REJ and the bridge. This also contributes to the rail displacement for Model 0A converging to the rail displacement for the site data.

- As the stiffness between the bridge and rail increases at the fixed REJ section, the track further interacts with the bridge deck and limits bridge displacement, as supported by Section 1.4.1 of UIC Code 774-3R (2001).

- The need for a rail expansion joint for a 314 m bridge is justified and high compressive rail stresses resulting in lateral buckling can be expected in the absence of an REJ when comparing the results to the maximum permissible additional rail stress documented in UIC Code 774-3R (2001) for ballasted track and BS PD CEN/TR 17231 (2017) for Slab Track.

6.1.6 Alternative Methods to Manage the Track-bridge Interaction Phenomenon

- Although the use of ballasted trackform reduced the maximum compressive rail stress by approximately 16% (283 MPa to 244 MPa), the rail stress is still significantly higher than the maximum permissible **additional** compressive stress as recommended by UIC Code 774-3R (2001) Section 1.7.2.

- The installation of ZLR's over a length of 20 m at the southern abutment results in a very minor reduction in peak compressive rail stress and can be deemed as ineffective on the on a 314 m continuous bridge when comparing the results to the maximum permissible additional rail stress documented in UIC Code 774-3R (2001) for ballasted track and BS PD CEN/TR 17231 (2017) for Slab Track. The numerical analysis presented in this dissertation and literature by Esveld et al. (1995), Rhodes & Baxter (2016), McManus et al. (2017) thus confirm that the use of ZLR's is not a feasible alternative to an REJ on a 314 m continuous bridge deck.

6.1.7 The Effect of Bridge Expansion Length

- The results from Model 3A demonstrate that **additional** compressive rail stress can be reduced to permissible values, as per BS PD CEN/TR 17231 (2017) (Slab Track), by reducing the total Majuba Rail Bridge expansion length from 314 m to 120 m.

- An interesting observation can be made from the results in Figure 5.21 noting that the recommended maximum bridge expansion length of 120 m compares well with results published by Esveld et al. (1995), Rhodes & Baxter (2016) and McManus et al. (2017) which adopted similar expansion lengths and further supports the need to challenge current permissible bridge expansion lengths across various codes and standards. These results also highlight that recommendations for a bridge expansion lengths of up to 200 m (SAR's in the 1980's) and the 495 m bridge expansion lengths on the Olifants River Bridge may result in unacceptable risk to most rail operators.

6.2   RECOMMENDATIONS

The following recommendations are made for future research in this field:

- The calibration of the numerical model was based on load cases due to bridge and rail thermal loading only. To further validate the numerical model, it is recommended that additional site investigations are undertaken to consider load case effects due to vehicle braking/acceleration and bending due to vehicle vertical loading.

- This study primarily focussed on and was limited to permissible additional stresses in the rail stress due to track-bridge interaction. Support reactions in the bridge structure are a key consequence to consider in the track-bridge interaction phenomenon. It is believed that methods proposed in this dissertation to reduce the additional rail stress may have negative consequences on the bridge structure support reactions. It is recommended that further site investigation and numerical analysis is undertaken to further understand the impacts on the structure support reactions.

- Methods proposed to reduce the maximum permissible stress in the rail, such as increased fixity fastenings, may have a negative impact on structural member sizes, however, the ability to remove a rail expansion joint has positive impacts on infrastructure and maintenance cost as well as passenger comfort. It is, therefore, recommended that a whole of lifecycle cost analysis is considered when comparing the capital cost required for increased structural member sizes as opposed to installation of rail expansion devices.

- While UIC Code 774-3R (2001) longitudinal track resistance values provide a reasonable initial calibration input, further site investigation and supplier engagement is required to confirm the longitudinal track resistance of a particular product including elastic fastenings, high/low restraint fastenings and rail expansion joints. Further validation of the rail creep results presented in Section 4.2.3 can be confirmed by using testing methods described in BS EN 13146-1 (2012) Test methods for fastening systems Part 1: Determination of longitudinal rail restraint and is recommended, as further scope to this study.

- Although varying the fastening strength (low or high restraint) in strategic locations along the length of the bridge deck may reduce peak rail stress, the additional load transferred from the rail to the Slab Track, bridge deck, bearings and ultimately piers can have a

negative impact on the structure and further bridge design and analysis is recommended if alternative fastening methods are proposed.

- To confirm the need for a rail expansion joint, the additional rail stress due to bridge expansion was compared to the **"maximum permissible additional compressive rail stress"** as recommended by UIC Code 774-3R (2001) for ballasted track and BS PD CEN/TR 17231 (2017) for Slab Track. However, as the site investigation and numerical models were limited to thermal loading only, the maximum additional compressive rail stress was reduced by 30%. This assumption was made on the basis that thermal loading can account for up to 70% of track-bridge interaction forces whereas train acceleration/braking and bending due to vertical loading accounts for the remaining 30% (Lee et al., 2015). It is recommended that this assumption is further validated by undertaking the necessary field tests and calibrated numerical modelling to determine/quantify the effect of train braking/acceleration and vertical load on additional rail stress before considering alternatives to an REJ.

- When modelling the track-bridge interaction phenomenon, it is recommended that the embankment length is sufficient to avoid rail displacements on the embankment influencing the peak stress expected on the bridge deck.

- The implementation of a ballasted trackform as opposed to Slab Track may have significant impacts on the bridge structural design due to additional dead load. In addition, track-bridge interaction can result in excessive relative displacement between ballast and sleepers impacting the stability of the track (Esveld et al., 1995). Further investigation into the use of ballasted trackform on long-span bridges is, therefore, recommended.

- The installation of ZLR's over a length of 20 m at the southern abutment was proposed to evaluate the effectiveness of ZLR's on the 314 m bridge. It is important to note that the level and extent of low/zero longitudinal resistance is a compromise between the restraint required to limit the rail gap size and the desire to minimise the track-bridge interaction forces (Clemons, 1986). It is recommended that this compromise is well understood and considered in track-bride interaction analysis.

- Noting that the confirmation of bridge expansion length was out of the primary scope of this study, it was assumed that lateral buckling permissible levels of rail stress was the critical failure mode associated with the 314 m Majuba Rail Bridge. Due to the season in which the site investigation was undertaken, site data associated with rail breaks due to

contraction of rails was not obtained and, therefore, rail break failure modes were not investigated. It is acknowledged that a larger temperature variation in temperature may occur due to seasonal effects, however, the numerical analysis has considered temperature variations load cases as recommended in the UIC Code 774-3R (2001). To confirm these assumptions, it is recommended that further investigations are undertaken in the winter months to consider rail break and vertical track buckling failure modes.

- Research shows a large variation in recommended parameters from 30 m for Network Rail, 90 m for UIC Code 774-3R to a maximum of 200 m by SAR in the 1980's. The evaluation in this dissertation indicates that expansion lengths recommended in various literature can be further challenged noting that the recommended maximum bridge expansion length of 120 m compares well with results obtained from Esveld et al. (1995), Rhodes & Baxter (2016) and McManus et al. (2017) which adopted similar expansion lengths and further supports the need to challenge current permissible bridge expansion lengths across various codes and standards. These results also highlight that recommendations for a bridge expansion lengths of up to 200 m (SAR's in the 1980's) and the 495 m bridge expansion lengths on the Olifants River Bridge may result in unacceptable risk to most rail operators. The vast difference in recommended values, ranging from 30 m - 200 m, supports the recommendation for further evaluation of track-bridge interaction phenomenon due to total bridge expansion length.

- Noting that the required bridge length of 314 m for the Majuba Rail Bridge is a function of typography, flood hydrology and geometric constraints, it is recommended that bridges of a similar length reduce expansion lengths by revising the static arrangement of the bridge by introducing bridge expansion joints.

- The numerical analysis also confirms that a bridge expansion length of up to 500 m without an REJ, as stated in the Transnet Freight Rail "User Requirement Specification for Rail Expansion Joints (BBG2478)", is unlikely and further review of the specification is recommended.

- Considering the Midas Civil Rail Structure Interaction Wizard takes UIC Code 774-3R (2001) as the basis for analysis, it is recommended that the numerical analysis undertaken in this study is confirmed with alternative modelling methods and software to validate the results.

7   REFERENCES

Anon., 2018. PY track slab and the PRASA stray current project. *The official publication of the Concrete Society of Southern Africa NPC,* 2018(155), pp. 8-16.

AREMA, 2003. *Practical Guide to Railway Engineering.* 2nd ed. Lanham, MD, USA: American Railway Engineering and Maintenance-of-way Association.

Bartlett, D. L., Tuora, J. & Smith, G. R., 1961. *Experiments on the stability of long welded rails,* London, UK: British Transport Commission.

Bastin, R., 2006. Development of German non-ballasted track forms. *Transport,* 159(1), pp. 25-39.

Benaim, R., 2019. *The Design of Prestressed Concrete Bridges.* 1st ed. CRC Press.

BS EN 13146-1, 2012. *Railway applications – Track – Test methods for fastening systems Part 1: Determination of longitudinal rail restraint.*

BS EN 13146-4, 2012. *Railway applications – Track – Test methods for fastening systems Part 4: Effect of repeated loading.*

BS EN 13481-5, 2012. *Railway Applications - Track - Performance requirements for fastening systems - Part 5: Fastening systems for ballastless track.*

Campbell Scientific, 2021. *Campbell Scientific.* [Online] Available at: https://www.campbellsci.com.au/cr800 [Accessed 25 May 2021].

Choi, I., 2020. *Case Study: L&T Construction | Rail Structure Interaction of Railway Bridge in Hyderabad, India.* [Online] Available at: https://www.youtube.com/ [Accessed 15 June 2021].

Clemons, R. E., 1986. *Continuously Welded Rail on BART Aerial Structures,* Washington D.C.: Transportation Research Board, Transportation Research Record No. 1071.

Committee of State Road Authorities, 1981. *Code of Practice for the Design of Highway Bridges and Culverts in South Africa TMH7 Parts 1 and 2,* Pretoria, South Africa.

Corven, J., 2016. *Post-Tensioned Box Girder Design Manual,* Washington DC: Federal Highway Administration.

De Wet, H., 1989. *Track Stability Considerations in the Design of Railway Bridges.* Brisbane, Australia, Proceedings of the Fourth International Heavy Haul Railway Conference.

Dickinson, R. E., 2003. Land-Atmosphere Interactions - Overview. In: J. R. Holton, ed. *Encyclopedia of Atmospheric Sciences.* Seattle: Elsevier Science Ltd., pp. 1116-1120.

Dupont, 2021. [Online] Available at: https://www.dupont.com/knowledge/

durable-rail-pads-for-freight-lines.html [Accessed 25 04 2021].

Emerson, M., 1976. *Bridge temperature estimated from the shade temperature,* Crowthorne, England: Crowthorne: TRRL Report SR 696.

Emerson, M., Black, W. & Moss, D., 1976. *Bridge temperatures derived from measurement of movement,* Crowthorne: Transport and Road Research Laboratory.

Esveld, C., 2001. *Modern Railway Track.* 2nd ed. Delft: Delft University of Technology.

Esveld, C., 2003. *Recent Developments in Slab Track,* Delft, Netherlands: Publication of the Department of Civil Engineering, Section of Roads & Railways, Deflt University.

Esveld, C., Delhez, R., Godart, P. & Mijs, J., 1995. Avoidance of expansion joints in high-speed CWR. *Rail Engineering International,* 3(1), pp. 7-9.

Getzner, 2019. *Long-Term Test of Rail Pads on a Heavy Traffic Route*.

Gräbe, P. J., Freyer, R. V. & Furno, R. F., 2007. *An Intelligent Condition Monitoring System for the Management of Continuously Welded Rails*, Proceedings of the International Heavy Haul Association Conference, Kiruna, Sweden, pp. 579-586.

Gräbe, P. J. & Jacobs, D., 2015. The effects of fastening strength on the variation in stress-free temperature in continuous welded rail. *Journal of Rail and Rapid Transit,* 230(3).

Gräbe, P. J. & Lubout, N., 2012. Performance of resilient rail pads used in Tubular Modular Track under South African service conditions. *SAICE Civil Engineering,* May, 2012(4), pp. 20-22.

Gräbe, P. J. & van Schoor, B., 2012. An inside look at the stresses due to lateral forces in Tubular Modular Track. *SAICE Civil Engineering,* 20(4), pp. 15-18.

Grissom, G. T. & Kerr, A. D., 2006. Analysis of Lateral Track Buckling using new frame-type equations. *International Journal of Mechanical Science,* Volume 48, pp. 21-32.

Hoang, T. et al., 2019. *Monitoring of non-ballasted railway tracks in tunnel: development of a robot for the automatic detection of damaged concrete blocks.* Tokyo, Japan, 12th World Congress on Railway Research (WCCR).

Krkoška, L. & Moravčik, M., 2015. The analysis of thermal effect on concrete box girder bridge. *Theoretical Foundation of Civil Engineering,* 111(1), pp. 470-477.

Kumar, R. & Upadhyay, A., 2012. Effect of temperature gradient on track-bridge interaction. *Interaction and Multiscale Mechanics,* 5(1), pp. 1-12.

Kuppa, S. & Roeder, C., 1991. *Thermal movements in bridges*: Final Report to NSF.

Lee, K. C., Jang, S. Y. & Jung, D. K., 2015. *Rail-Structure Interaction Analysis of Sliding Slab Track on Bridge.* San-Jose, California, Proceedings of the 2015 Joint Rail Conference.

Lee, K., Jang, S. & Lee, J., 2017. *Development of Sliding Slab Track to Reduce Track–Bridge Interaction.* Chengdu, International Conference on Rail Transportation.

Lichtberger, B., 2011. *Track Compendium.* 2 ed. Hamburg, Germany: Eurailpress.

Lim, N., Park, H. & Kang, Y., 2003. Stability of Continuously Welded Track. *Journal of Computers and Structures,* 81(22-23), pp. 2219-2236.

Lombard, P. C., 1978. *Continuously Welded Rails.* Durban, South Africa, Proceeding of the 6th 5-Yearly SAICE Conference.

Louw, P., 2009. Railway Track Material and Maintenance in South Africa. *SAICE Civil Engineering,* 17(4), pp. 43-52.

Maree, H., 1987. Forces in the railway track structure on the Olifants River Bridge. *Reports in Applied Measurement,* 3(1).

Maree, J. S., 1993. *Aspects of resilient pads.* Beijing, China, International Heavy Haul Association (ed.) Proceedings of the 5th International Heavy Haul Association Conference, pp. 433-439.

Marutla, M. A., Mistry, K., van Aardt, J. H. P. & Mtetwa, C. Q., 2012. *Manual for Track Maintenance (BBB0481),* Johanessburg: Transnet Freight Rail.

McManus, A., Costa, L. & Gupta, A., 2017. *Rail Structure Interaction For Multiple Span Railway Viaducts With Direct Fixed Track,* Australia: Austroads.

METER Group, 2018. [Online] Available at: http://library.metergroup.com/Manuals /20635_ATMOS41_Manual_Web.pdf [Accessed 24 May 2021].

Meyer, J. & Mistry, K. C., 2014. *User requirment specification for rail expansion joints (BBG2478),* Johannesburg, South Africa: Transnet Freight Rail.

Meyer, J., Mistry, K. & Marutla, F., 2013. *Specification for Rail Fastening Systems (BBF9273),* Johannesburg, South Africa: Transnet Freight Rail.

Midas Civil, 2021. *Rail Structure Interaction Wizard in midas Civil.* [Online] Available at: https://www.midasbridge.com/en/blog/tipstutorials/rail-structure-interaction-wizard-in-midas civil [Accessed 15 June 2021].

Mirković, N., Popović, Z., Lazarević, L. & Vilotijević, M., 2017. *Track/bridge interaction - the aspect of bridge structure.* Doboj, VI International Symposium of transport and communications.

Mundrey, J. S., 2017. *Railway Track Engineering.* 5th ed. India: Mc Graw Hill.

Ni, Y. Q., Hua, X. G., Wong, K. Y. & Ko, J. M., 2007. Assessment of Bridge Expansion Joints Using Long-Term Displacement and Temperature Measurement. *Journal of Performance of Constructed Facilities,* 21(2).

Rhodes, D. & Baxter, M., 2016. *Interaction between Ballastless Track and Bridge Structures on High Speed Lines.* Manchester, UK, Journal of Proceedings: The Permanent Way Institution & The Union of European Engineer Associations.

Rhodes, D. & Cox, S. J., 2013. *Rail fastenings for heavy haul and extreme longitudinal forces.* New Dehli, India, International Heavy Haul Association (ed.) Proceedings of the International Heavy Haul Association Conference, pp. 123-126.

Rhodes, D., Leeves, G. G. & Cox, S. J., 1989. *Rail Pads for Concrete Sleepers in Heavy Haul Track.* Brisbane, Australia, International Heavy Haul Association (ed.) Proceedings of the International Heavy Haul Association Conference, pp. 286-290.

Rhodes, D., Maree, J. S. & Barthram, P., 2005. *Track design for extreme traction and braking forces.* Rio de Janeiro, Brazil, Proceedings of the 7th International Heavy Haul Conference, pp. 271-276.

Rodrigues, C., Mendonca, C., Jorge, C. & Bicalho, B., 2009. *Managing the Rail Thermal Stresses Levels at MRS Tracks – Brazil.* Shanghai, China, Proceeding of the 9th International Heavy Haul Conference.

Roeder, C. W., 2002. *Thermal Movement Design Procedure for Steel and Concrete Bridges,* Seattle, WA: National Cooperative Highway Research Program NCHRP 20-07/106.

Roeder, C. W., 2002. *Thermal Movement Design Procedure for Steel and Concrete Bridges,* Washington: National Cooperative Highway Research Program.

Selig, E. T. & Waters, J. M., 1994. *Track Geotechnology and Substructure Management.* 1st ed. Derby, England: Thomas Telford.

Shaw, F. J., Gräbe, P. J. & Maree, J. S., 2007. *Finite Element Analyses of Standard Gauge Conventional Track,* Johannesburg, South Africa: Spoornet Railway Engineering and Technology Management.

Sonneville AG, 2011. *Low Vibration Track System (LVT) System Description,* Müntschemier, Switzerland: Sonneville AG.

Stanton, J. F. & Roeder, C. W., 1982. *Elastomeric Bearings Design, Construction and Materials,* Seattle, WA: National Cooperative Highway Research Program NCHRP 248.

STN EN 1991-1-5 , 2003. *Actions on Structures. Part 1-5: General Actions - Thermal actions,* Brussels: European Committee for Standardization.

Strauss, A. et al., 2018. Nonlinear Finite Element Analysis of Continuous Welded Rail–Bridge Interaction: Monitoring-Based Calibration. *Journal of Civil Engineering and Management,* 24(4), pp. 344-354.

Sung, W., Shih, M., Lin, C. & Go, C., 2005. The critical loading for lateral buckling of continuous welded rail. *Journal of Zhejiang University Science,* 6A(8), pp. 878-885.

Szelazek, J., 1992. Ultrasonic Measurement of Thermal Stresses in Continuously Welded Rails. *Journal of NDT & E,* 25(2), pp. 77-85.

Tayabji, S. & Bilow, D., 2001. Concrete Slab Track State of the Practice. *Transportation Research Record Journal of the Transportation Research Board,* 10(3141/1742-11), pp. 87-96.

Transportation Research Board, 2000. *Track Design Handbook for Light Rail Transit.* Washington D.C.: National Academy Press.

Turner, H., Kerkovius, A., Oborn, T. & Trantino, V., 2011. *Seaford Rail Viaduct: launching a kilometre.* Sydney, Australia, Proceedings of the 8th Austroads Bridge Conference.

Tzanakakis, K., 2013. *The Railway Track and Its Long Term Behaviour.* 1st ed. Berlin: Springer.

UIC Code 774-3R, 2001. Track/bridge Interaction: Recommendations for calculations. *Paris, France.*

University of Pretoria, 2010. *Introductory Course on Multi-Disciplinary Concepts in Railway Engineering,* Pretoria, Gauteng, South Africa: Continuing Education at the University of Pretoria.

Wagner, H. & Gräbe, P. J., 2018. Slab track test section for University of Pretoria Railway Research Facility. *SAICE Civil Engineering,* 2018(4), pp. 36-38.

Wegner, A., 2009. *Quality Assessment of Continuously Welded Tracks by Nondestructive Testing of Stress-Free Temperature.* Shanghai, China, Proceedings of the 9th International Haul Conference.

APPENDIX A   DERIVATIONS

EFFECTIVE BRIDGE TEMPERATURE

The equation for determining effective bridge temperature is derived by considering two adjacent bridge sections of unit length. One section being concrete and the other steel. Each section has an associated area (A_1, A_2), Elastic Modulus (E_1, E_2) and Thermal Expansion Coefficient (α_1, α_2). Assuming the concrete and steel sections are both subjected to the same change in temperature (ΔT), a unit length of concrete would expand by $\alpha_1.\Delta T$ and a unit length of steel would expand by $\alpha_2.\Delta T$, if the sections were free to expand independently. However, the composite bridge section is bonded together and, therefore, both the concrete and steel sections must expand together by a length (x). The axial load in the concrete and steel sections can be determined as follows:

$$P_{conc} = A_1 \, E_1 \, (\alpha_1 \, \Delta T - x) \qquad \text{(Eq. A-1)}$$
$$P_{steel} = A_2 \, E_2 \, (\alpha_2 \, \Delta T - x) \qquad \text{(Eq. A-2)}$$

Where:

P = Axial load of concrete or steel (N)

A = Area of concrete or steel (m^2)

E = Elastic Modulus of concrete or steel (MPa)

α = Expansion coefficient of concrete or steel ($^1/_{\circ C}$)

ΔT = Change in tempearture (°C)

In an unconstrained system where the bridge is free to expand, the resultant axial load is zero and thus $P_{conc} = P_{steel}$ therefore:

$$A_1 \, E_1 \, (\alpha_1 \, \Delta T - x) = A_2 \, E_2 \, (\alpha_2 \, \Delta T - x) \qquad \text{(Eq. A-3)}$$

or

$$x = \left(\frac{A_1 E_1 \alpha_1 + A_2 E_2 \alpha_2}{A_1 E_1 + A_2 E_2} \right) \Delta T \qquad \text{(Eq. A-4)}$$

Comparing Equation A-5 with $L = \alpha \, T$, it can be seen that $\left(\frac{A_1 E_1 \alpha_1 + A_2 E_2 \alpha_2}{A_1 E_1 + A_2 E_2} \right)$ is equivalent to the "mean" coefficient of expansion of the non-homogenous section i.e., α_m. The displacement of a composite bridge is as a result of a mean expansion coefficient (α_m) and change in effective bridge temperature (ΔT_e).

Now assuming that the concrete and steel sections are subjected to a change in temperature of ΔT_1 and ΔT_2 respectively, the equation becomes:

$$x = \left(\frac{A_1 E_1 \alpha_1 \Delta T_1 + A_2 E_2 \alpha_2 \Delta T_2}{A_1 E_1 + A_2 E_2}\right) \qquad \text{(Eq. A-5)}$$

Let $x = \alpha_m T_e$ where T_e is the change of effective bridge temperature, then from Equation A-5 and A-6:

$$\left(\frac{A_1 E_1 \alpha_1 \Delta T_1 + A_2 E_2 \alpha_2 \Delta T_2}{A_1 E_1 + A_2 E_2}\right) = \left(\frac{A_1 E_1 \alpha_1 + A_2 E_2 \alpha_2}{A_1 E_1 + A_2 E_2}\right) \Delta T \qquad \text{(Eq. A-6)}$$

or

$$\Delta T_e = \left(\frac{A_1 \alpha_1 \Delta T_1 + A_2 \alpha_2 \Delta T_2}{A_1 \alpha_1 + A_2 \alpha_1}\right) \qquad \text{(Eq. A-7)}$$

If the bridge material is homogenous, then $E_1 = E_2$ and $\alpha_1 = \alpha_2 = \alpha$ and Equation A-8 can be simplified to:

$$\Delta T_e = \left(\frac{A_1 \Delta T_1 + A_2 \Delta T_2}{A_1 + A_2}\right) \qquad \text{(Eq. A-8)}$$

Where ΔT_e represents the change in effective temperature for a bridge structure.

FORCE INDUCED IN THE RAIL

The force (P) induced in a rail, in the central zone of CWR, when a change in temperature has occurred may be derived from the analogy of a beam fixed at both ends undergoing a temperature increase.

The derivation of thermal loading can be described as follows:

Strain due to temperature change:

$$\varepsilon_t = \frac{\Delta L}{L} = \alpha \, \Delta t \qquad\qquad \text{(Eq. A-9)}$$

If both ends are restrained a force is generated:

$$\varepsilon_P = \frac{\sigma_P}{E} = \frac{P}{A.E} \qquad\qquad \text{(Eq. A-10)}$$

For a beam fixed at both ends:

$$\varepsilon_t - \varepsilon_P = 0 \qquad\qquad \text{(Eq. A-11)}$$

Substituting Equation (A-9) and (A-10) into (A-11) yields Equation (A-12):

$$P = \alpha \, \Delta T \, E \, A \qquad\qquad \text{(Eq. A-12)}$$

Where:

ε_T = Strain due to temperature change
ε_P = Strain due to induced force
L = Length of rail (m)
α = Expansion coefficient of steel ($1/_{°C}$)
ΔT = Change in temperature (°C)
E = Elastic Modulusof rail steel (GPa)
A = Cross sectional area of rail (m^2)
P = Force induced in the rail (N)
σ_P = Stress induced in rail caused by induced force (MPa)

The temperature change (ΔT) is the difference between the current rail temperature (T_R) and the stress free temperature.

$$\Delta T = \text{Rail temperature} - \text{SFT} \qquad\qquad \text{(Eq. A-13)}$$

APPENDIX B   TEMPERATURE & DISPLACEMENT DATA
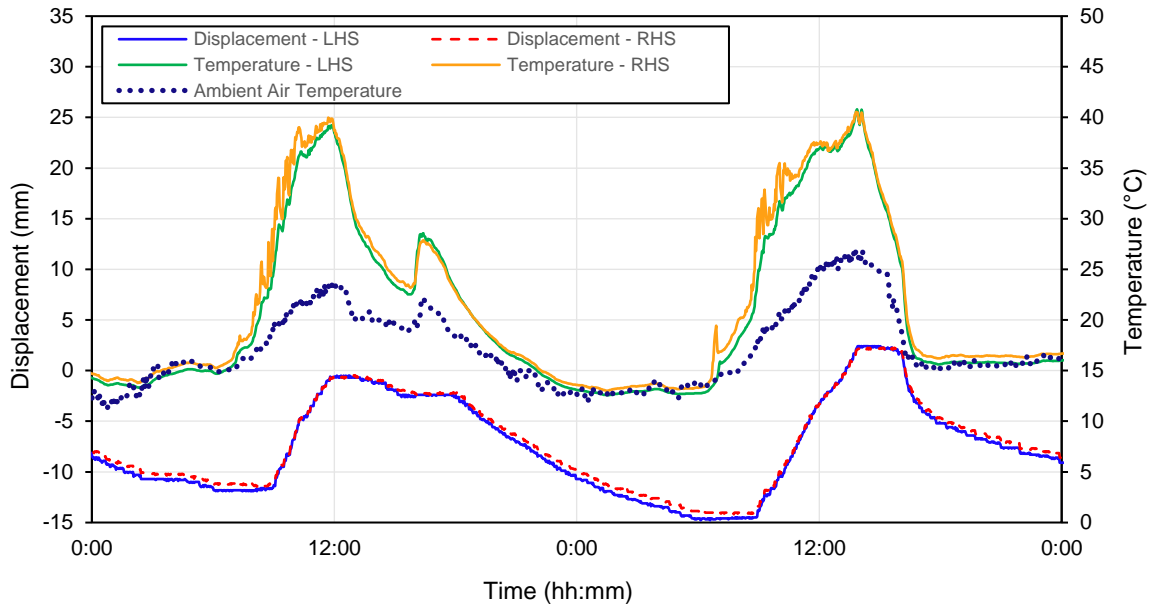
**Figure B.1: Site A - Rail Temperature and Rail Displacement in March 2018**
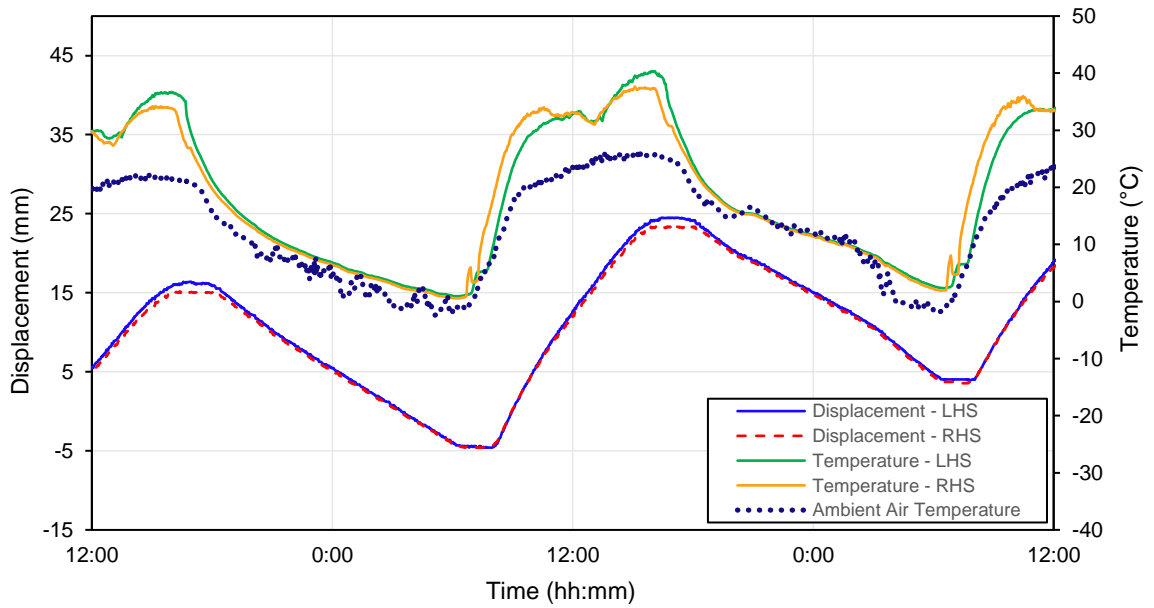
Figure B.2: Site A - Rail Temperature and Rail Displacement in September 2018
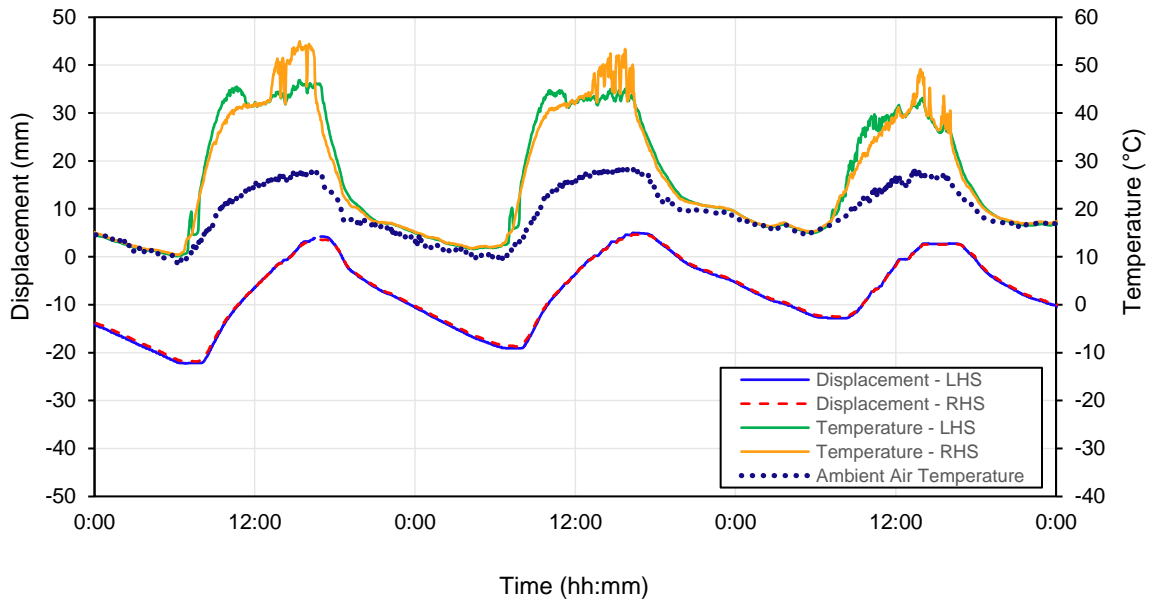
Figure B.3: Site A - Rail Temperature and Rail Displacement in March 2019

Table B-1: Site A - Rail Temperature and Rail Displacement in March 2018

Period	Description	ΔX LHS (mm)	ΔX RHS (mm)	ΔT LHS (°C)	ΔT RHS (°C)
Day 1 AM Peak	Time	6:08:00	8:10:00	2:20:00	2:16:00
	Value	-11.90	-11.48	13.30	13.79
Day 1 PM Peak	Time	12:08:00	12:58:00	11:52:00	11:42:00
	Value	-0.50	-0.47	39.22	39.98
Day 2 AM Peak	Time	6:08:00	7:46:00	1:28:00	1:26:00
	Value	-14.80	-14.19	12.58	13.02
Day 2 PM Peak	Time	13:54:00	14:06:00	13:52:00	13:50:00
	Value	2.40	2.25	40.79	40.54

Table B-2: Site A - Rail Temperature and Rail Displacement in September 2018

Period	Description	ΔX LHS (mm)	ΔX RHS (mm)	ΔT LHS (°C)	ΔT RHS (°C)
Day 1 AM Peak	Time	16:34:00	16:24:00	16:00:00	15:10:00
	Value	16.38	15.16	36.71	34.25
Day 1 PM Peak	Time	6:50:00	6:36:00	6:14:00	6:08:00
	Value	-4.60	-4.60	0.94	0.55
Day 2 AM Peak	Time	16:26:00	15:54:00	15:56:00	15:06:00
	Value	24.51	23.37	40.36	37.68
Day 2 PM Peak	Time	6:34:00	7:18:00	6:28:00	6:24:00
	Value	3.94	3.54	2.33	1.90

Table B-3: Site A - Rail Temperature and Rail Bridge Displacement in March 2019

Period	Description	ΔX LHS (mm)	ΔX RHS (mm)	ΔT LHS (°C)	ΔT RHS (°C)
Day 1 AM Peak	Time	6:52:00	7:30:00	6:14:00	6:18:00
	Value	-22.21	-21.84	10.15	10.36
Day 1 PM Peak	Time	17:00:00	16:56:00	15:22:00	15:22:00
	Value	4.22	3.56	46.92	54.95
Day 2 AM Peak	Time	7:36:00	7:36:00	4:28:00	4:10:00
	Value	-19.08	-18.70	11.62	11.71
Day 2 PM Peak	Time	16:20:00	16:20:00	15:46:00	15:44:00
	Value	4.99	4.64	45.11	53.34
Day 3 AM Peak	Time	7:40:00	7:38:00	5:44:00	5:48:00
	Value	-12.83	-12.51	14.96	15.27
Day 3 PM Peak	Time	16:08:00	16:32:00	14:00:00	13:50:00
	Value	2.78	2.60	43.13	49.17
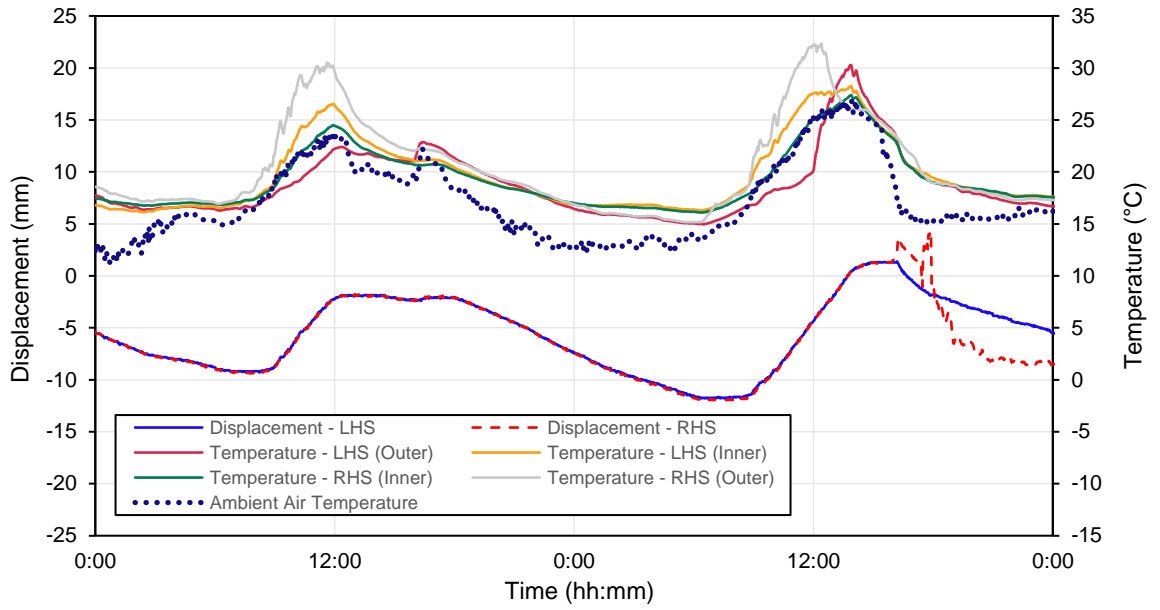
Figure B.4: Site A - Bridge Temperature and Bridge Displacement in March 2018
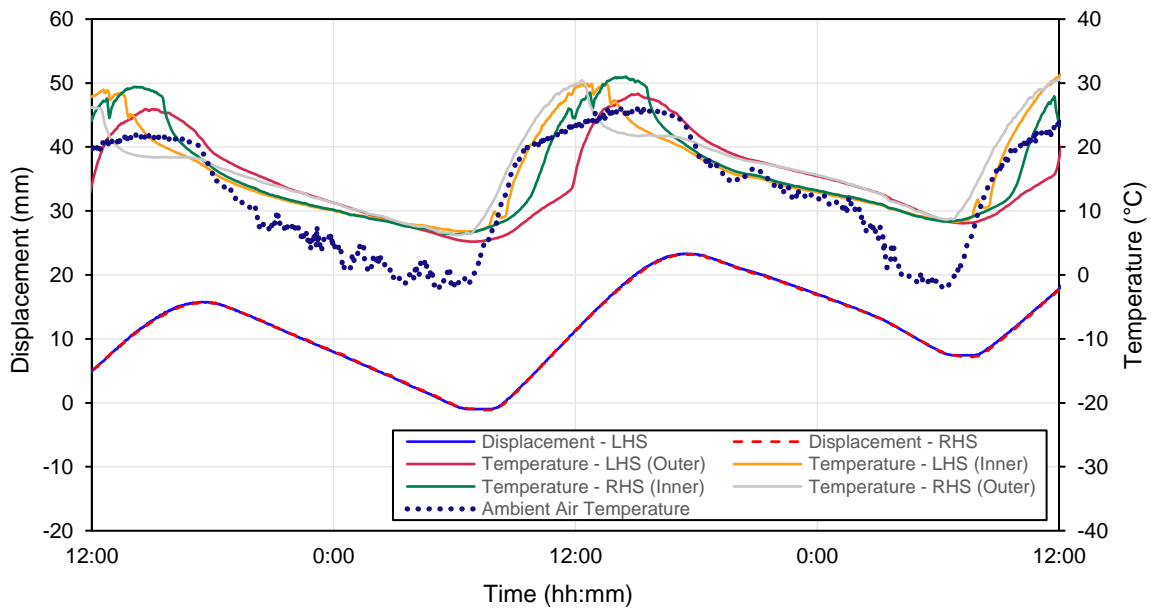
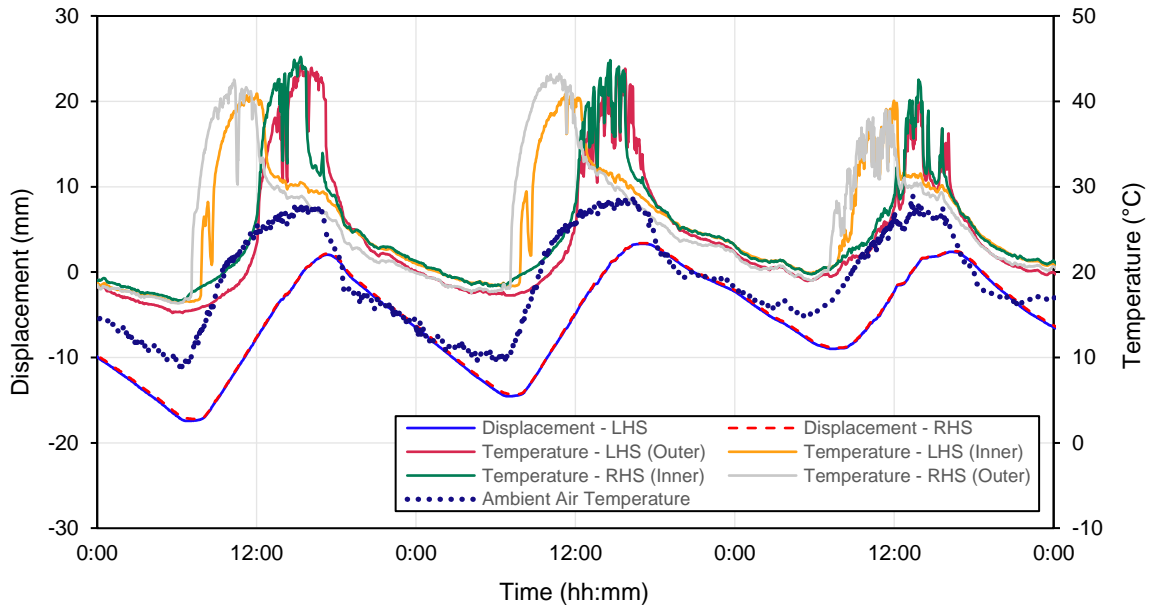**Figure B.5: Site A - Bridge Temperature and Bridge Displacement in September 2018**

Figure B.6: Site A - Bridge Temperature and Bridge Displacement in March 2019

Table B-4: Site A - Bridge Temperature and Bridge Displacement in March 2018

Period	Description	ΔX LHS (mm)	ΔX RHS (mm)	ΔT LHS Outer (°C)	ΔT LHS Inner (°C)	ΔT RHS Inner (°C)	ΔT RHS Outer (°C)
Day 1 AM Peak	Time	8:14:00	7:48:00	6:10:00	2:26:00	2:28:00	6:10:00
	Value	-9.30	-9.40	16.29	16.13	16.74	16.93
Day 1 PM Peak	Time	12:20:00	12:40:00	16:24:00	11:56:00	11:54:00	11:38:00
	Value	-1.85	-1.79	22.87	26.55	24.50	30.50
Day 2 AM Peak	Time	6:24:00	6:58:00	6:28:00	6:16:00	6:16:00	5:40:00
	Value	-11.80	-11.96	14.97	16.32	16.11	15.16
Day 2 PM Peak	Time	15:06:00	15:58:00	13:50:00	13:54:00	13:54:00	12:24:00
	Value	1.33	1.49	30.25	28.26	27.39	32.35

Table B-5: Site A - Bridge Temperature and Bridge Displacement in September 2018

Period	Description	ΔX LHS (mm)	ΔX RHS (mm)	ΔT LHS Outer (°C)	ΔT LHS Inner (°C)	ΔT RHS Inner (°C)	ΔT RHS Outer (°C)
Day 1 PM Peak	Time	17:18:00	17:22:00	14:38:00	12:34:00	14:06:00	12:02:00
	Value	15.76	15.71	25.94	28.96	29.42	26.20
Day 1 AM Peak	Time	6:52:00	7:24:00	6:46:00	6:44:00	6:06:00	6:10:00
	Value	-1.03	-1.14	5.21	6.78	6.35	6.21
Day 2 PM Peak	Time	17:12:00	17:18:00	15:06:00	12:36:00	14:30:00	12:20:00
	Value	23.31	23.26	28.34	29.95	31.02	30.43
Day 2 AM Peak	Time	7:00:00	7:30:00	7:12:00	6:34:00	6:32:00	6:24:00
	Value	7.37	7.14	8.08	8.28	8.32	8.62

Table B-6: Site A - Bridge Temperature and Bridge Displacement in March 2019

| Period	Description	ΔX LHS (mm)	ΔX RHS (mm)	ΔT LHS Outer (°C)	ΔT LHS Inner (°C)	ΔT RHS Inner (°C)	ΔT RHS Outer (°C)
Day 1 AM Peak	Time	6:56:00	7:12:00	5:40:00	5:50:00	6:10:00	6:02:00
	Value	-17.43	-17.21	15.22	16.40	16.61	16.33
Day 1 PM Peak	Time	17:20:00	17:20:00	15:22:00	12:02:00	15:20:00	10:18:00
	Value	2.03	2.19	44.20	40.91	45.21	42.55
Day 2 AM Peak	Time	6:48:00	7:22:00	6:56:00	7:04:00	6:28:00	4:10:00
	Value	-14.53	-14.33	17.26	18.32	18.26	17.53
Day 2 PM Peak	Time	16:56:00	17:04:00	15:44:00	11:46:00	14:38:00	10:48:00
	Value	3.31	3.40	43.84	40.84	44.83	43.22
Day 3 AM Peak	Time	7:16:00	7:32:00	5:28:00	5:28:00	5:46:00	5:46:00
	Value	-8.99	-8.86	18.97	19.90	19.76	19.01
Day 3 PM Peak	Time	16:18:00	16:16:00	13:54:00	11:58:00	13:50:00	11:22:00
	Value	2.37	2.47	39.83	40.06	42.56	39.02

APPENDIX C   RAIL STRAIN & CREEP DATA
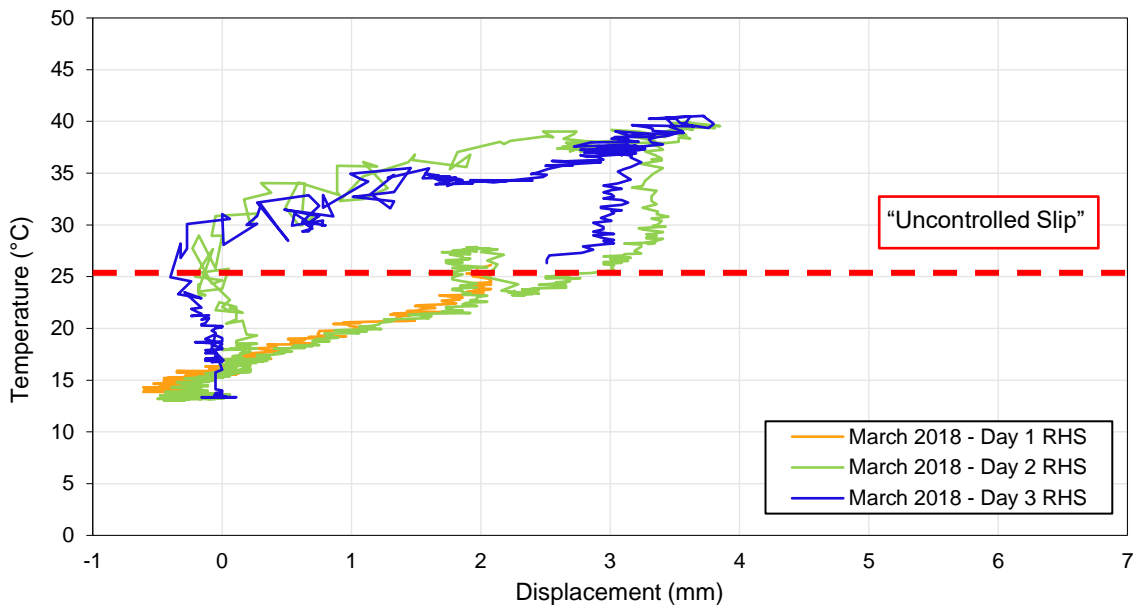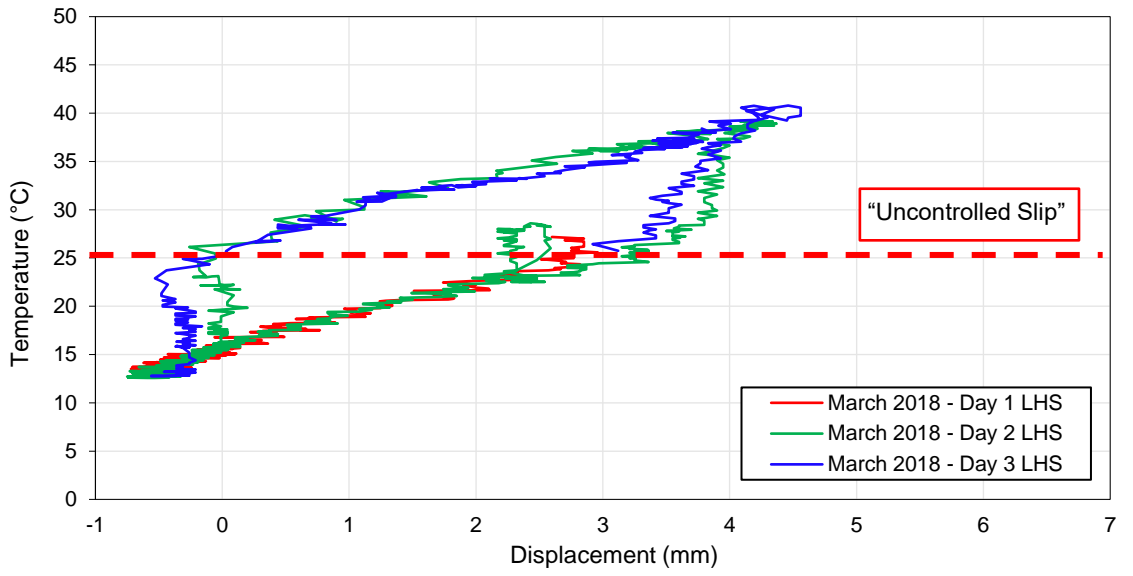
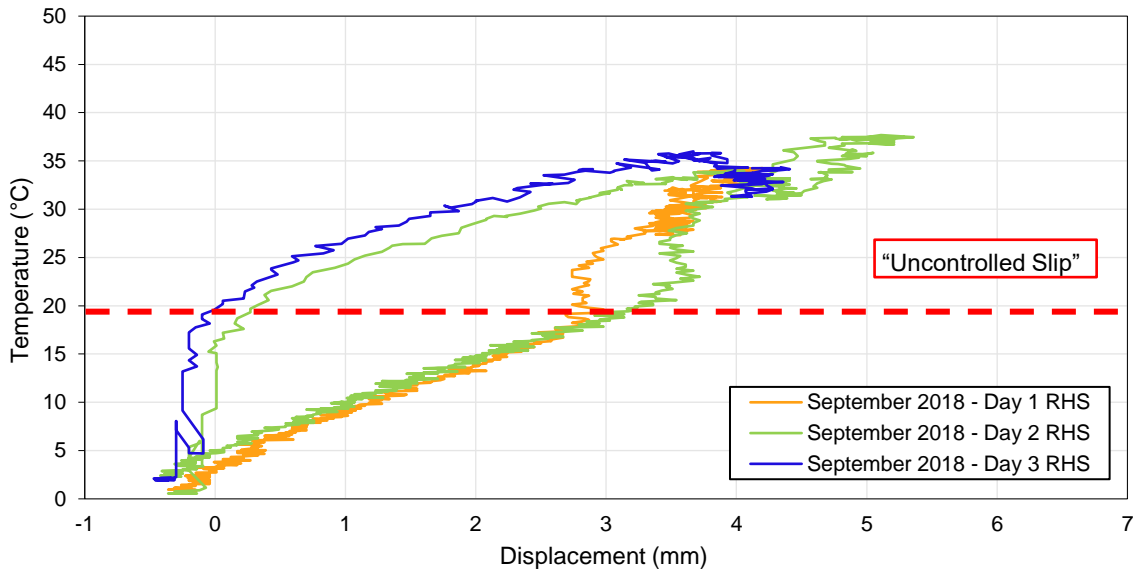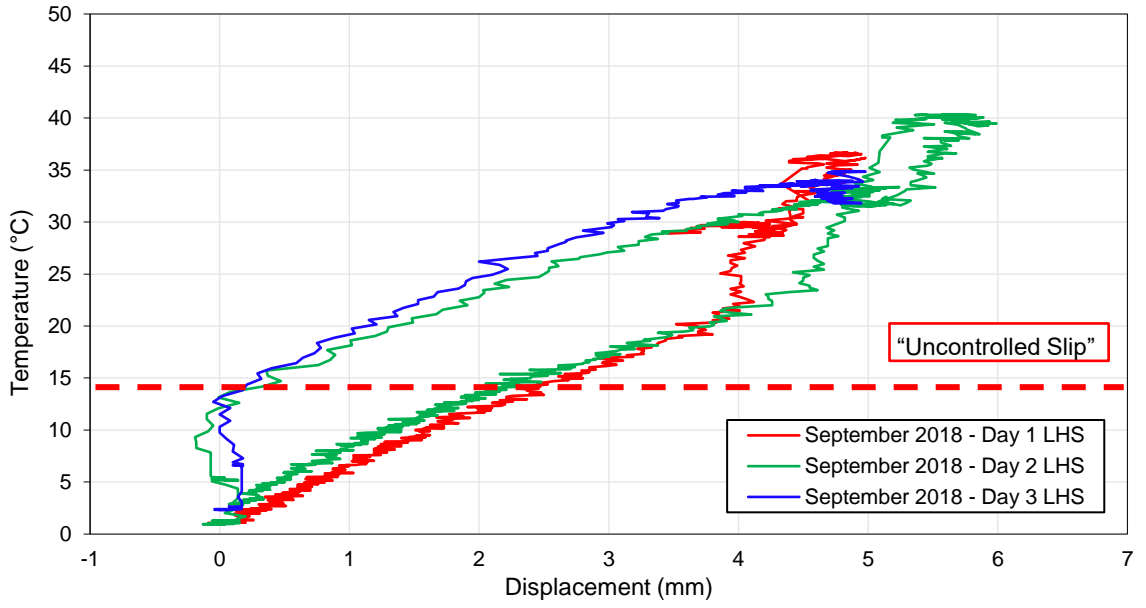**Figure C.1: Rail creep as a function of temperature (track resistance) – March 2018**

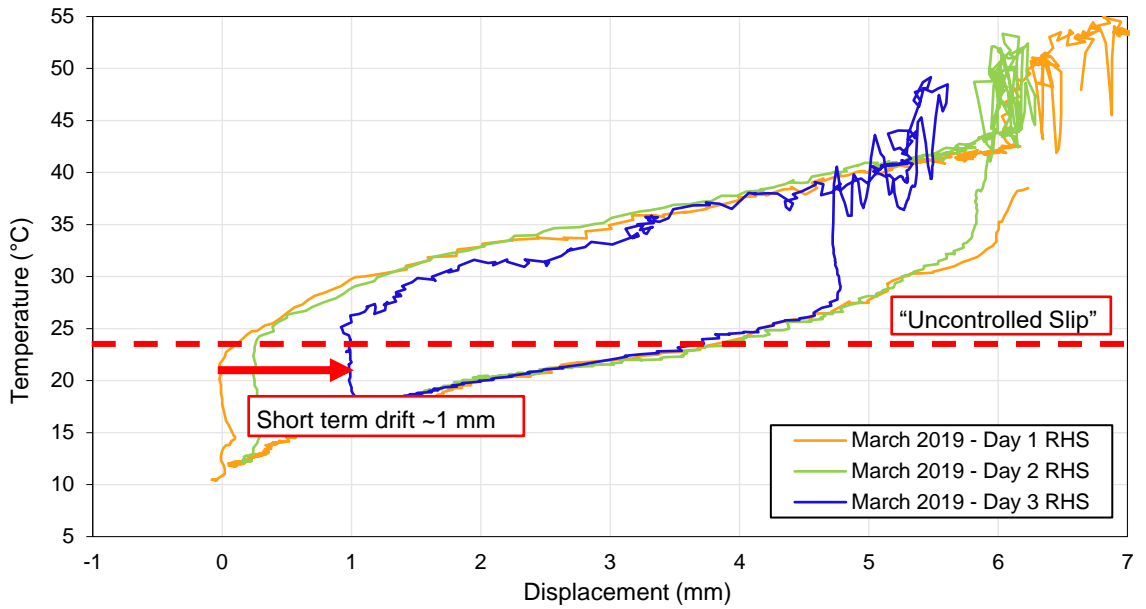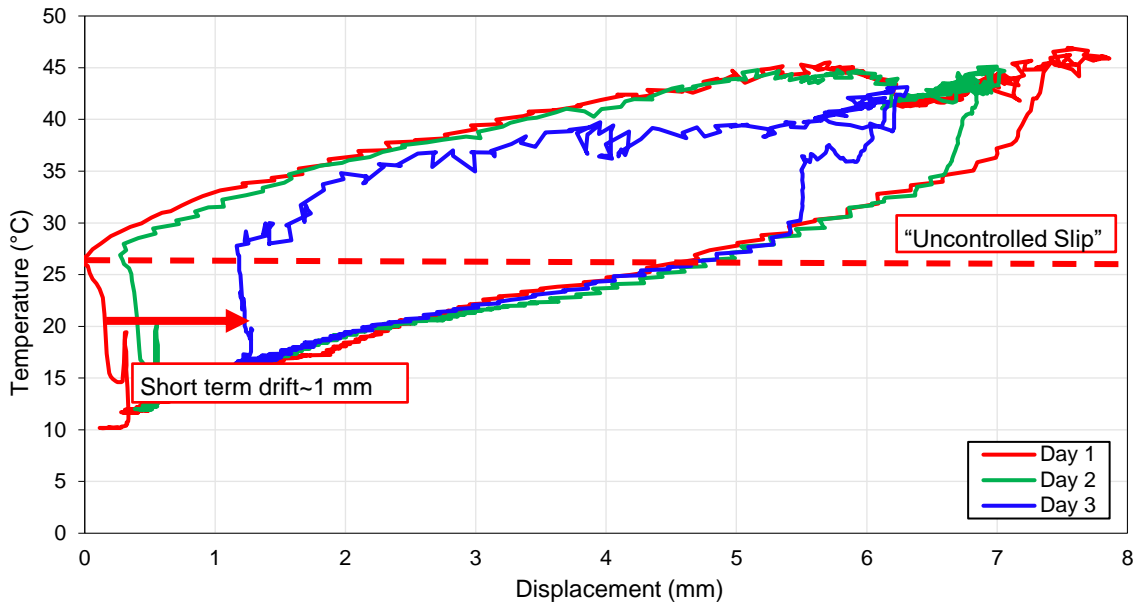**Figure C.2: Rail creep as a function of temperature (track resistance) – September 2018**

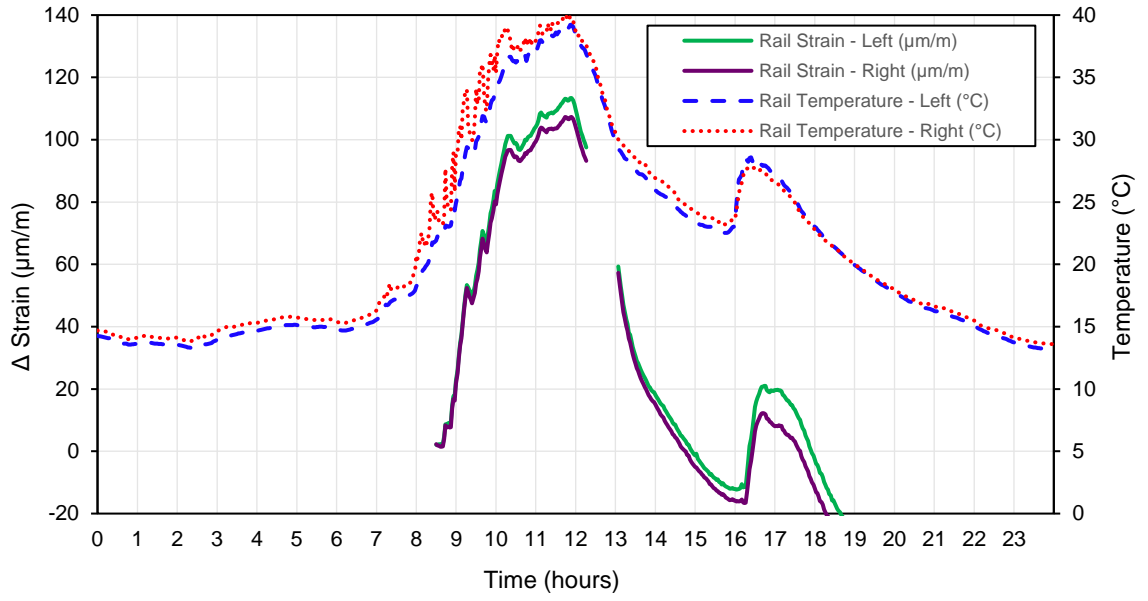**Figure C.3: Rail creep as a function of temperature (track resistance) – March 2019**
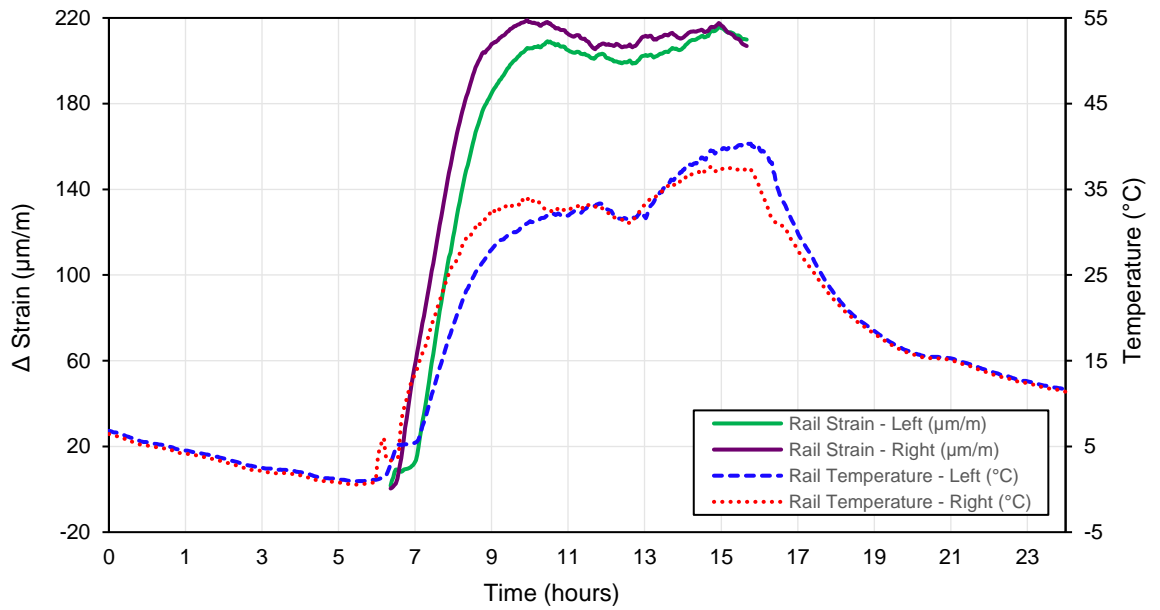
Figure C.4: Rail strain and temperature – Site 1
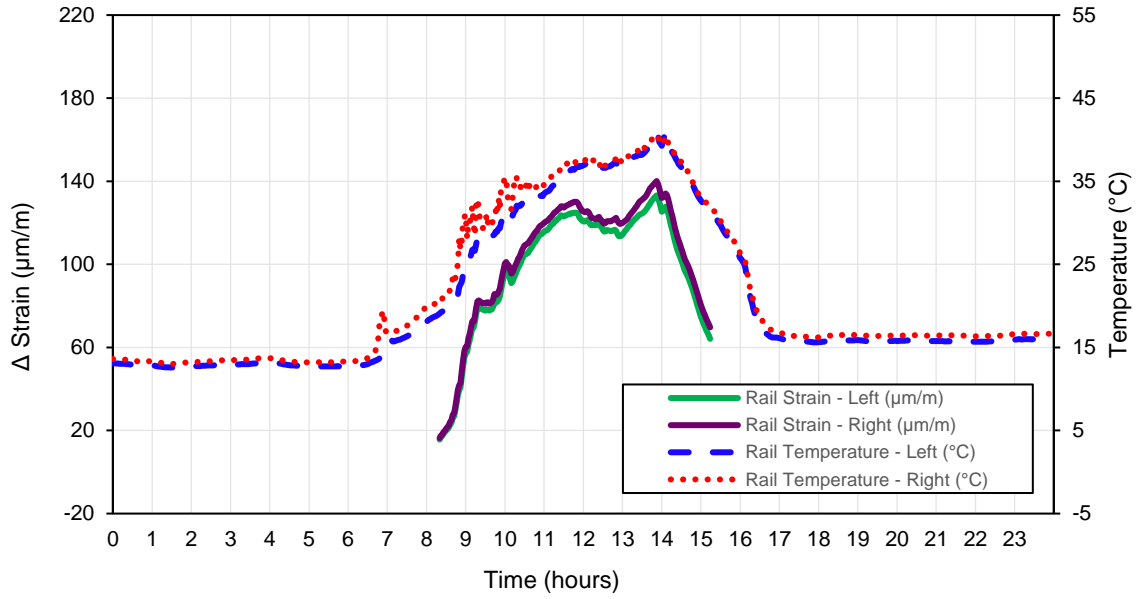

Figure C.5: Rail strain and temperature – Site 2
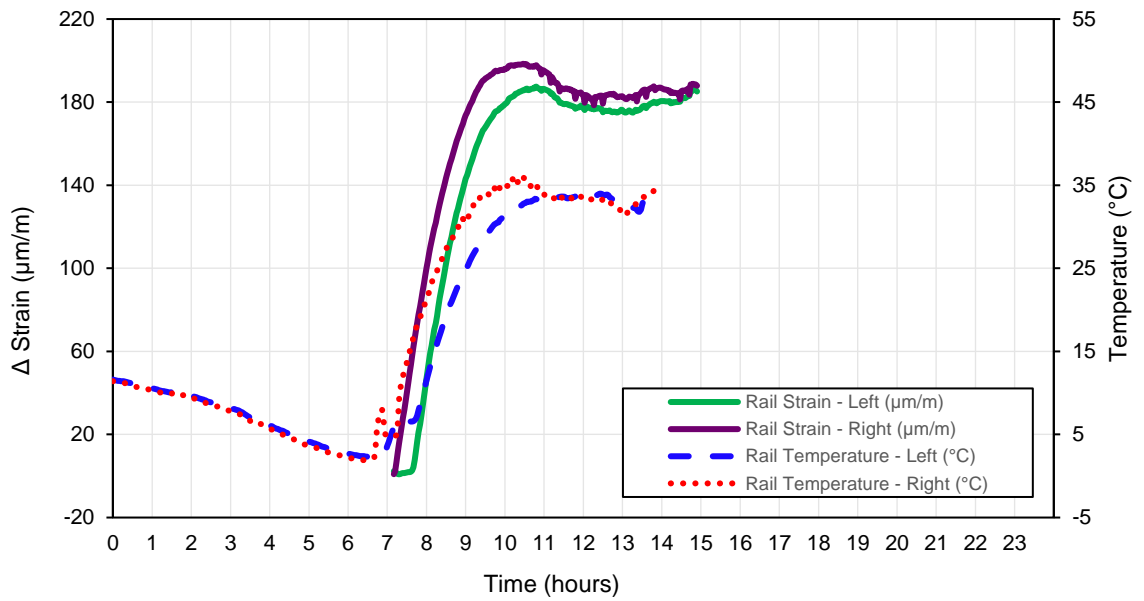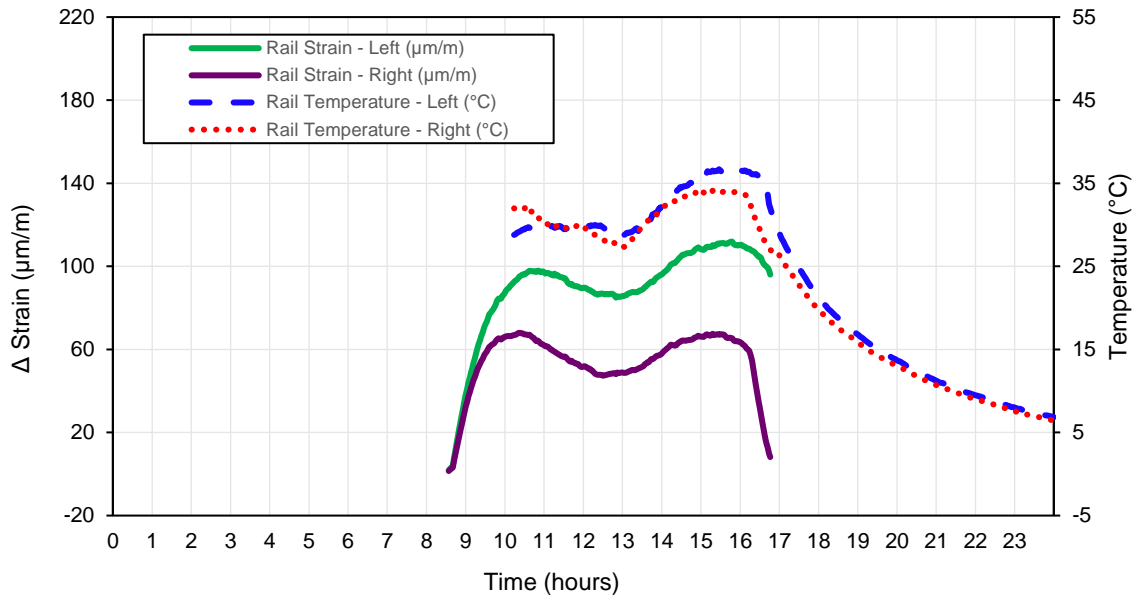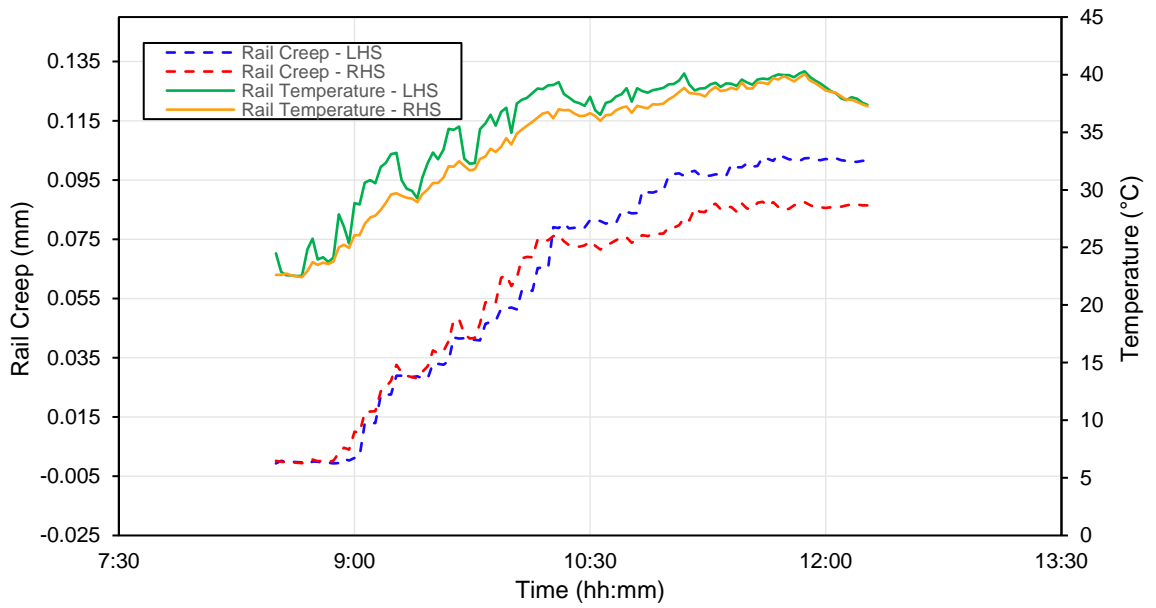
Figure C.6: Rail strain and temperature – Site 3

Figure C.7: Rail strain and temperature – Site 4

Figure C.8: Rail strain and temperature – Site 5

Figure C.9: Site 1 - Rail Temperature and Rail Creep at km 35.693
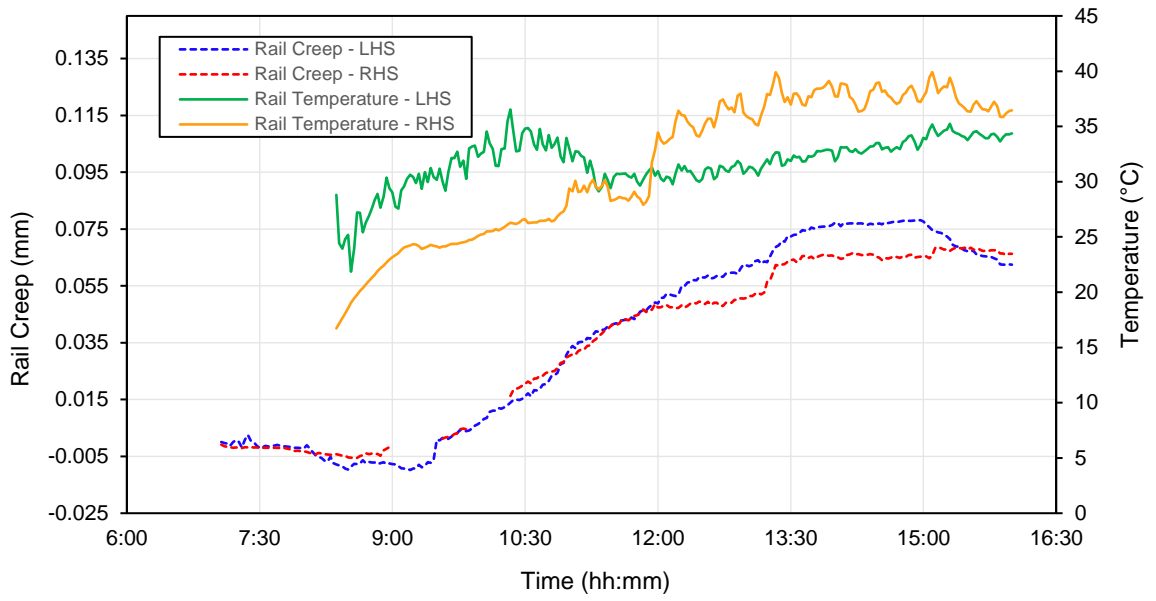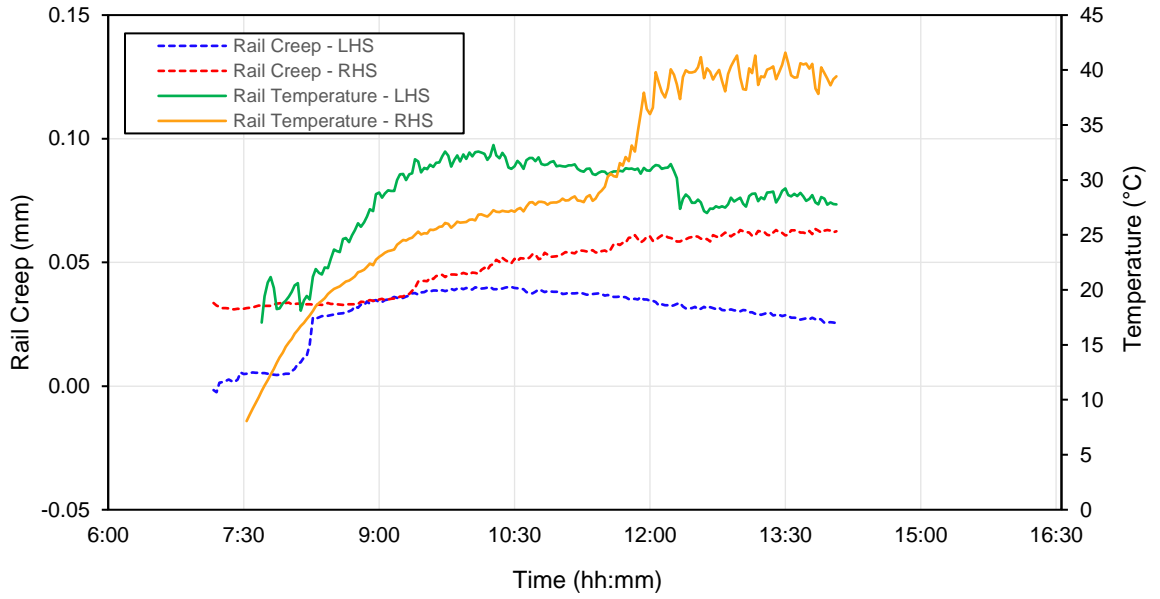
Figure C.10: Site 2 – Rail Temperature and Rail Creep at km 35.625
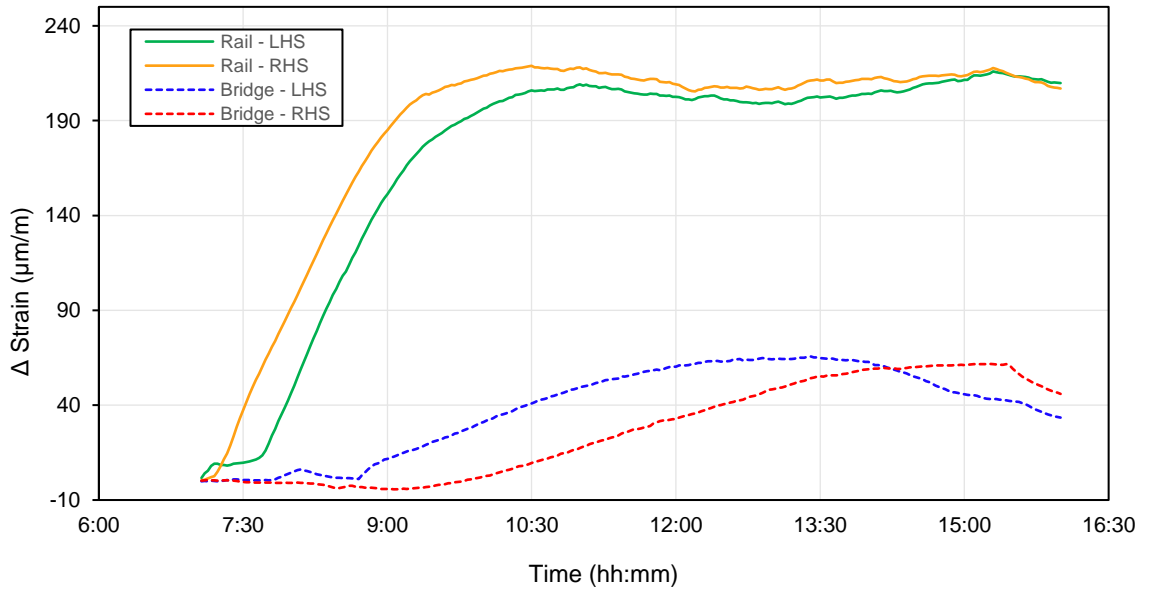
Figure C.11: Site 2 – Rail and Bridge Strain at km 35.625
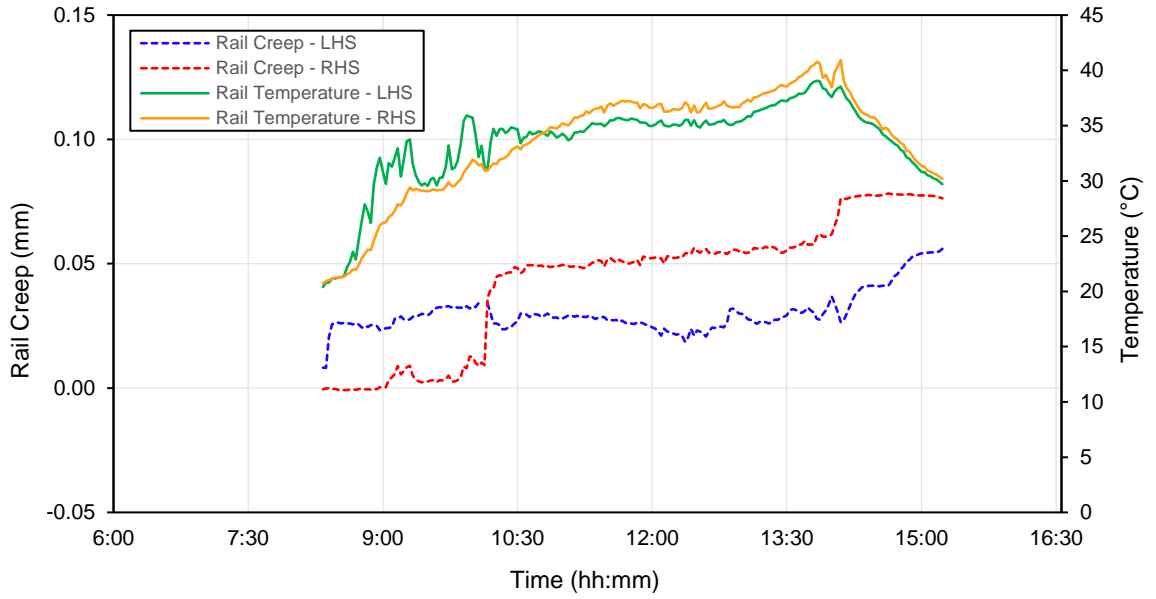
Figure C.12: Site 3 – Rail Temperature and Rail Creep at km 35.557
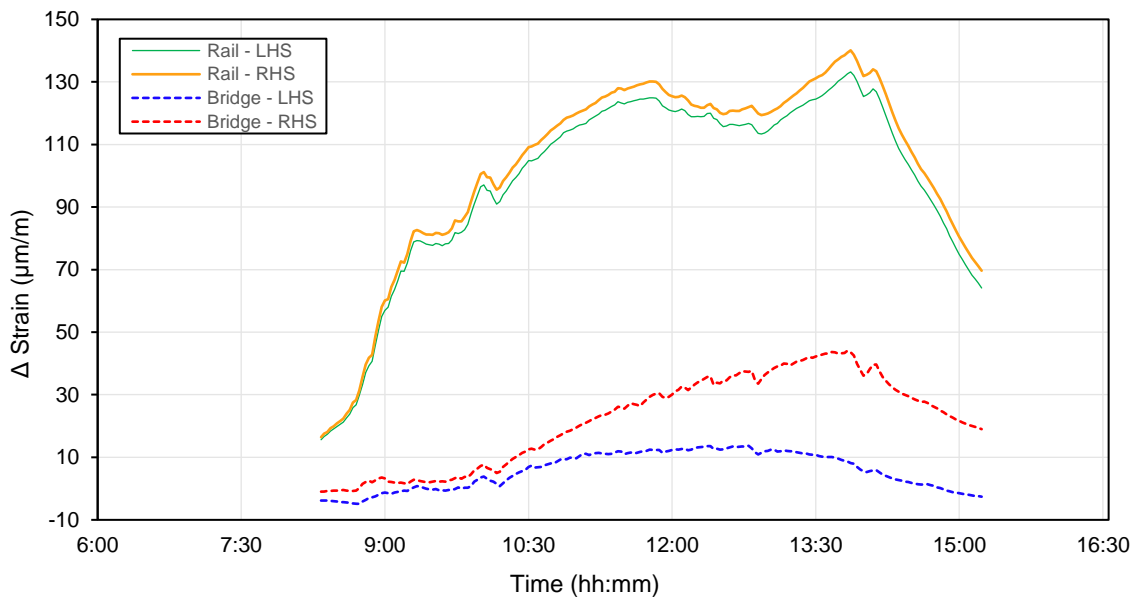
Figure C.13: Site 3 – Rail and Bridge Strain at km 35.557

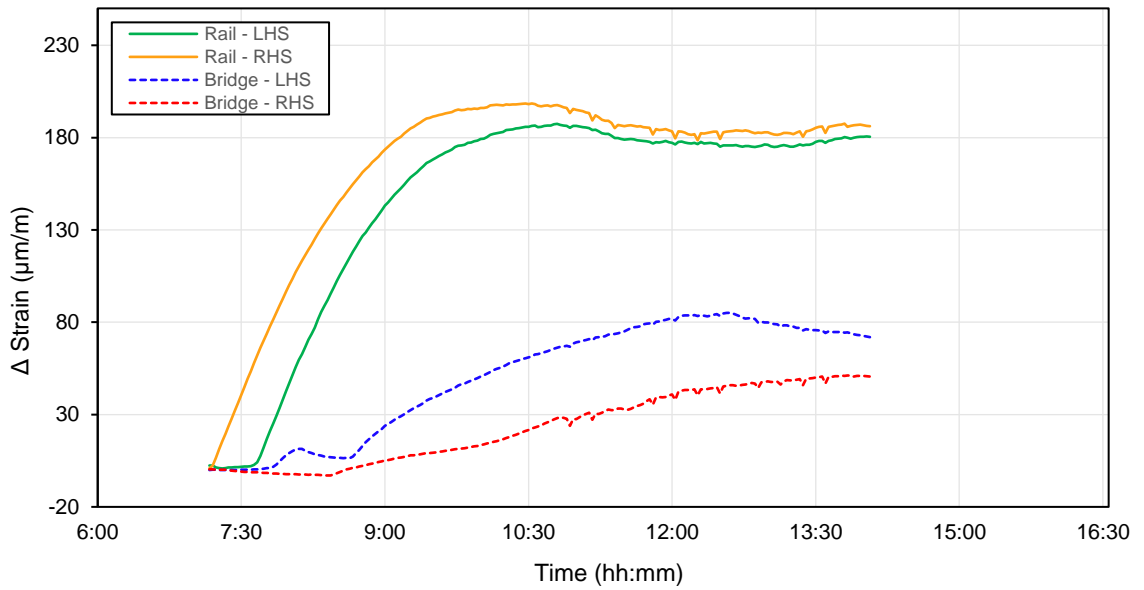**Figure C.14: Site 4 – Rail Temperature and Rail Creep at km 35.484**

Figure C.15: Site 4 – Rail and Bridge Strain at km 35.484
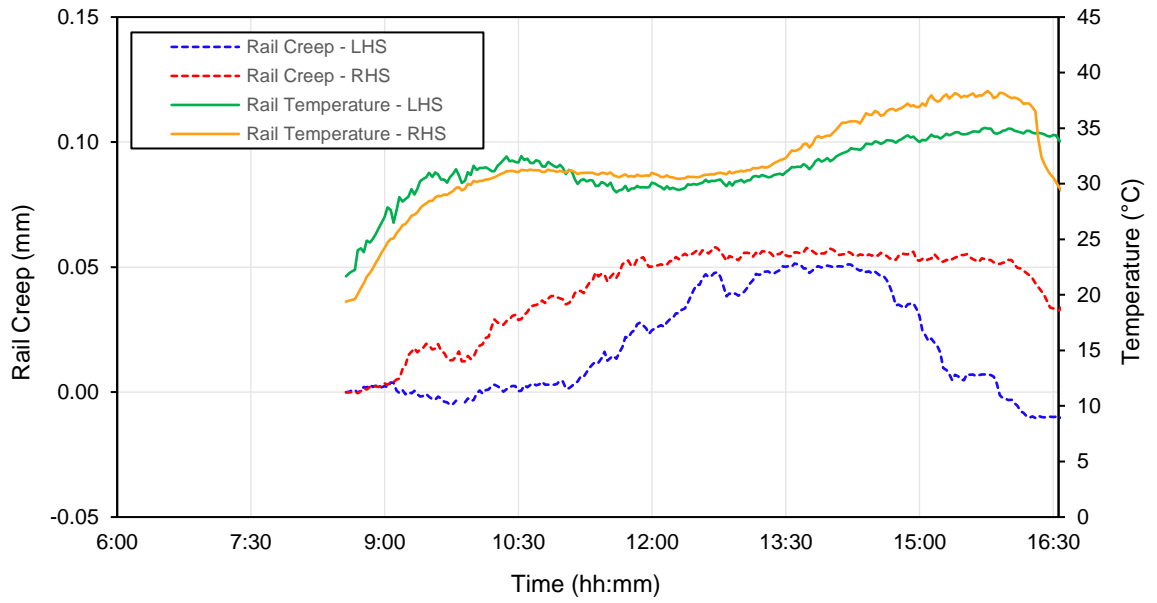
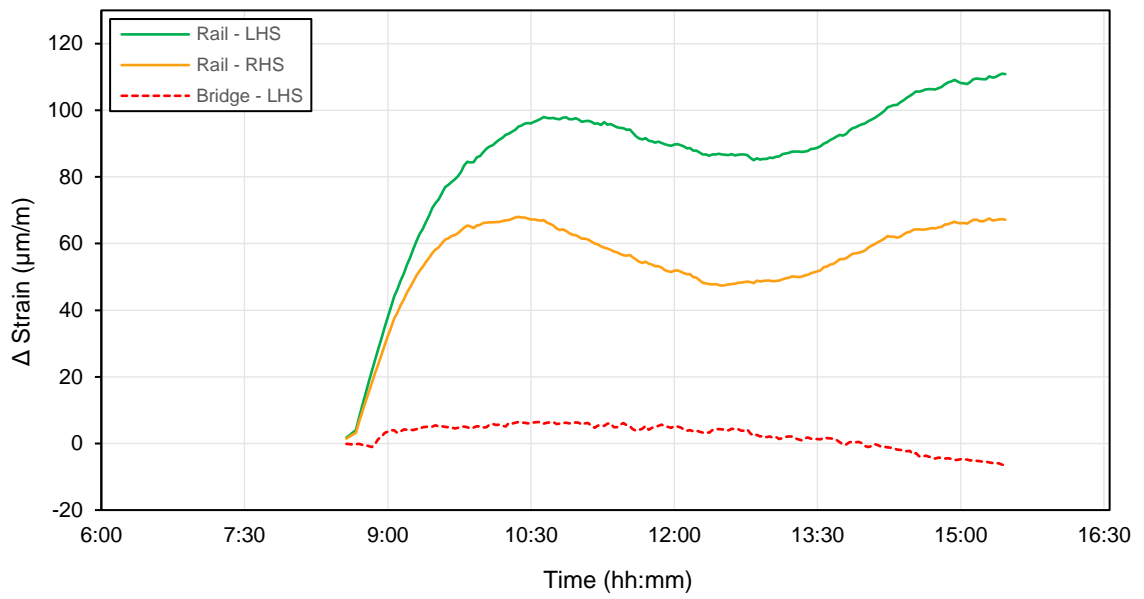**Figure C.16: Site 5 – Rail Temperature and Rail Creep at km 35.415**

Figure C.17: Site 5 – Rail and Bridge Strain at km 35.415